

FLUIDS, FORM, AND FUNCTION: THE ROLE OF FLUID DYNAMICS
IN THE EVOLUTION OF STALACTITES, ICICLES, AND AQUATIC
MICROORGANISMS

by

Martin Bowen Short

A Dissertation Submitted to the Faculty of the

DEPARTMENT OF PHYSICS

In Partial Fulfillment of the Requirements
For the Degree of

DOCTOR OF PHILOSOPHY

In the Graduate College

THE UNIVERSITY OF ARIZONA

2006

THE UNIVERSITY OF ARIZONA
GRADUATE COLLEGE

As members of the Dissertation Committee, we certify that we have read the dissertation prepared by Martin Bowen Short entitled FLUIDS, FORM, AND FUNCTION: THE ROLE OF FLUID DYNAMICS IN THE EVOLUTION OF STALACTITES, ICICLES, AND AQUATIC MICROORGANISMS and recommend that it be accepted as fulfilling the dissertation requirement for the Degree of Doctor of Philosophy

Raymond E. Goldstein Date: May 9, 2006

James C. Baygents Date: May 9, 2006

J. Warren Beck Date: May 9, 2006

Ke Chiang Hsieh Date: May 9, 2006

Srinivas Manne Date: May 9, 2006

Final approval and acceptance of this dissertation is contingent upon the candidate's submission of the final copies of the dissertation to the Graduate College.

I hereby certify that I have read this dissertation prepared under my direction and recommend that it be accepted as fulfilling the dissertation requirement.

Dissertation Director: Raymond E. Goldstein Date: May 9, 2006

STATEMENT BY AUTHOR

This dissertation has been submitted in partial fulfillment of requirements for an advanced degree at the University of Arizona and is deposited in the University Library to be made available to borrowers under rules of the Library.

Brief quotations from this dissertation are allowable without special permission, provided that accurate acknowledgment of source is made. Requests for permission for extended quotation from or reproduction of this manuscript in whole or in part may be granted by the head of the major department or the Dean of the Graduate College when in his or her judgment the proposed use of the material is in the interests of scholarship. In all other instances, however, permission must be obtained from the author.

SIGNED: Martin Bowen Short

ACKNOWLEDGEMENTS

Wow. By the time you actually get to the point of writing the acknowledgements for your doctoral dissertation, the list of people to thank is so long that the task seems almost Herculean in magnitude. I mean, what, you're maybe late twenties, early thirties by the time you graduate? So, you've lived on the order of 10,000 days on this planet, and each day you interact with who knows how many people, each indelibly leaving their mark upon you, even if you don't know it at the time. You know, that whole "no man is an island" thing isn't just a lot of pretty words from some dead poet.

So, with such a daunting task before you, how might you begin? I suppose a good first try would be a chronological listing of all the major characters that have appeared thus far in your life, beginning with – who else? – your parents. But, why start there, at an essentially arbitrary position within the timeline? After all, if it weren't for your grandparents, your parents wouldn't exist for you to thank, etcetera. No, the only logical recourse is to begin at the beginning: the dawn of time. Unfortunately, the University only allows one page of acknowledgements, clearly too small a space to list the names of every existent thing in the universe since the Big Bang. Furthermore, such a list is, as far as I know, impossible to create due to the relative dearth of historical records from periods greater than a couple thousand years ago. Instead it would probably be easier to just make some vague, nebulous comment such as, "I would like to thank God," and leave it at that. Somehow, though, this is unsatisfying, as you would ideally like those you thank to thank you in return for thanking them, and I am doubtful that God participates in such tit-for-tat pleasantries.

Perhaps, then, a minimalist's approach would suffice; enumerate the top, say, ten people who have had a direct influence on your life-path, and write a little blurb explaining their contribution and thanking them profusely for offering it. This task is undeniably easier than that described in the previous paragraph, but is also rife with veritable interpersonal landmines. This is because any such list will inevitably omit some person(s) who feel that his/her/their contribution to your life and (hopefully) success is entirely worth mentioning and just who do you think you are leaving me out while including the likes of so-on and so-forth when they weren't there for you during the bad times like I was and... Well, as you can see, it may be best not to open that particular can of worms, as only pain and terrible retribution can follow.

What path, then, exists to extricate myself from this seemingly Sisyphusian situation? On the one hand, I cannot name all of the people whom I should, for their numbers are too great; while on the other, I cannot pare the list down for fear of discounting even one whom I should not. And so I am lead to the only possible solution: I thank *you*, dear reader. Whoever you are, be ye family, friend, foreigner, or foe, without you these words would be nothing but black squiggles on a stark, white background, or, worse yet, simply a long string of ones and zeroes floating about through the uncaring aether. It is you who give life to the ideas within this humbly submitted work by the mere act of reading them, and for this I am eternally grateful.

For my family

TABLE OF CONTENTS

LIST OF FIGURES	7
ABSTRACT	8
1. PROLOGUE	9
2. CAST IN STONE	11
2.1. INTRODUCTION	11
2.2. PRESENT STUDY.....	12
3. FROZEN FLUID FORMATIONS.....	21
3.1. INTRODUCTION	21
3.2. PRESENT STUDY.....	22
4. LIVING LARGE	30
4.1. INTRODUCTION	30
4.2. PRESENT STUDY.....	32
5. EPILOGUE.....	41
REFERENCES	43
APPENDIX A: STALACTITE GROWTH I	45
APPENDIX B: STALACTITE GROWTH II.....	50
APPENDIX C: ICICLE GROWTH.....	63
APPENDIX D: EVOLUTIONARY TRANSITIONS IN <i>VOLVOX</i>	69

LIST OF FIGURES

Figure 2.1: Stalactites in Kartchner Caverns State Park, Benson, AZ.	12
Figure 2.2: Geometry of a growing stalactite.....	14
Figure 2.3: (a) Numerical stalactite growth. The different colored lines represent the shape at increasing times, starting from black and moving to green. When aligned as shown at the tip, these profiles collapse onto a uniformly translating shape (dashed line). (b) The numerically integrated ideal stalactite shape.	17
Figure 2.4: Comparison between the ideal stalactite shape (black line) and the average of 20 properly scaled stalactite images (green dots and red error bars). The error bars increase further up the shape because there are fewer long stalactites.	19
Figure 3.1: A collection of icicles.	22
Figure 3.2: Geometry of a growing icicle.	24
Figure 3.3: The ideal icicle shape.....	28
Figure 3.4: Comparing the ideal icicle (black line) to the average of eight properly scaled icicle images (red points and error bars). Error bars generally increase up the shape because there are fewer long icicles. The small error bars near the end indicate that only one icicle is present there.	29
Figure 4.1: Various species of Volvocine algae and their respective sizes. The species shown here are: A) <i>Chlamydomonas reinhardtii</i> , B) <i>Gonium pectorale</i> , C) <i>Eudorina elegans</i> , D) <i>Pleodorina californica</i> , E) <i>V. carteri</i> , and F) <i>V. aureus</i> . Note the daughter colonies within the last two species, indicating full germ/soma separation.	31
Figure 4.2: (a) Illustrating the bottleneck radius. Once metabolic demands (green) outstrip diffusional currents (red), the organism begins to starve. (b) Advection bypasses the bottleneck. On this log-log plot, advective current (blue) is parallel to metabolic needs at radii greater than the advective radius. Since the bottleneck radius (indicated by Λ) is greater than this, the bottleneck is completely circumvented.	34
Figure 4.3: (a) Verifying the fluid flow model. The theoretical tangential flow at the colony's surface (blue) is compared to the average of 10 suitably scaled flows measured by PIV around actual <i>Volvox</i> colonies (black points and error bars). (b) Concentration field of nutrients near a colony at various values of Pe, color scale bar at right. As Pe increases, the boundary layer in front of the colony gets thinner and a depletion plume extends further in the back.	36
Figure 4.4: The advantage of being large. At small radii, the advantage per cell conferred by advection over pure diffusion increases precipitously with increasing size. At larger sizes, though, this advantage saturates.	39

ABSTRACT

This dissertation is devoted to better understanding the role that fluids play in the selection of the shapes and functions of objects and creatures in nature. Toward that end, three specific examples are considered: stalactites, icicles, and species of colonial green algae known as *Volvox*. In the cases of stalactites and icicles, the object's growth is considered as a free-boundary problem. For stalactites, the coupling of thin-film fluid dynamics with calcium carbonate chemistry leads to a local, geometric growth law that is proportional to the thickness of the water layer covering the surface at any point. Application of this law to a uniformly translating shape allows a universal stalactite form to be derived; the comparison of this shape to images of actual stalactites supports the theory. In the case of icicles, the transport of the latent heat of fusion is coupled with the dynamics of both the thin-film of water encompassing the icicle and a thermally buoyant boundary layer in the immediately surrounding air. The uniformly translating shape solution is found to be parameter-free, and is, in fact, the same shape exhibited by stalactites. A comparison between this shape and icicle images validates the theory. The final example considers how advection of nutrients due to the stirring of water by the flagella of a *Volvox* colony leads to a metabolite uptake rate that is much greater than would occur by diffusion alone. Moreover, nutrient acquisition by pure diffusion would limit the size of *Volvox* species to a certain bottleneck radius at the point where diffusional uptake just meets metabolic demands, whereas advection increases the uptake in such a way as to avoid this problem entirely, thus enabling the evolution of the larger *Volvox* species.

1. PROLOGUE

Nothing is as ubiquitous on Earth as the fluids that surround us in our everyday lives. From the water that we drink, which covers nearly three quarters of the Earth's surface and makes up roughly sixty-five percent of our own bodies, to the thousand kilometer thick atmosphere that we breathe, there is no escaping the constant presence, and accompanying influence, of fluids on our planet. The incredible power of this influence over the natural world is evident whether gazing through binoculars at the majestic Grand Canyon, forged by millennia of erosion from the Colorado River, or peering through a microscope as a lowly *E. coli* bacterium swims via its flagella, shaped over eons by a marriage of fluid dynamics and natural selection. Indeed, the physical forms and physiological functions of myriad other terrestrial objects and organisms like these are dependant upon, if not dictated by, the fluids that surround them.

In the following three chapters, we examine some specific instances of this sort of dependency in detail. Each chapter provides a summary of one or more of the papers presented in the appendices at the end of this dissertation and is divided into two segments: introduction and present study. In each introduction, a general overview of the topic will be given, in which we explain the issue at hand and present a brief review of previous research done in the area. Then, in each present study section, we summarize the methods, results, and conclusions of the relevant paper(s) within the appendices. These present study subsections are not intended to be rigorous presentations of the research they summarize; rather, they present only the major points and conclusions of the research. To accomplish this, many details have been omitted, especially within the vari-

ous calculations employed. Furthermore, all citations of previous works are found in the appropriate appendix, so they will not be provided in these sections. Therefore, the appendices are a crucial part of this dissertation and, for a complete understanding, they should be read along with the main body of the work. By so doing, we expect the reader will be provided with a convincing case for the power and importance of fluids in the natural world.

2. CAST IN STONE

That drop was falling when the Pyramids were new; when Troy fell; when the foundations of Rome were laid; when Christ was crucified; when the Conqueror created the British empire; when Columbus sailed; when the massacre at Lexington was “news.” It is falling now; it will still be falling when all these things shall have sunk down the afternoon of history, and the twilight of tradition, and been swallowed up in the thick night of oblivion.

-Mark Twain, *The Adventures of Tom Sawyer*

2.1. INTRODUCTION

The first stop on our intellectual journey is the stalactite, that iconic cave formation which dangles from the stony ceiling like the Sword of Damocles above the heads of intrepid spelunkers below. From as early as the first century A.D., the origin and nature of these speleothems have been the subjects of speculation and wonder around the globe, the number of explanations for which being nearly as plentiful as the formations themselves [1].

It was not, however, until the 19th century that the chemical and physical mechanisms underlying the growth of the stalactite were properly understood. Basically, these include the chemical reactions of calcium carbonate within an extremely thin water layer that covers the stalactite's surface, and they have been well described and characterized by works such as those of Dreybodt and Buhmann [2,3]. These investigations are successful insofar as they correctly explain the glacially slow growth of cave formations in general and offer a glimpse of the underlying connection between these growth rates and the details of the coating water layer. In fact, attempts have been made [4,5] to use such a connection to explain the shapes of the stalactite's alter ego, the floor-bound stalagmite; unfortunately, these explanations have not been rigorous in their descriptions of the fluid dynamics governing the layer and its relationship with the underlying geometry of the

speleothem.

In order to account for this connection, we have approached the problem of stalactite growth from a free-boundary perspective [6,7]. In this way, the overall stalactite shape influences the details of the fluid flow over the surface, which in turn dictates the way in which the substrate grows. As we shall see, this coupling of the geometry, chemistry, and fluid flow characteristics predicts a universal mathematical form for stalactites which compares quite



Figure 2.1: Stalactites in Kartchner Caverns State Park, Benson, AZ.

well with the real thing. Thusly, fluids make their mark upon the subterranean world.

2.2. PRESENT STUDY

The long, slow process of speleothem generation begins with water percolating down through the soil above a cave. As the water travels downward, it eats away at calcium carbonate minerals (among others) that are present in the overlying soil. Since this soil has a far greater effective partial pressure of CO_2 than the atmosphere, significant quantities of this gas may accumulate during the water's journey. This lowers the pH of the water, allowing more calcium carbonate to dissolve, and the cycle continues.

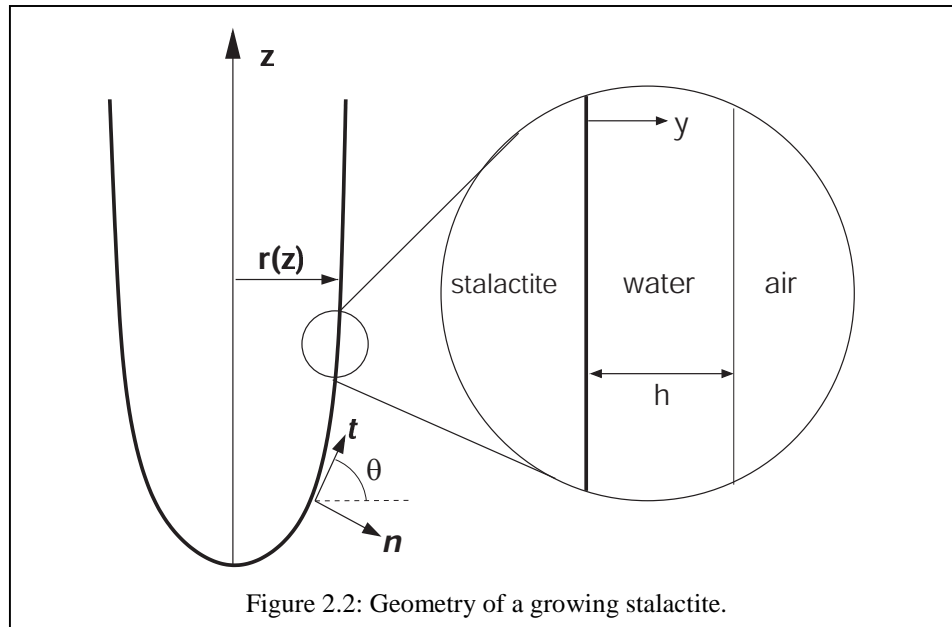
Eventually the water, now laden with calcium ions and various aqueous carbonate species, enters the cave through openings in the ceiling. Upon exposure to the cave's at-

mosphere and its lower CO_2 partial pressure, carbon dioxide begins to outgas from the solution. Simultaneously, this causes the dissolved calcium to become supersaturated, forcing it out of solution via growth on the underlying rock. Thus, a speleothem is born.

In order for this formation to become a stalactite, though, it is typically required for a “soda straw” to be generated first. This is essentially an elongated limestone tube through which water flows until it drips off the end. Each drip leaves behind a small rim of growth, elongating the tube over time. At some point, however, water may begin to flow on the outside of the soda straw, leading eventually to a stalactite, which may or may not have a still-dripping soda straw at its core.

A typical stalactite may have a length of 50 cm and a radius of 5 cm. Of course, stalactite measurements vary widely, but these figures are representative. Over this formation flows an average of about 10 to 100 ml of water per hour, corresponding to approximately one drip every few minutes. As we shall soon show, this relatively low flow rate over a structure of this size results in a water film thickness h of only tens of microns, with a peak fluid velocity of only a few millimeters per second. Hence, the fluid flow in question may be considered laminar and non-inertial.

Due to the low Reynolds number involved in the flow over a typical stalactite, Stokes flow may be assumed. Furthermore, because the water layer thickness is so small compared to the stalactite’s radius, we can approximate the flow as that underneath an inclined plane with a width equal to the circumference of the stalactite at that point and an inclination angle equal to the local tangent angle of the stalactite’s profile (see Figure 2.2). By solving the gravity-driven Stokes equation subject to the appropriate boundary



conditions and enforcing conservation of fluid flow along the length of the stalactite, we arrive at an expression for the layer thickness,

$$h = \left(\frac{3Q\nu}{2\pi g r \sin \theta} \right)^{1/3}, \quad (2.1)$$

where Q is the volumetric flow rate, ν is the kinematic viscosity of water, g is gravitational acceleration, r is the local radius, and θ is the local tangent angle. If we now substitute known values into this expression, we recover our initial thickness estimate of tens of microns. Of course, (2.1) is not valid very near the tip of the stalactite. In this region, capillary effects become important and cause drops to form and eventually fall. In fact, the tip region will remain off limits for the rest of this analysis, and anything happening there will become a parameter within the rest of the theory.

The second crucial ingredient for stalactite growth lies in the chemistry indicated above by which the cave formations grow. Thankfully, most of the details related to this

have been previously worked out, so we only quote the major results here. It has been shown that, for typical chemical species concentrations, the stoichiometry of the reactions involved demands that for every molecule of CaCO_3 added to the surface of the speleothem, one CO_2 molecule must be created in the fluid layer via the conversion of bicarbonate. This carbon dioxide generation is described by the rate equation

$$\frac{d[\text{CO}_2]}{dt} = -k_+[\text{CO}_2] + k_-[\text{HCO}_3^-], \quad (2.2)$$

in which

$$k_+ = k_{+1} + k_{+2}[\text{OH}^-], \quad k_- = k_{-1}[\text{H}^+] + k_{-2}, \quad (2.3)$$

and $k_{\pm 1}$ and $k_{\pm 2}$ are rate constants for the two pathways available for this conversion. For typical values of the pH, k_+ and k_- evaluate to around 0.1 to 1 sec^{-1} . It should also be noted that these CO_2 generating reactions are the slowest of all the reactions occurring, and are, therefore, the rate limiting step in the chemical process.

By taking an inverse of the rate constants above, we arrive at a timescale for the chemical reactions of 1 to 10 seconds. Compare this, then, to the timescale for diffusion of a chemical species with diffusion constant $D = 10^{-5} \text{ cm}^2/\text{sec}$ across the fluid layer, $h^2/D \approx 10^{-1}$ seconds. Clearly, diffusion is significantly faster than the slowest chemical reactions. This implies that the concentrations of chemical species across the fluid layer will be nearly constant, allowing us to use the average values of such species in equations such as (2.2). Along similar lines, we can argue that, because growth is so slow (only around one centimeter per *century*), chemical concentrations will vary little along the length of the stalactite. Hence, advective transport down the stalactite is negligible, per-

mitting us to focus only on what is happening locally when deriving a growth law. Finally, one can show through a detailed analysis that atmospheric diffusion of CO_2 is also unimportant, leaving the overall rate limiting step of the growth process as the carbon dioxide generation described by (2.2).

Using this information, then, we can make a simple derivation of the growth law for stalactites. The flux of CO_2 out of the water at any point is just the local layer thickness multiplied by the time rate of change of the carbon dioxide concentration at that point. In other words, reactions occur at a constant rate volumetrically, so the thicker the water is, the more CO_2 is being generated there. Using the one-to-one relationship between carbon dioxide generation and CaCO_3 growth equates stalactite growth to this calculated CO_2 flux. A multiplication of this factor by the molar volume of calcium carbonate translates the flux into a normal growth velocity of the stalactite's surface that may be written as

$$v_g = v_c \left(\frac{\ell}{r \sin \theta} \right)^{1/3}, \quad (2.4)$$

with v_c a characteristic velocity that depends upon the concentrations of aqueous bicarbonate and atmospheric carbon dioxide along with the rate constants k_+ and k_- , and ℓ a length scale dependant upon the flow rate Q . Typical values place v_c at 0.1 to 1 centimeter per century, consistent with known tip elongation rates.

A superficial examination of (2.4) reveals that the growth velocity should be much higher near the tip of the stalactite, where r and θ are small. This should have the general effect of emphasizing long, pointy structures, as stalactites tend to be. A more de-

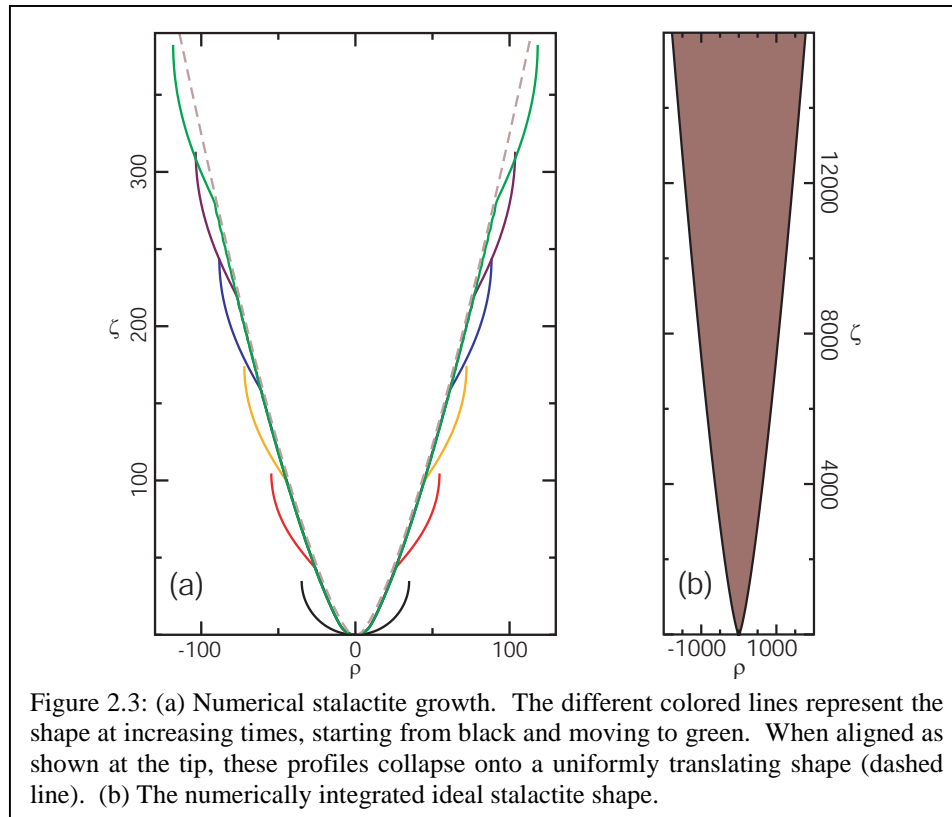


Figure 2.3: (a) Numerical stalactite growth. The different colored lines represent the shape at increasing times, starting from black and moving to green. When aligned as shown at the tip, these profiles collapse onto a uniformly translating shape (dashed line). (b) The numerically integrated ideal stalactite shape.

tailed analysis in the form of numerical calculations verifies this behavior and can be seen in Figure 2.3(a). Most interestingly, the numerical output seems to indicate that there is an attractor of these dynamics in shape space that is a uniformly translating shape; i.e., a shape that does not deform as time goes by, but simply reveals more and more of itself.

Analytically determining the functional form of this shape is not very difficult. First, we note that, in general, uniformly translating shapes are described by dynamics in which the normal growth velocity at any point is such that $v_g = v_t \cos \theta$, where v_t is the velocity of the tip. To find our shape, then, we apply this formula to the growth velocity as given in (2.4), rewrite trigonometric quantities in terms of the derivative of the stalactite's profile $z'(r)$, and scale z and r by a length scale $a = \ell(v_c / v_t)^3$ to give dimen-

sionless variables ζ and ρ . Through this procedure, one finds that the uniformly translating stalactite shape obeys the differential equation

$$\frac{\zeta'}{\left(1+(\zeta')^2\right)^2} - \frac{1}{\rho} = 0. \quad (2.5)$$

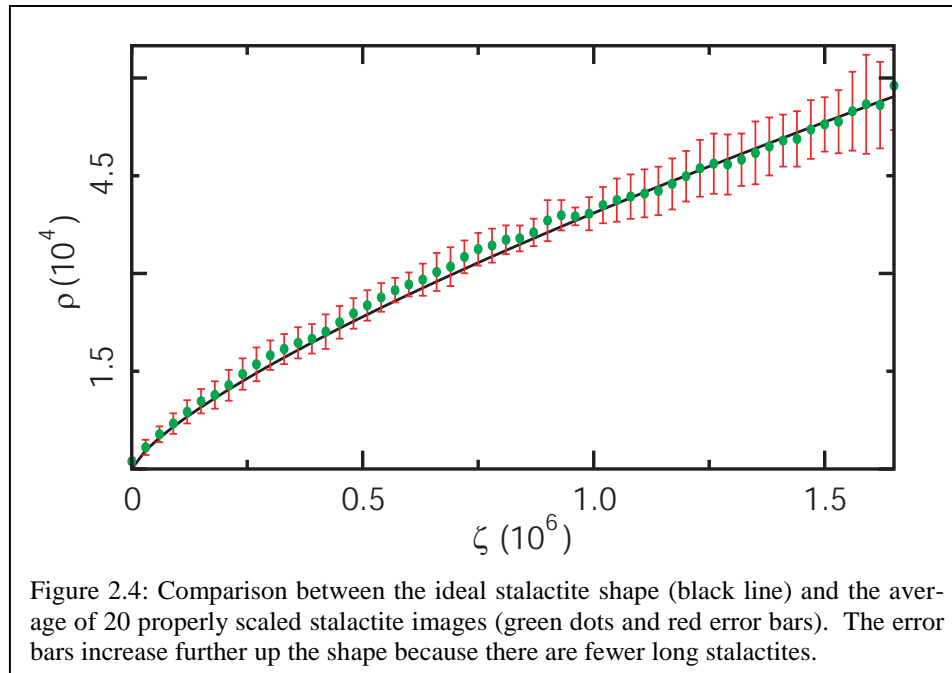
Unfortunately, an exact integration of (2.5) is not available, though results of a numerical integration are shown in Figure 2.3(b). However, an expansion at large ρ shows that the asymptotic shape is a power law in which

$$\zeta \sim \rho^{4/3}. \quad (2.6)$$

Since a is typically quite small (perhaps 10^{-5} cm), this asymptotic regime is reached at very small radii, making this four-thirds power law a very good approximation for the overall shape, barring the tip.

The shape described by (2.6) is interesting for multiple reasons. First, it displays a slight convexity that is quite distinct from a cone, reminiscent of the carrot-like profile often observed in stalactites. Secondly, this ideal shape is parameter-free; all details of the flow rate and chemical species concentrations are lost in the rescaling to dimensionless variables. This means that, if the theory is indeed correct, all stalactites should tend toward the same mathematical form, the only difference between individuals being the factor a that dictates how much of the ideal form is displayed. In a way, the scaling parameter a magnifies the ideal shape onto reality, selecting how much or how little of this universal form to reveal.

To test the validity of the theory, we compared the ideal shape as found by numerically integrating (2.5) with the profiles of actual stalactites. To accomplish this, we



first took many high-resolution digital pictures of stalactites in Kartchner Caverns State Park, selecting those that were the most axisymmetric and smooth. Second, we ran edge detection algorithms on these pictures to extract the profiles $z(r)$ for each stalactite. Then, using *Mathematica*, we performed a least-squares comparison between each profile and the ideal shape to determine the optimal value of a for that stalactite. Finally, we scaled the profiles by their respective a values and then averaged them all together. The fruits of this analysis can be found in Figure 2.4. The results are quite striking, in that the theory and the actual shapes agree well (within one standard deviation) over many orders of magnitude.

In conclusion, through our research on speleothem growth, we were able to uncover a growth law for stalactites that combines the details of the aqueous chemical reactions and the dynamics of the water in which they occur. Through a free-boundary approach, we have found that this law leads to a uniformly translating and universal stalac-

tite shape that compares well with the forms of actual stalactites. Truly, just as the very existence of stalactites depends upon fluid flow, so too do the details of their mathematical form.

3. FROZEN FLUID FORMATIONS

Some say the world will end in fire; / Some say in ice. / From what I've tasted of desire /
I hold with those who favor fire. / But if it had to perish twice, / I think I know enough of
hate / To know that for destruction ice / Is also great / And would suffice.

-Robert Frost, "Fire and Ice"

3.1. INTRODUCTION

When looking at the stalactites from our first example (Figure 2.1), it is hard not to be reminded of their frigid look-alikes, icicles. Like stalactites, icicles have fascinated mankind since antiquity, but the mechanisms underlying icicle growth have been known for much longer, and are well described in numerous publications [8-10]. Icicle growth is, of course, the result of the transport of latent heat from the freezing water covering the surface of the icicle into the surrounding, colder atmosphere. Once the heat escapes into the atmosphere, it creates a thermally buoyant boundary layer that rises along the icicle's surface. Superficially, this process is not completely dissimilar to that of stalactite growth; each involves a quantity that is being transported through a thin, flowing fluid layer surrounding the underlying structure. Could this conceptual similarity explain the uncanny physical resemblance of the two objects?

To be certain, previous works have taken steps to model the growth of icicles [8,9], though not through a strict free-boundary approach. Unfortunately, though the overall growth rates and characteristics are well predicted by these theories, little mention has been made of the exact shape adopted by the icicles modeled therein. Interestingly, the analysis of Szilder and Lozowski [9] points toward a slightly convex shape like that displayed by real icicles; however, they dismiss this, claiming that their shape "does not deviate substantially from simple conical geometry."

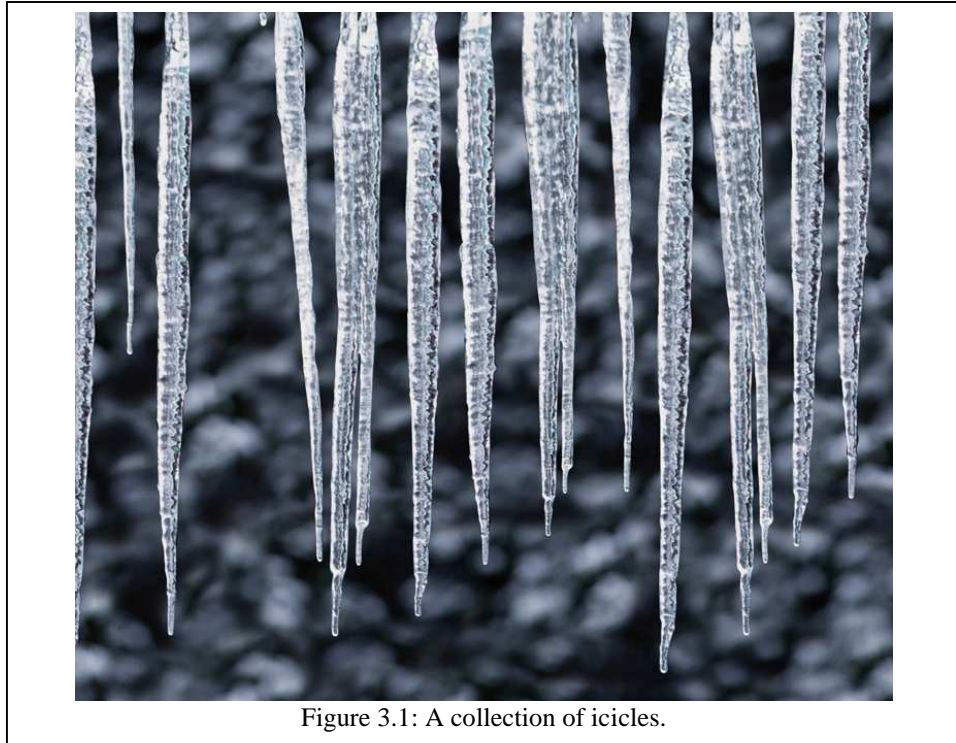


Figure 3.1: A collection of icicles.

To address the issue of icicle shape, we have, as with stalactites, taken a free-boundary approach to the problem [11]. We find that icicles also tend toward one universal shape, the functional form of which compares very well with actual icicle images. These results are uncanny, insofar as the shape calculated thusly is (at least asymptotically) identical to that found for stalactites; indeed, the resemblance between the two is more than skin-deep, and the power of fluid mechanics to dictate shape is once again displayed.

3.2. PRESENT STUDY

The process involved in the generation of icicles is in many ways quite similar to that involved in stalactites. In this case, the water involved is typically melted snow present on a roof, or possibly on the branches of a tree. This near freezing water forms a hanging

droplet on whatever the substructure might be, and if the air temperature is below freezing, some (or all) of the droplet may turn to ice as the latent heat of fusion is transferred into the atmosphere. If we assume slow growth, only the water at the point of contact with the substructure will freeze, the rest will drop away, and a new drop will take its place. Eventually, something like a small ice soda straw might form which may then begin to form the icicle proper, similar to stalactites. Interestingly, many still-growing icicles will continue to have an unfrozen liquid core, as water that reaches the tip after flowing along the outside of the icicle is drawn up through the tube by capillary action (the presence of this unfrozen core will be important in our later analysis).

The water layer covering the icicle's surface is very similar to that on a stalactite as well. Of course, icicles are typically smaller than the average stalactite, being only around 10 cm in length and a couple of centimeters in radius, and the volumetric flow rates on icicles are typically a little higher than on stalactites. But despite this, the thickness h of the layer is still quite small (maybe 100 microns) and can be described by the same equation, (2.1). The major difference between the two cases, though, is that the volumetric flux Q on an icicle is not constant, as it is on a stalactite. This is, of course, because water is being converted to ice as it travels down the icicle.

To describe the variance of Q on an icicle, we simply write a mass balance equation that relates the rate at which Q changes with the arclength s as measured from the icicle's tip. The resulting equation is

$$\frac{dQ}{ds} = 2\pi r v_g . \quad (3.1)$$

If we now enforce the condition on v_g for uniformly translating shapes described in Sec-

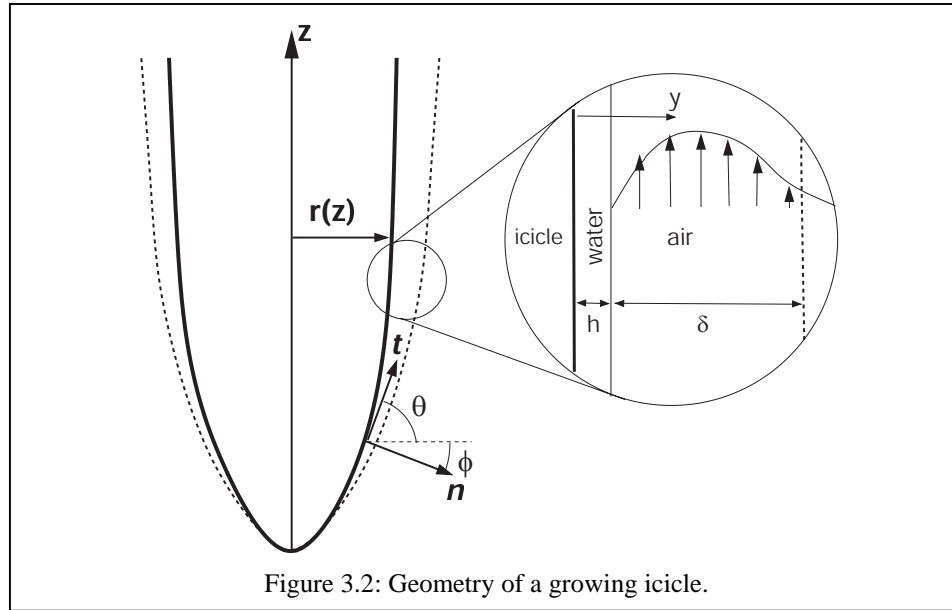


Figure 3.2: Geometry of a growing icicle.

tion 2.2 ($v_g = v_t \cos \theta$), and note that $ds \cos \theta = dr$, we can exactly integrate (3.1) to yield

$$Q = Q_t + \pi r^2 v_t, \quad (3.2)$$

where Q_t is the volumetric flow rate at the tip. So, as long as the icicle does not become too large, and the tip velocity is not too great, the icicle will remain coated with water and growth can occur along the entire length. For the remaining analysis, we will assume this to be the case.

At this point though, the similarities between icicle and stalactite growth end. With stalactites, the water layer thickness controls the growth via chemical reactions, but for icicles, the controlling step does not occur within the water layer (as long as it exists). Rather, another flowing fluid controls the icicle's fate: the rising thermal boundary layer in the air near the icicle's surface (Figure 3.2). But to understand the existence and details of this layer, we must first analyze how heat is transported within this system.

As previously stated, for the water on the icicle to freeze, it must give up its latent heat of fusion L (measured per unit volume in this case) to the atmosphere. The first step in doing this is the rapid conduction of the heat across the thin water layer. Due to the isothermality of the ice-water interface at the melting temperature T_m and the low Péclet number involved, the transport of this heat down the icicle is negligible, and the heat is assumed to travel perpendicular to the surface only. In addition, because of the liquid water core within a standard icicle, there is an internal ice-water interface that is also at T_m . This means that no heat is transferred from the icicle's core to the outer surface, hence any heat flux we calculate there is composed solely of the latent heat being released.

Once this heat has come to the water-air interface, it enters the atmosphere, raising the local air temperature slightly as it does so. This air is now warmer than the surrounding atmosphere, and so it becomes buoyant and begins to rise. The heat flux across this layer can be well approximated by a simple conduction equation, even though advection plays an important role; the actual flux is found by simply multiplying this approximated conduction-only flux by an order one constant that is essentially unimportant, as we shall see. So, the heat flux from a point along the icicle where the thickness of the natural convection layer is δ is given by

$$F = \frac{\kappa_a \Delta T}{\delta}, \quad (3.3)$$

where κ_a is the thermal conductivity of air and ΔT is the difference between the ambient temperature T_a and the water-air interface temperature T_i at the point in question.

To find a formula for this thickness δ , we use as an example the natural convection boundary layer for a flat, vertical, isothermal plate. It turns out that there is a similarity solution for this system, and the thickness of the boundary layer is found through the equation

$$\delta = C \left(\frac{\nu_a^2 z}{g\beta\Delta T} \right)^{1/4}, \quad (3.4)$$

where C is an order one constant that depends on the Prandtl number of air, and ν_a and β are the kinematic viscosity and volumetric expansion coefficient of air, respectively.

Though (3.4) was not derived with icicles in mind, it can be used to describe the thickness of an icicle's buoyant air layer for the following reasons. First, using a temperature difference of 10° K, δ is around a few millimeters to a centimeter at most. This is significantly less than the typical icicle radius, so flatness is approximated. Second, though the icicle's surface is not vertical, the slope changes very slowly at areas not near the tip, so that g and z could be modified by approximately constant factors related to the average slope. These constants can be subsumed into the factor C of (3.4), thus leaving it essentially unaltered. Third, the interface temperature T_i can be shown (by equating water and air heat fluxes) to be

$$T_i = T_m - (T_m - T_a) \frac{h\kappa_a / \delta\kappa_w}{1 + h\kappa_a / \delta\kappa_w}, \quad (3.5)$$

where κ_w is the thermal conductivity of water. Because of the great disparity between h and δ , the ratio of the two is quite small, meaning that the water-air interface temperature is only different from the melting temperature by maybe 10^{-2} to 10^{-3} ° K. In this way, the

icicle is practically isothermal. Finally, because the velocity of the air layer (cm/sec) is much greater than the velocity of the water layer (mm/sec), the no-slip condition used to derive (3.4) is essentially attained.

Having justified our use of (3.4), we can at this point combine it with (3.3) and divide by the latent heat per volume of water to derive the normal growth velocity of the icicle's surface. This gives us the equation

$$v_g = v_c \left(\frac{\ell}{z} \right)^{1/4}, \quad (3.6)$$

where v_c is a characteristic velocity and ℓ is a length scale, both depending upon the temperature difference ΔT . Estimates for v_c , again at a ΔT of 10° K, place it at around 10^{-4} cm/s, in good agreement with known elongation rates.

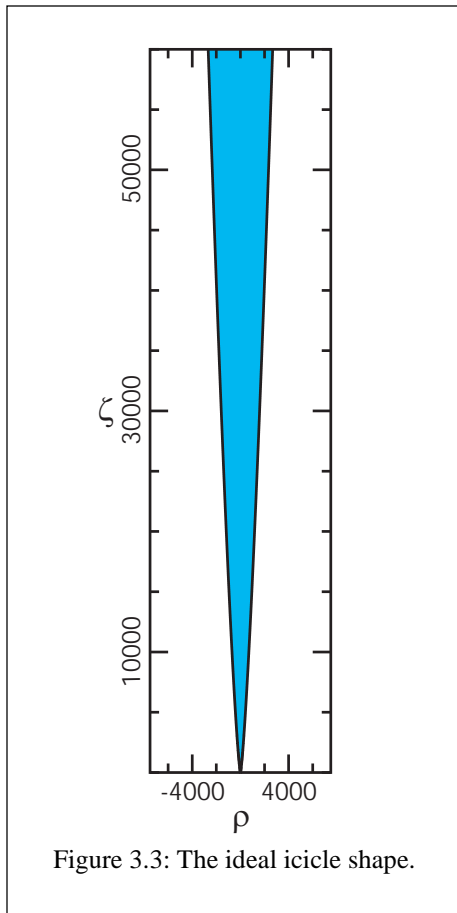
To find the ideal icicle profile, we do as we did with the stalactites and apply our growth velocity to a uniformly translating shape. After rewriting the trigonometric quantities in terms of the slope $r'(z)$ and scaling r and z by the lengthscale $a = \ell(v_c / v_t)^4$ to define the dimensionless variables ρ and ζ , we find that the icicle shape is governed by the differential equation

$$\rho' = \frac{1}{\sqrt{\zeta^{1/2} - 1}}. \quad (3.7)$$

Unlike the differential equation for the stalactite shape (2.5), we can readily integrate (3.7) to find that the shape of an ideal icicle (Figure 3.3) is

$$\rho = \frac{4}{3} (\zeta^{1/2} + 2) \sqrt{\zeta^{1/2} - 1}. \quad (3.8)$$

Note that the shape described here is, like the stalactite shape, parameter-free, implying a

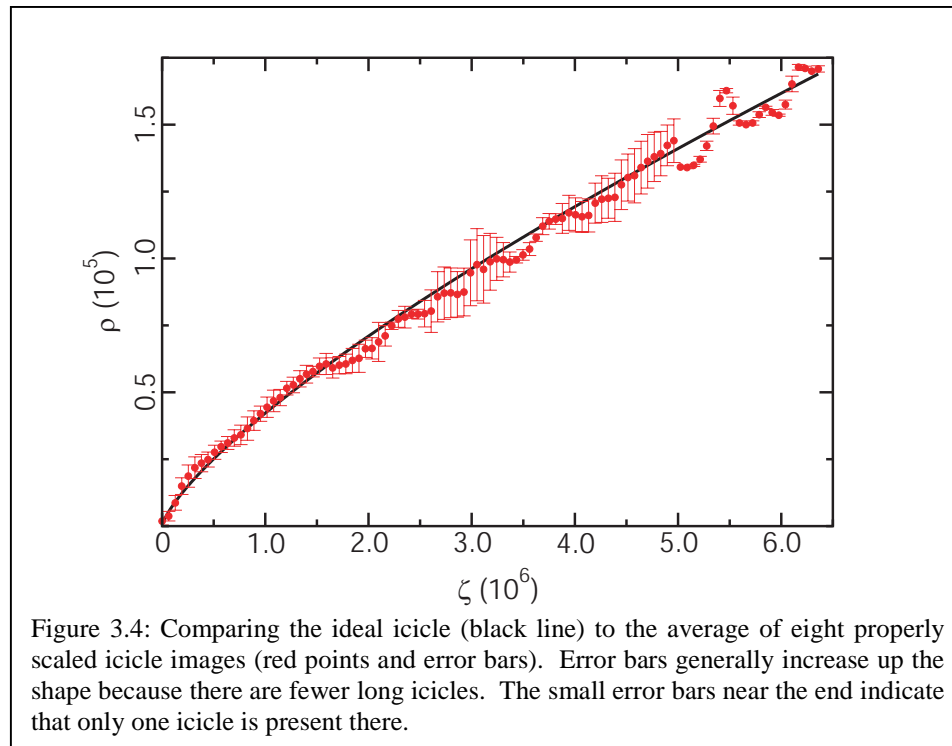


universality of form between icicles. Furthermore, at large values of ζ , this shape exhibits the same power law as the stalactite shape (2.6); i.e., the ideal icicle form is the slightly convex four-thirds power law seen before. Finally, then, we can understand why there is such a pronounced visual similarity between icicles and stalactites.

Before moving on, we note a curious fact about the calculations presented thus far. If one calculates the shape of an icicle using the heat flux as calculated through the water layer thickness, rather than through the air layer thickness, the same asymptotic shape is found. The underlying cause of

this is not understood. Note that the calculation outlined above does not require any exact details of the water layer's flow; it is sufficient to simply acknowledge that the water thickness is small compared to the buoyant layer and to demand that the icicle be covered with water from top to tip. Hence, the shape (3.8) is not in any way due to the scaling of the water layer thickness. But, when calculating the shape via the water layer, such details are of pivotal importance. The fact that the two routes lead to the same answer, then, is somewhat mysterious and is, at the very least, an odd coincidence.

With that noted, we now move to the testing of our theory. The process behind this is practically identical to that for testing the stalactite theory, except for the fact that



the icicle images were taken from the Internet, rather than being taken by us (icicles are quite rare in Tucson, Arizona, after all). The results of such a comparison are shown in Figure 3.4, and the agreement is clearly quite good. It should furthermore be noted that an attempt to fit the data to a cone, rather than our four-thirds power law, fails miserably, as systematic deviations are quite clearly present.

To conclude, our icicle research has verified that the rate-limiting step in icicle formation is the transfer of heat through a thermally buoyant boundary layer of air near the icicle's surface. This layer can be well approximated as that due to a flat, vertical, isothermal plate, and the resulting shape obtained is in very good agreement with images of natural icicles. Finally, the connection between icicles and stalactites is now clear, as both have been shown to exhibit the same asymptotic shape, despite the very different physical mechanisms underlying their respective growth processes.

4. LIVING LARGE

If Creatures of so low an Order in the great Scale of Nature are endued with Faculties to enable them to fill up their Sphere of Action with such Propriety, we likewise, who are advanced so many Gradations above them, owe to ourselves, and to Him who made us and all things, a constant Application to acquire that degree of Rectitude and Perfection to which we also are endued with Faculties of attaining.

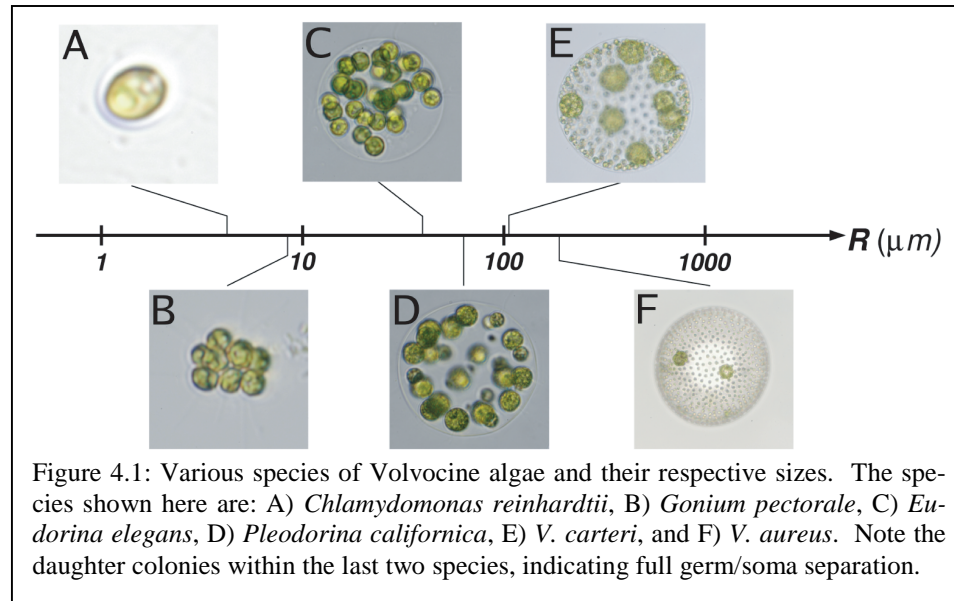
-John Ellis, *A Natural History of the Corallines*

4.1. INTRODUCTION

Within the lakes, ponds, rivers, and oceans of the world reside innumerable species and families of microorganisms. Among these are the Volvocales, a family of various species of flagellated, colonial green algae ranging in size from the single-cell *Chlamydomonas reinhardtii* to the 100,000 cell behemoth *V. gigas* (Figure 4.1) [12]. And among these various species, generically referred to as *Volvox*, *V. carteri* is a giant, coming in at a whopping 200 microns in diameter. Now, this may seem small to us humans, but in the microscopic world of phytoplankton, size really does matter, and sometimes in unexpected ways.

For example, the larger an organism is, the more food it generally needs to survive. For large land animals like elephants and rhinos, this means spending more time eating, and eating more at any given time. But for very small microorganisms, the rate at which one can “eat” is often limited by diffusion. For larger species of *Volvox*, this presents a serious problem, because the rate of diffusive nutrient intake grows only linearly with the organism’s radius, while the number of cells grows quadratically (the cells live on the surface of the sphere). What, then, is a large species such as *V. carteri* to do?

One answer, provided by Mother Nature herself, is to swim. Clearly, swimming provides a means for an organism to move from a nutrient-poor to a nutrient-rich envi-



ronment. However, that is only half the story. It has long been known, for example, that aquatic plants grow larger when living in a rapidly flowing stream than in a still pond [13]. This is because the plant living in the flowing stream gains nutrients not only by diffusion, as the lake plant does, but also through advection, the transport of a concentration field by fluid flow. In a similar way, the swimming of *Volvox* colonies brings advection into play, thereby supplementing their diffusional diets.

But, is advection enough to have allowed the larger *Volvox* species to evolve? The relative importance of advection to diffusion is measured by a dimensionless parameter known as the Péclet number (Pe), and at large Pe , uptake rates are often expressed as power laws in this parameter. For example, the type of fluid flow field generically exhibited by a *Volvox* colony leads to an uptake rate that scales as the square root of Pe times the organism's radius [14]. But in order to use this result, we must know how the Péclet number is related to the size of the organism in question.

To address this, we have developed a model for the swimming of these spherical

organisms that describes the fluid flow field around the colony and predicts the organism's swimming speed, thus enabling a calculation of the Péclet number and the role of advection in nutrient uptake [15]. Rather miraculously, our analysis shows that the advective uptake rate and the number of surface cells scale identically with increasing size, illustrating how advection has enabled evolutionary transitions toward these larger species. Moreover, the analysis explains the transition to germ/soma cell differentiation in the larger species, and describes an evolutionary advantage to growing larger in size as well. We see, then, how fluids have played a vital role in the evolution of life on Earth.

4.2. PRESENT STUDY

As just discussed, it has long been known that aquatic microorganisms use flagella (or similar constructs) to move about their environment, presumably to seek out areas of greater nutrient concentration, among other things. However, it has also been postulated that flagella may serve an important role in mixing the fluid in which the organism lives, thereby increasing the overall uptake rate of nutrients through advection. Models describing this mixing behavior quantitatively are not plentiful, though.

To address this gap in our scientific knowledge, we have created such a model based upon *Volvox*. The choice of this organism is not at random; the spherical body plan they display is very amenable to modeling. The surface of this spherical creature is home to (at least most of) the organism's cells, each with two flagella oriented outward into the surrounding fluid. This one-cell-thick layer covers the core of the sphere, known as the extracellular matrix (ECM), a gelatinous substance secreted by the surface cells. The ECM is thought by some to be a nutrient storehouse, where the surface cells can save

away extra metabolites that they have collected for a rainy day (or, possibly, a non-rainy day). The larger *Volvox* species also contain germ cells within the ECM where reproduction occurs. In the smaller species, the surface cells both swim and reproduce, depending upon where in the life-cycle the organism resides.

The major question at hand is how flagellar beating enhances nutrient transport in *Volvox* and similar organisms. Before answering this, however, we should address the issue of nutrient uptake by pure diffusion to see if, and when, this method of food procurement fails. If we model the spherical *Volvox* of radius R as a perfect absorber (i.e., it takes up any and all nutrients near it), the metabolite current entering the organism via pure diffusion is given by

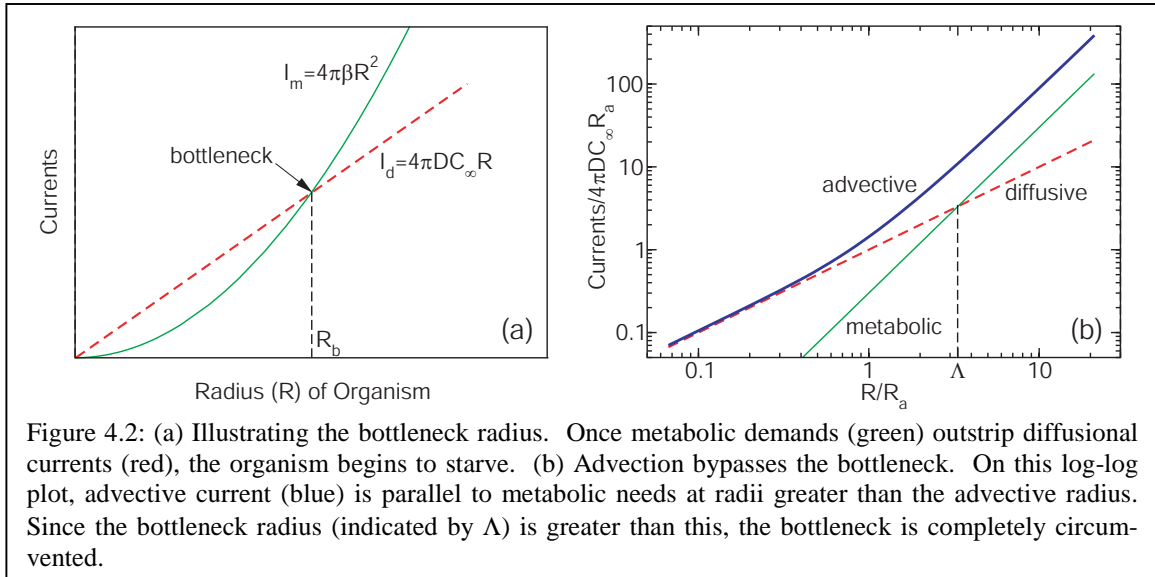
$$I_d = 4\pi DC_\infty R, \quad (4.1)$$

where D and C_∞ are the diffusion constant and far-field concentration of the metabolite in question, respectively. Note that this current scales linearly in colony radius.

Now, let us compare this to the nutritional requirements for this organism. The ECM has no nutritional needs, *per se*, and the germ cells will take their food from the ECM, leaving only the cells on the sphere's surface to be accounted for. With the definition that these cells have nutritional requirements β per unit area, the total metabolic current that the organism requires is

$$I_m = 4\pi R^2 \beta. \quad (4.2)$$

Since these metabolic demands scale quadratically with the radius while the diffusional supply scales only linearly, there will clearly be a point at which I_m is equal to I_d . To find this point, which we will refer to as the “bottleneck radius”, one must simply equate (4.1)



with (4.2) and solve for the radius, yielding

$$R_b = \frac{DC_\infty}{\beta}. \quad (4.3)$$

At sizes larger than this, then, these organisms should starve as nutrient demand outstrips diffusional supply (Figure 4.2(a)). However, estimates place the bottleneck radius in the range of 50-200 microns, smaller than many of the larger *Volvox* species. Evidently, diffusion is not the only means of nutrient acquisition for these organisms.

In fact, diffusion for the larger *Volvox* species is negligible compared to advection. This can be seen by examining the Péclet number involved for these large species; this ratio of advective to diffusive importance is written as

$$\text{Pe} = \frac{2RU}{D}, \quad (4.4)$$

where U is the organism's free-swimming speed. Measurements from large colonies place Pe in the hundreds, clearly showing that advection dominates diffusion. In such circumstances, the advective current I_a is often expressed as a power law in Pe . In order

to find the power law in this particular case, though, a fluid flow model must first be developed.

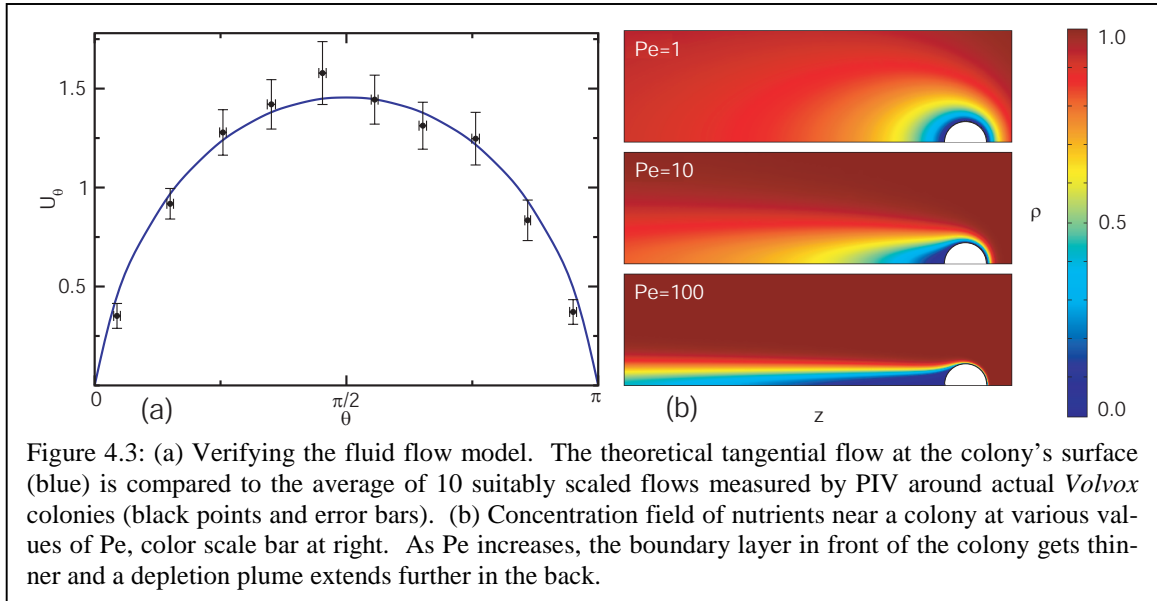
The details of our model are nearly identical to the typical calculation of Stokes flow past an inert sphere. We may assume Stokes flow in this case because, though Pe is high, the Reynolds number is still quite low. So, we model the *Volvox* as a sphere moving in the \hat{z} direction in the lab frame at speed U , then switch to a co-moving frame so that the fluid speed asymptotically approaches $-U\hat{z}$. There is no fluid flow into or out of the organism, so the radial velocity at $r = R$ is zero. To account for the action of the flagella, we demand a constant shear stress $f\hat{\theta}$ on the fluid at the *Volvox*' surface, where $\hat{\theta}$ is the typical polar angle direction for a spherical coordinate system using the \hat{z} direction already defined. This approach is coarse-grained, ignoring all of the details of the flagellar beating, but is a good approximation given the relative smallness of the flagella compared to typical colony radii. Finally, the velocities are scaled by U and the radial coordinate by R . So modeled, the radial and polar components of the fluid velocity are found to be

$$u_r = -\left(1 - \frac{1}{r}\right)P_1(\mu) - \frac{U_c}{U} \sum_{l=1}^{\infty} (r^{-l} - r^{-l-2})g_l P_l(\mu), \text{ and} \quad (4.5)$$

$$u_\theta = -\left(1 - \frac{1}{2r}\right)P_1^1(\mu) + \frac{U_c}{U} \sum_{l=1}^{\infty} ((l-2)r^{-l} - lr^{-l-2})\frac{g_l}{l(l+1)}P_l^1(\mu), \text{ where} \quad (4.6)$$

$$g_l = -\int_{-1}^1 P_l^1(\mu)d\mu, \quad (4.7)$$

the characteristic speed $U_c = fR/4\eta$ (with η the dynamic viscosity of water), P_l are Legendre polynomials, and $\mu = \cos\theta$.



To test the validity of this model, we first evaluate the tangential flow in (4.6) at the surface of the sphere ($r = 1$) for the case in which U is zero. This is then compared to particle imaging velocimetry (PIV) data for the flow speeds along the surfaces of actual *Volvox* colonies held in place with micropipettes. For each colony's data, the speeds are normalized to best fit the ideal curve through a least squares fit algorithm. Once the velocities for each colony have been thusly scaled, the data are all combined and averaged together. Figure 4.3(a) shows a comparison between this composite data and the theoretical flow rate as a function of polar angle θ ; the agreement between the two is good, with the theory lying within one standard error of the measurements.

Thus satisfied with the validity of our theory, we proceed to use the flow field just calculated to model the advection in our system. First, in order to find the free-swimming speed of a *Volvox* colony, we enforce a condition of zero net force on the organism. This involves calculating the various stresses and pressure acting on the sphere and then integrating them over the surface. The result of such a calculation is that the

swimming speed is given by

$$U = U_c g_1 = \frac{f \pi R}{8 \eta}; \quad (4.8)$$

simply speaking, the larger the colony, the faster it swims. Using this result, we can rewrite the Péclet number in (4.4) as

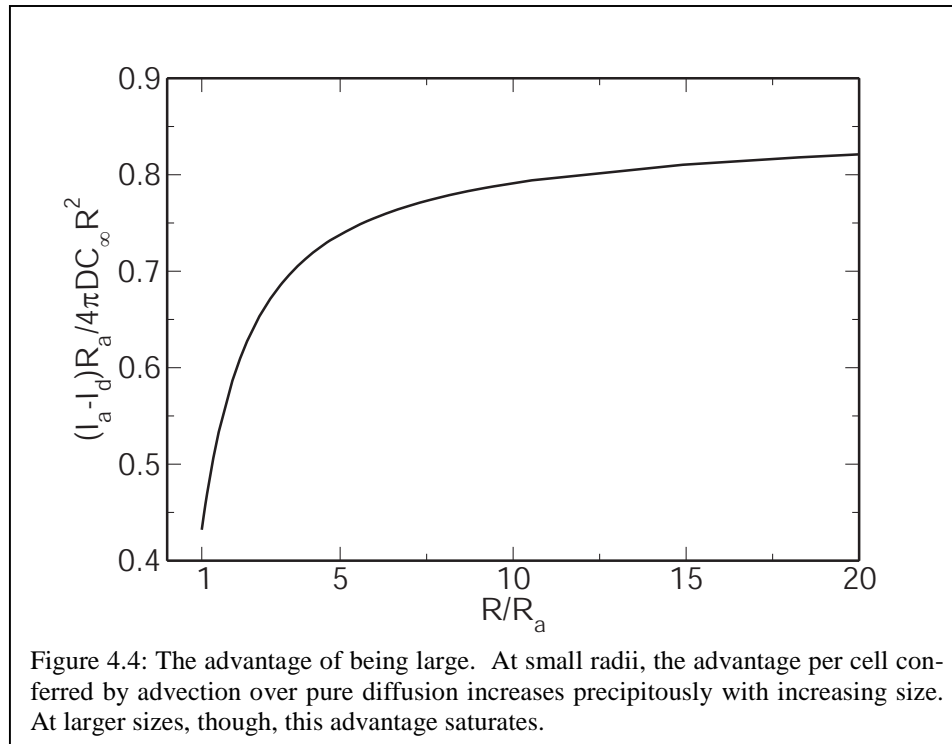
$$\text{Pe} = \left(\frac{R}{R_a} \right)^2, \quad (4.9)$$

where R_a is a new length scale we refer to as the advective radius. Estimates place the value of this parameter at around 10 microns, which is around the size of a single surface cell and is much less than the bottleneck radius estimated previously.

The fluid flow field described by (4.5) and (4.6) can now be used to study the advection of nutrients toward a *Volvox* colony by looking for solutions of the time-independent advection-diffusion equation for a passive scalar subject to this flow field and the appropriate boundary conditions. This was accomplished through the use of *Femlab*, a finite-element analysis software package. Figure 4.3(b) shows the output of this program and illustrates the concentration field at various values of Pe. As Pe increases, the concentration boundary layer in the front of the colony gets smaller and smaller, leading to larger and larger uptake rates. Specifically, for Pe greater than one, the advective current follows the law $I_a \sim R \text{Pe}^{1/2}$, which, in conjunction with (4.9), means that the advective current grows quadratically with colony radius R at radii larger than R_a . Quite amazingly, this scaling is the same seen in (4.2), which describes the metabolic needs of a colony. Hence, advection bypasses the diffusive bottleneck, allow-

ing evolutionary transitions toward larger colony size; this effect is summarized in Figure 4.2(b).

Further indirect evidence of the importance of advection can be deduced from the evolution of germ/soma separation in the Volvocales. On the small end of the species spectrum, the colonies are composed of only one type of cell that both swims and reproduces when the time is right. As we move up the spectrum, we eventually come across *Pleodorina californica*, the first species to exhibit soma differentiation, in which only some of the surface cells reproduce while the others are purely for swimming. Moving further up, the species eventually exhibit total germ/soma differentiation, in which the reproductive (germ) cells have moved to the inside of the sphere, leaving swimming-only (somatic) cells on the outside. Now, the undifferentiated cells of the smaller species are subject to what is known as the “flagellation constraint”; this means that during the reproductive phase of these cells, all swimming stops. Therefore, no advection will occur during the reproductive phase of these small colonies, just when they need nutrients the most, and diffusion alone must provide nutrition. However, it turns out that the colonies without any differentiation are smaller than our low estimate for the bottleneck radius (50 μm), so advection is not necessary for their survival. In fact, *Pleodorina* is of comparable size to this low bottleneck estimate, and the first of the complete germ/soma separated species is around the size of the high estimate (200 μm). We see, then, that the need to swim in order to survive has been evolutionarily translated into the separation of cells by function, so that the colonies above the bottleneck radius will not have to stop swimming to reproduce.



We have shown thus far that advection due to flagellar beating facilitates the evolutionary transition to larger colony size in the Volvocales. However, it seems that this advective facilitation may also present an *advantage* toward growing larger in size. As shown in Figure 4.4, the extra current per unit area (i.e., per cell) that advection offers over pure diffusion grows precipitously over the range of radii from 1-10 R_a , after which it saturates. The consequences of this are clear: for very small colonies, it is advantageous to increase in size, as this will lead to a large payoff per cell in terms of enhanced nutrient current for the same amount of individual work. Call it microscopic socialism, if you will. Past a certain size, though, this payoff becomes small, negating the advantage enjoyed by the smaller species.

In conclusion, the work presented here has shown that, at least in Volvoclean species, advection due to the beating of flagella is extremely important in facilitating evo-

lutionary transitions to larger and more-multicellular organisms. In addition, germ/soma separation seems to be a consequence of the necessity of the larger colonies to continually swim, and the advantage conferred by advection may even present an incentive for smaller colonies to evolve into larger ones. Clearly, the interaction of these organisms with the fluid surrounding them has had enormous influence over their evolutionary history and is responsible for much of their biological form and function.

5. EPILOGUE

In this section, we will highlight a few of the questions that remain unanswered regarding the various research subjects presented in Chapters 2 through 4, beginning with stalactites. Research into speleothem morphology is relatively sparse, and many questions on this subject remain. For example, could analyses similar to that of Chapter 2 be done for other standard speleothem types to explain their basic shapes? Many explanations for the stalagmite shape have been put forth over the years [4,5], though they are not quite equivalent to the free-boundary approach we have employed. However, other formations such as draperies, shields, and helictites offer a fertile and relatively untouched ground for further investigation.

Another unsolved problem in this field involves the ripples or “crenulations” seen on the surfaces of many speleothems [16]. These ripples do not seem to be simply random deformities, as their wavelengths are quite consistently around one centimeter, indicating that there is a common cause behind them all. The underlying mechanism behind their formation is, at present, unknown, but could likely be found through a sufficiently detailed and careful linear stability analysis of the combined reaction-diffusion and fluid flow systems.

Interestingly, this issue of surface ripple formation is also one of the outstanding problems of icicle research. Unlike the stalactite’s ripples, though, there have been some attempts at explaining the existence of icicle ripples [17-19], and the results of these analyses are encouraging. However, though these papers do predict average ripple wavelengths that match with observations, they do not explain the uniformity of wavelengths

observed in nature. Furthermore, none of them take into account the buoyant air layer discussed in our analysis, and are therefore somewhat suspect. It is probable that the true explanation for icicle ripples will require an incorporation of the dynamics of the buoyant air layer as seen in Chapter 3 of this dissertation.

Finally, we turn to the subject of *Volvox*, for which the remaining questions are legion. Regarding our analysis, one may wonder if the boundary conditions we have employed (a perfect absorber) are realistic. For example, it may be the case that uptake rates are tied to rates of waste removal, changing the analysis significantly. Experiments designed to verify or discount this assumption are currently underway.

Also of interest are time-dependent models of *Volvox* swimming. Clearly, the shear stress on the colony's surface is not constant in time, reflecting the flagellar beating cycle. What effect any small-scale time-variation has in general is not well known. Perhaps, though, long-scale variations can lead to phenomena such as phototactic steering, in which the presence of light decreases flagellar activity, leading to net torques on the *Volvox* that orient it toward said light [20,21].

Obviously, these few questions merely scratch the surface of the large body of work remaining to be done on the areas of research presented herein. Moreover, the topics presented here are but the smallest sampling of those that relate to the larger theme of fluids and their influence over our natural world. In the end, this dissertation is but a footnote in that regard, though it is my hope that others will find this footnote both as interesting and as enlightening as I have.

REFERENCES

- [1] C. Hill and P. Forti, *Cave Minerals of the World* (National Speleological Society, Huntsville, AL, 1997).
- [2] W. Dreybrodt, "Chemical kinetics, speleothem growth and climate," *Boreas* **28**, 347 (1999).
- [3] D. Buhmann and W. Dreybrodt, "The kinetics of calcite dissolution and precipitation in geologically relevant situations of karst areas. 1. Open system," *Chem. Geol.* **48**, 189 (1984).
- [4] G. Kaufmann, "Stalagmite growth and palaeo-climate: the numerical perspective," *Earth Planet. Sci. Lett.* **214**, 251 (2003).
- [5] H.W. Franke, "The theory behind stalagmite shapes," *Stud. Speleol.* **1**, 89 (1965).
- [6] M.B. Short, J.C. Baygents, J.W. Beck, D.A. Stone, R.S. Toomey III, & R.E. Goldstein, "Stalactite growth as a free-boundary problem: A geometric law and its platonic ideal," *Phys. Rev. Lett.* **94**, 018501 (2005).
- [7] M.B. Short, J.C. Baygents, & R.E. Goldstein, "Stalactite growth as a free-boundary problem," *Phys. Fluids* **17**, 083101 (2005).
- [8] L. Makkonen, "A model of icicle growth," *J. Glaciology* **34**, 64 (1988).
- [9] K. Szilder and E.P. Lozowski, "An analytical model of icicle growth," *Ann. Glaciol.* **19**, 141 (1994).
- [10] J. Walker, "Icicles ensheathe a number of puzzles: just how does the water freeze?," *Sci. Am.* **258**, 114 (1988).
- [11] M.B. Short, J.C. Baygents, & R.E. Goldstein, "A free-boundary theory for the shape of the ideal dripping icicle," *Phys. Fluids* **18**, 083101 (2006).
- [12] D.L. Kirk, *Volvox: Molecular-Genetic Origins of Multicellularity and Cellular Differentiation* (Cambridge University Press, Cambridge, U.K., 1998).
- [13] K.J. Niklas, *Plant Allometry* (University of Chicago Press, Chicago, IL, 1994).
- [14] V. Magar, T. Goto, & T.J. Pedley, "Nutrient uptake by a self-propelled steady squirmer," *Q. J. Mech. Appl. Math.* **56**, 65 (2003).

- [15] M.B. Short, C.A. Solari, S. Ganguly, T.R. Powers, J.O. Kessler, & R.E. Goldstein, “Flows driven by flagella of multicellular organisms enhance long-range molecular transport,” *Proc. Natl. Acad. Sci. U.S.A.* **103**, 8315 (2006).
- [16] C.A. Hill, “On the waves,” *Sci. News* (Washington, D. C.) **163**, 111 (2003).
- [17] N. Ogawa and Y. Furukawa, “Surface instability of icicles,” *Phys. Rev. E* **66**, 041202 (2002).
- [18] K. Ueno, “Pattern formation in crystal growth under parabolic shear flow,” *Phys. Rev. E* **68**, 021603 (2003).
- [19] K. Ueno, “Pattern formation in crystal growth under parabolic shear flow II.” *Phys. Rev. E* **69**, 051604 (2004).
- [20] W.G. Hand and W. Haupt, “Flagellar activity of the colony members of *Volvox aureus* Ehrbg. during light stimulation,” *J. Protozool.* **18**, 361 (1971).
- [21] J.D. Fabricant Hiatt and W.G. Hand, “Do protoplasmic connections function in the phototactic coordination of the *Volvox* colony during light stimulation?,” *J. Protozool.* **19**, 488 (1972).

APPENDIX A: STALACTITE GROWTH I

PHYSICAL REVIEW LETTERS

*Providing rapid publication of short reports of important fundamental research, with coverage of major advances
in all aspects of physics and of developments with significant consequences across subdisciplines.*

<p style="text-align: center;">Editors</p> <p>JACK SANDWEISS GEORGE BASBAS STANLEY G. BROWN REINHARDT B. SCHUHMAN</p> <p style="text-align: center;">Associate Editors</p> <p>ROBERT GARISTO BRANT M. JOHNSON</p> <p style="text-align: center;">Senior Assistant Editors</p> <p>JEROME MALENFANT SAMINDRANATH MITRA CHRISTOPHER WESSELBORG</p> <p style="text-align: center;">Assistant Editors</p> <p>DONAVAN HALL SAAD E. HEBBOUL MARIE KAPLAN YONKO MILLEV JOHN RIPKA JANE THROWE DANIEL UCKO DENIZ VAN HEIJNSBERGEN</p> <p style="text-align: center;">Adjunct Associate Editors</p> <p>THOMAS DUKE M. MUTHUKUMAR FRANK NARDUCCI</p>	<p style="text-align: center;">Editorial Board (Divisional Associate Editors) JACK SANDWEISS, Chairman</p> <p><i>Astrophysics</i> M. BARING, R. PRICE, D. SCOTT, C. STUBBS</p> <p><i>Atomic, Molecular, and Optical Physics</i> R. W. BOYD, P. G. BURKE, K. BURNETT, E. CORNELL, W. M. ITANO, J. MACEK, G. NIENHUIS, W. SCHLEICH, H. T. C. STOFF, S. STRINGARI, J. E. THOMAS, M. UEDA</p> <p><i>Biological Physics</i> D. CHATENAY, M. MAGNASCO</p> <p><i>Chemical Physics</i> S. T. CEYER, N. MAKRI</p> <p><i>Condensed Matter Physics</i> T. ANDO, A. AUERBACH, G. E. W. BAUER, C. W. J. BEENAKKER, C. BRUDER, M. H. W. CHAN, B. DEVEAUD, F. GUINEA, B. KEIMER, T. R. KIRKPATRICK, M. V. KLEIN, J. D. MAYNARD, L. W. MOLENKAMP, P. G. RADSELLI, D. RAMAKER, R. RESTA, S. SACHDEV, S. L. SONDHI, H. SPOHN, Y. TAKADA, J. TOBOCHNIK, J. TRANQUADA, H. M. VAN DRIEL, G. VIGNALE, P. WOLFLE</p> <p><i>Fluid Dynamics</i> R. E. ECKE, R. PANDIT</p> <p><i>Laser Science</i> J. BERGOU, P. BUCKSBAUM</p> <p><i>Materials Physics</i> N. C. BARTELT, P. C. CANFIELD, J. M. D. COEY, G. COMSA, A. PINCZUK, M. D. STILES, J. A. VENABLES</p> <p><i>Nuclear Physics</i> J. BARRETTE, D. H. BECK, H. ESBENSEN, P. -H. HEENEN, M. HUYSE, S. E. PRATT, W. WEISE</p> <p><i>Particles and Fields</i> P. ARGYRES, D. BRYMAN, S. GOTTLIEB, A. YU. SMIRNOV, F. ZWIRNER</p> <p><i>Physics of Beams</i> F. ZIMMERMANN</p> <p><i>Plasma Physics</i> H. BERK, D. MEYERHOFER, D. L. NEWMAN, S. ZWEBEN</p> <p><i>Polymer Physics</i> G. H. FREDRICKSON, P. F. GREEN</p> <p><i>Foundations of Quantum Mechanics</i> E. MERZBACHER</p> <p><i>Quantum Information</i> W. K. WOOTTERS</p>	<p style="text-align: center;">The American Physical Society One Physics Ellipse College Park, MD 20740-3844</p> <p><i>President</i> MARVIN L. COHEN <i>President-Elect</i> JOHN BAHCALL <i>Vice-President</i> JOHN J. HOPFIELD <i>Editor-in-Chief</i> MARTIN BLUME <i>Treasurer and Publisher</i> THOMAS J. McLEATH <i>Executive Officer</i> JUDY R. FRANZ</p> <hr/> <p style="text-align: center;">APS Editorial Office 1 Research Road, Box 9000 Ridge, NY 11961-9000 Phone: (631) 591-4060 Fax: (631) 591-4141 Email: prl@aps.org Web: http://publish.aps.org/ Submissions: prtex@aps.org or http://publish.aps.org/ESUB/</p> <hr/> <p style="text-align: center;">Member Subscriptions: APS Membership Department One Physics Ellipse College Park, MD 20740-3844 Phone: (301) 209-3280 Fax: (301) 209-0867 Email: membership@aps.org</p> <hr/> <p style="text-align: center;">Institutional Subscriptions: APS Subscription Services Suite 1N01 2 Huntington Quadrangle Melville, NY 11747-4502 Phone: (516) 576-2270, (800) 344-6902 Fax: (516) 349-9704 Email: subs@aps.org</p>
--	--	---

Letters intended for this journal must be short and self-contained. A description of editorial Policies and Practices is published in the first January and July issues and can be found on our Web server. Instructions for manuscript preparation are given in the Information for Contributors published in the first issue of each volume and available on our Web server. Rules pertaining to allowed length and memos regarding production requirements appear at the end of some issues of the journal.

Manuscripts should be submitted electronically in acceptable format (see <http://publish.aps.org/ESUB/> or inquire at prtex@aps.org). If this is not possible, send four copies to the Editorial Office. Submission is a representation that the manuscript has not been published previously and is not currently under consideration for publication elsewhere. Authors should provide indexing codes according to the PACS scheme (available at <http://publish.aps.org/PACS/>). An executed APS copyright-transfer form (effective only on acceptance for publication) must be provided; the form is available on our Web server and appears at the end of the 12 November 2004 issue of *Physical Review Letters*. To help defray editorial and production expenses, authors of published Letters are expected to pay a publication charge of \$675 (\$245 for a Comment or Reply). Charges are lower (\$550 for a Letter, \$195 for a Comment or Reply) for properly prepared electronic submissions. Acceptable formats are REV_LTEX (preferred), L^AT_EX, plain TEX, MS Word, PostScript figures. Reprints are offered for sale to authors.

For information about subscription prices and about the online version of the journal, see our Web server, or inquire at assocpub@aps.org. Member inquiries regarding subscriptions, renewals, address changes, missing or damaged copies, microfilm, and single-copy orders should be addressed to the APS Membership Department. Institutional subscribers should address subscription inquiries to APS Subscription Services. For address changes please send both old and new addresses, and if possible, send the mailing label from a recent issue.

Copyright © 2005 by The American Physical Society. All rights reserved.
Physical Review Letters™ is a trademark of The American Physical Society.

Rights and Permissions

Copying: No part of this publication may be reproduced, stored in a retrieval system or transmitted in any form or by any means, electronic, mechanical, photocopying, recording or otherwise, without the written permission of the publisher, except as stated below. Single copies of individual articles may be made for private use or research. Authorization is given to copy articles beyond the use permitted by Sections 107 and 108 of the U.S. Copyright Law, provided the copying fee of \$23.00 per copy per article is paid to the Copyright Clearance Center, 222 Rosewood Drive, Danvers, MA 01923, USA.

Reproduction of an entire Article in a reprint collection, or for advertising or promotional purposes, or republication in any form requires permission from APS. Permission must be sought from the Associate Publisher, The American Physical Society, One Physics Ellipse, College Park, MD 20740-3844; email: assocpub@aps.org.

Other Use: Permission is granted to quote from the journal with the customary acknowledgment of the source. Permission must be sought from the APS Associate Publisher to reproduce a figure, table, or excerpt of an Article.

Authorization for private use or research does not extend to systematic or multiple reproduction, to copying for promotional purposes, to distribution in any format, or to republication in any form. In all such cases, specific permission from APS must be obtained.

Physical Review Letters [ISSN: 0031-9007 (print), 1079-7114 (online); CODEN PRLTAO; printed in USA] is published weekly by The American Physical Society, 1 Research Road, Box 9000, Ridge, NY 11961-9000.

POSTMASTER: Send address changes to *Physical Review Letters*, APS Subscription Services, Suite 1N01, 2 Huntington Quadrangle, Melville, NY 11747-4502. The 2005 print + online base price is \$2915. Periodicals postage rates are paid at Huntington Station, NY, and additional mailing offices.

Reprinted article with permission from M.B. Short *et al.*, *Physical Review Letters* **94**, 018501 (2005).
Copyright 2005 by the American Physical Society.

Stalactite Growth as a Free-Boundary Problem: A Geometric Law and Its Platonic Ideal

Martin B. Short,¹ James C. Baygents,^{2,3} J. Warren Beck,^{1,4} David A. Stone,⁵
Rickard S. Toomey III,⁶ and Raymond E. Goldstein^{1,3}

¹Department of Physics, University of Arizona, Tucson, Arizona 85721, USA

²Department of Chemical and Environmental Engineering, University of Arizona, Tucson, Arizona 85721, USA

³Program in Applied Mathematics, University of Arizona, Tucson, Arizona 85721, USA

⁴Accelerator Mass Spectrometry Facility, University of Arizona, Tucson, Arizona 85721, USA

⁵Department of Soil, Water, and Environmental Science, University of Arizona, Tucson, Arizona 85721, USA

⁶Kartchner Caverns State Park, P.O. Box 1849, Benson, Arizona 85602, USA

(Received 11 August 2004; published 7 January 2005)

The chemical mechanisms underlying the growth of cave formations such as stalactites are well known, yet no theory has yet been proposed which successfully accounts for the dynamic evolution of their shapes. Here we consider the interplay of thin-film fluid dynamics, calcium carbonate chemistry, and CO₂ transport in the cave to show that stalactites evolve according to a novel local geometric growth law which exhibits extreme amplification at the tip as a consequence of the locally-varying fluid layer thickness. Studies of this model show that a broad class of initial conditions is attracted to an ideal shape which is strikingly close to a statistical average of natural stalactites.

DOI: 10.1103/PhysRevLett.94.018501

PACS numbers: 91.65.-n, 47.15.Gf, 47.54.+r, 68.70.+w

The astonishing variety and beauty of structures found in limestone caves, from stalactites and stalagmites to soda straws, draperies, and helictites, have been the subject of human wonder for hundreds if not thousands of years [1]. There is little debate about the fundamental chemical processes responsible for their development. Water enters the cave from the overlying environment with significant concentrations of dissolved carbon dioxide and calcium. As the partial pressure of CO₂ in the cave is lower than that in the overlying rock, CO₂ outgases from the water. This raises the pH and leads to supersaturation and then precipitation of calcium carbonate. Yet, this chemical picture is only part of the story, for it does not in any direct way answer the most obvious morphological question: why are stalactites long and slender, often roughly conical? While some studies address the dynamics of speleothem morphology, [2–4], none quantitatively explains this most basic fact.

Here, we view the growth of stalactites as a free-boundary problem akin to those found in the theory of crystal growth [5], and derive a geometric law of motion in which the growth rate depends on the local radius and inclination of the stalactite surface. This approach is used to explain quantitatively the long, slender forms of stalactites by leading to the discovery of a universal shape toward which general initial conditions evolve. Found under a set of limiting assumptions, this may be thought of as the *Platonic ideal* of speleothem growth. While real stalactites have more complex shapes due to instabilities and cave inhomogeneities, we find that comparison with the average shapes of natural stalactites shows very good agreement. This work serves to emphasize a broad class of problems that demands considerable attention—*free-boundary dynamics in precipitative pattern formation*. Beyond speleothems, these include structures as diverse as hydrothermal

vents [6], chemical gardens [7], mollusc shells [8], and tubes whose growth is templated by bubbles [9]. Further development of greatly-accelerated model systems [10] to allow quantitative tests of such theories is thus an important goal.

The fluid layer flowing down the surface of a growing stalactite controls precipitative growth, so we first establish its typical thickness and velocity. Consider a cylindrical stalactite of radius R , length ℓ , over the surface of which flows an aqueous film of thickness h . We show below that the Reynolds number is low enough that the Stokes approximation is valid, and that $h \ll R$ over nearly the entire stalactite, so the velocity profile in the layer may be deduced by assuming a flat surface. Let y be a coordinate perpendicular to the surface and θ the tangent angle with respect to the horizontal [Fig. 1(a)]. The Stokes equation for gravity-driven flow is $\nu d^2u/dy^2 = g \sin\theta$, where $\nu = 0.01 \text{ cm}^2/\text{s}$ is the kinematic viscosity of water. No-slip and stress-free boundary conditions at the solid-liquid and liquid-air interfaces yield $u(y) = u_0[2(y/h) - (y/h)^2]$, where $u_0 = (gh^2/2\nu)\sin\theta$. The volumetric flux $Q = 2\pi R \times \int_0^h dy u(y) = (2\pi g/3\nu)Rh^3 \sin\theta$. Measuring Q in cm^3/h

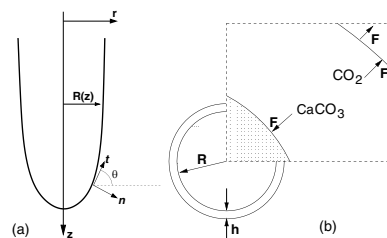


FIG. 1. Geometry of fluid flow along the surface of a stalactite (a) and model for determination of growth rate (b).

and R in cm, we find

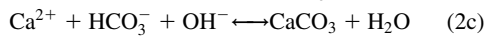
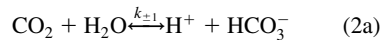
$$h \approx 11 \mu\text{m} \left(\frac{Q}{R \sin\theta} \right)^{1/3}, \quad (1a)$$

$$u_0 \approx 0.060 \text{ cm/s} \left(\frac{Q^2 \sin\theta}{R^2} \right)^{1/3}. \quad (1b)$$

Typically, $1 < R < 10$ cm and the flow rates are well below $100 \text{ cm}^3/\text{hr}$ [11], so the layer thickness is tens of microns and the surface velocities below several mm/s. On the scale of the water layer thickness, the Reynolds number is $\text{Re}_w = u_0 h / \nu \sim 0.007(Q/R)$, well in the laminar regime, as anticipated. Of course, the thickness law (1a) will cease to hold near the bottom tip of the surface, where $\theta \sim 0$ and h would appear to diverge. In reality a pendant drop periodically detaches there, on a scale set by the competition between surface tension σ and gravity—the capillary length $l_c = (\sigma/\rho g)^{1/2} \sim 0.3$ cm. We see below that our theory dictates a small-distance cutoff that is subsumed within the capillary length.

Next we address gross features of the precipitation process. The accretion rate of calcium carbonate can be deduced from stalactite elongation rates v , which are ~ 1 cm/century. Since stalactites are so slender, the volumetric increase can be estimated by considering the addition of a disk at the top of the stalactite, where the typical radius is ~ 5 cm. Hence, $\sim 80 \text{ cm}^3$ or ~ 200 g of CaCO_3 is added per century. Assuming a volumetric flow rate of $\sim 40 \text{ cm}^3/\text{h}$, toward the lower end of the measured range [11], the volume of water that flows over the stalactite in a century is $\sim 36\,000$ liters. With a typical concentration of calcium in solution of 150 ppm (mg/l), the total mass of calcium in that fluid volume is 5.4 kg, yielding a fractional precipitation of ~ 0.04 , sensibly small given the ubiquity of stalagmites below stalactites [12].

The dependence of the precipitation rate on fluid layer thickness is crucial; we extend important earlier work [13] to derive this. Consider a growing spherical body covered by fluid and surrounded by still atmosphere in which CO_2 diffuses [Fig. 1(b)]. The fluid has average calcium ion concentration $[\text{Ca}^{2+}]$ and proton concentration $[\text{H}^+]$, the latter assumed constant in the layer, as is valid for thin films. The ratio $\epsilon \equiv h/R$ is an important small parameter. Of the chemical reactions occurring in the fluid layer, the most important are [13]:



It is critical to note that for each molecule of CaCO_3 that adds to the surface of the crystal, one molecule of CO_2 must be generated in the solution via pathways (2a) and (2b), whose relative importance depends upon $p\text{H}$. Hence, for growth (or dissolution) to occur, CO_2 and HCO_3^- must

not be in chemical equilibrium. Of course, (2c) lies outside of equilibrium as well, but can be shown to be fast compared to (2a) and (2b) in the case of thin films, so that it is not rate-limiting. Reaction (2d), on the other hand, will be considered always equilibrated, leaving $[\text{HCO}_3^-]$, $[\text{CO}_3^{2-}]$, and $[\text{H}^+]$ related by the equilibrium constant K . Therefore, through the use of an electroneutrality condition, $[\text{HCO}_3^-]$ may be expressed solely in terms of $[\text{H}^+]$ and $[\text{Ca}^{2+}]$ as

$$[\text{HCO}_3^-] = \frac{2[\text{Ca}^{2+}] + (1 - \beta)[\text{H}^+]}{1 + 2\alpha}, \quad (3)$$

where $\alpha = K/[\text{H}^+]$, $\beta = K_W/[\text{H}^+]^2$, and K_W is the water dissociation constant.

To derive a growth law, we find the flux of Ca^{2+} onto the surface of the sphere from the diffusion equation

$$\partial_t[\text{Ca}^{2+}] = D_{\text{Ca}^{2+}} \nabla^2[\text{Ca}^{2+}]. \quad (4)$$

We impose upon $[\text{Ca}^{2+}]$ zero flux at $r = R + h$ and a flux $-F$ at $r = R$ for all t , and employ our knowledge of $[\text{Ca}^{2+}]$ at $t = 0$. All diffusive transients are assumed to have decayed, so $\partial_t[\text{Ca}^{2+}]$ is a constant. The dynamics of $[\text{CO}_2]$ are assumed to be in quasi-steady state; therefore, substituting (3) into the chemical dynamics of the reaction-diffusion equation for CO_2 leaves us with

$$D_{\text{CO}_2} \nabla^2[\text{CO}_2] = k_+[\text{CO}_2] - k_-[\text{Ca}^{2+}] - k_0, \quad (5)$$

where

$$k_0 \equiv \frac{1}{2}(1 - \beta)k_-[\text{H}^+], \quad (6a)$$

$$k_+ \equiv k_{+1} + \beta k_{+2}[\text{H}^+], \quad (6b)$$

$$k_- \equiv \frac{2(k_{-1}[\text{H}^+] + k_{-2})}{1 + 2\alpha}. \quad (6c)$$

We impose zero flux of $[\text{CO}_2]$ at $r = R$ and flux $F/(1 + \epsilon)^2$ at $r = R + h$, recalling that the number of Ca^{2+} molecules deposited equals the number of CO_2 molecules released. Finally, since diffusion of atmospheric carbon dioxide $[\text{CO}_2]_a$ is in steady state, we have the Stefan condition

$$\nabla^2[\text{CO}_2]_a = 0, \quad (7)$$

with boundary conditions of a flux $F/(1 + \epsilon)^2$ at $r = R + h$ and an asymptotic value of $[\text{CO}_2]_\infty$.

To find the growth rate, we must solve the simultaneous diffusion equations that hold in each domain, subject to boundary conditions. The lengthy details of this calculation will be presented elsewhere. Here, we summarize them as follows: solve (4) in terms of F and $[\text{Ca}^{2+}]$, use this solution at $t = 0$ in (5) to find $[\text{CO}_2]$ in terms of these same quantities, solve (7) in terms of F and $[\text{CO}_2]_\infty$, use the solutions to (5) and (7) to find $[\text{CO}_2]$ and $[\text{CO}_2]_a$ at $r = R + h$, relate the two through Henry's constant H , and thus deduce F . For a sphere, one finds

$$F \approx h(k_-[\text{Ca}^{2+}] + k_0 - k_+ H[\text{CO}_2]_\infty) \times \left[1 + \epsilon \left(1 - \frac{HR^2 k_+}{D_a} \right) + O(\epsilon^2) \right]. \quad (8)$$

Note that F does not depend explicitly upon atmospheric diffusion until order ϵ . This first correction takes the form of a ratio of the time scale for diffusion of the newly created CO_2 into the atmosphere to that for conversion of CO_2 back into HCO_3^- . It is also very small, being only $\sim 10^{-3}$. In contrast with other dendritic growth phenomena [5], atmospheric diffusion is not rate-limiting, and thus the dynamics is local.

If the local concentration gradients within the fluid are dominantly perpendicular to the flow within the layer, then advective contributions to precipitation can be ignored in computing the growth rates. In the present calculation, where we ignore instabilities that can produce ripples, where the *diffusion time* $t_D = h^2/D \sim 0.1$ s for equilibration in the layer is extremely small compared to the *contact time* $t_\ell = \ell/u_0 \sim 10^3$ s for a fluid parcel to traverse the typical length $\ell \sim 100$ cm of the stalactite, and where t_ℓ itself is extremely small compared to the *growth time* $t_v = h/v \sim 10^7$ s; this is a valid approximation. Hence, it follows from (1a) and (8) at leading order that there is a *geometrical law* for growth in which the component of the growth velocity \mathbf{v} normal to the surface is given by the local radius $r(z)$ and tangent angle θ ,

$$\hat{\mathbf{n}} \cdot \mathbf{v} = v_c \left(\frac{\ell_Q}{r \sin \theta} \right)^{1/3}, \quad (9)$$

where $v_c = v_m \ell_Q (k_- [\text{Ca}^{2+}] + k_0 - k_+ H[\text{CO}_2]_\infty)$ is the characteristic velocity, v_m is the molar volume of CaCO_3 , and $\ell_Q = (3\nu Q/2\pi g)^{1/4} \sim 0.01$ cm is a characteristic length. The velocity v_c depends upon the $p\text{H}$ through k_0 and k_\pm , crossing from positive (growth) to negative (dissolution) at a critical $p\text{H}$ that depends on $[\text{Ca}^{2+}]$ [Fig. 2(a)]. Cave water is close to the typical crossing point, giving $v_c \sim 0.1$ mm/yr, quite consistent with observations.

The growth model (9) generalizes the work of Kaufmann [4] by explicit inclusion of the dependence of film thickness on stalactite radius and surface inclination—that is, it recasts the dynamics as a true free-boundary problem. As a model for axisymmetric surface evolution, Eq. (9) depends on the absolute orientation of the surface through θ , as it must when gravity breaks the symmetry and drives the fluid flow. As such, it differs fundamentally from geometrical models of interface evolution [14], which depend only on invariants such as the curvature $\kappa = \partial\theta/\partial s$. Its dependence on angle is reminiscent of the effects of surface tension anisotropy [5], but with a vastly more singular form [Fig. 2(b)] producing a high and rapidly-varying growth rate near the tip, where θ is small, and a roughly constant growth rate for the nearly vertical regions ($\theta \sim \pi/2$). This extreme amplification near the tip produces the slender form of stalactites.

Numerical studies of this growth law [Fig. 2(c)] show that an initially rounded shape develops a conical instability at its lowest point; a downward bump, which has a smaller local radius, also has a locally thicker fluid layer in order

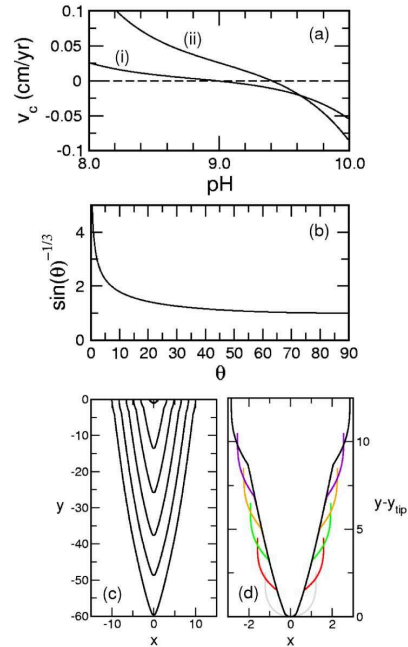


FIG. 2 (color online). Aspects of the growth law. (a) Growth velocity v_c versus $p\text{H}$, using CO_2 partial pressure in the cave atmosphere of 3×10^{-4} atm, a temperature of 20°C , (i) $[\text{Ca}^{2+}]$ of 100 ppm and volumetric fluid flow $Q = 2$ cm³/h, and (ii) $[\text{Ca}^{2+}] = 300$ ppm and $Q = 20$ cm³/h. Formulas for constants taken from [13]. (b) The function of tangent angle θ in Eq. (9). (c) A rounded initial condition evolves into a fingered shape. (d) Aligning the tips of the growing shapes in (c) shows at early times a rapid collapse to a common form.

to conserve mass. This increased thickness produces a higher precipitation rate and the protuberance grows. Interestingly, the growing tip approaches a uniformly translating shape for a wide range of initial conditions [Fig. 2(d)]. This asymptotic shape $z(r)$ can be found by noting that the normal velocity (9) at any point on such a surface must equal $v_t \cos \theta$, where v_t is the tip velocity. Observing that $\tan \theta = dz/dr$ and rescaling symmetrically r and z as $\rho \equiv (r/\ell_Q)(v_t/v_c)^3$ and $\zeta \equiv (z/\ell_Q)(v_t/v_c)^3$ yields the differential equation

$$\frac{\zeta'(\rho)}{[1 + \zeta'(\rho)^2]^2} - \frac{1}{\rho} = 0. \quad (10)$$

Equation (10) has no real solution at $\rho = 0$. This is to be expected as the growth law (9) can not be valid exactly at the tip, where capillarity must modify the thickness of the film. The first real solution appears at $\rho = \rho_m \equiv 16/3\sqrt{3}$, and for $\rho > \rho_m$, there are two distinct real solutions of (10) for ζ' , the solution of interest having $\zeta'' \geq 0$. Since $\ell_Q \sim 0.01$ cm, and assuming that $v_t \geq v_c$, r_m will be much less than the capillary length, so this solution is valid every-

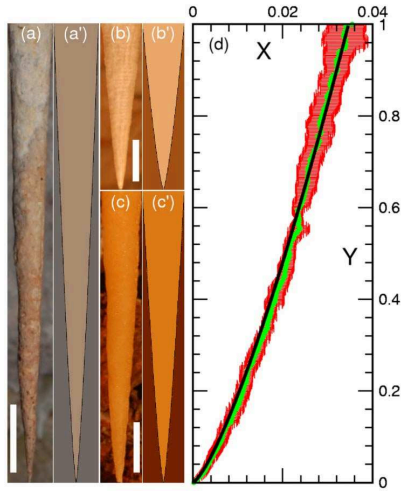


FIG. 3 (color online). Comparison between observed stalactite shapes and the Platonic ideal. Three examples (a)–(c) are shown, each next to an ideal shape of the appropriate aspect ratio and size (a')–(c'). Scale bars in each are 10 cm. (d) Master plot of stalactite shapes, rescaled as described in text. The average of 20 stalactites is shown with green circles and red uncertainties, and compared with the ideal (black curve).

where except the stalactite tip. One easily verifies that at large ρ there is a power-law form $\zeta \sim \rho^{4/3}$, which, while close to the conical form $\zeta \sim \rho$, produces an aspect ratio $\delta = \ell/w$, with ℓ the length and w the width, that increases with overall length. A systematic expansion yields the quite accurate approximation

$$\zeta(\rho) \approx \frac{3}{4}\rho^{4/3} - \rho^{2/3} - \frac{1}{3}\ln\rho + \text{const.} \quad (11)$$

A direct test of the relevance of the Platonic ideal was achieved by comparing it to the shapes of natural stalactites. Using a high-resolution digital camera, images of many stalactites in Kartchner Caverns (Benson, AZ) were recorded, each with a pair of fiducial marks projected from two parallel lasers to provide a local scale. It is important to emphasize that because the rescalings used to derive Eq. (10) are symmetric in r and z , a direct comparison between actual stalactites and the ideal requires only a global rescaling of the image. Moreover, as δ for the ideal increases with ℓ , this theory predicts that all stalactites will lie on the ideal curve provided the differential equation defining that curve is integrated up to a suitable length. Therefore, we can visually compare stalactite images to the ideal shape rather simply; Fig. 3 shows three representative examples of such a direct comparison, and the agreement is very good. Deviations are of course noted at the tip, where capillarity effects associated with the pendant drops alter the shape. For a more precise comparison, we extracted the contours of 20 stalactites by a standard edge-detection algorithm applied to the

images, yielding $r(z)$ for each. The optimal scaling factors for each were found by a least squares comparison with the ideal function. Finally, this set of rescaled data was averaged and compared directly to the theoretical curve [Fig. 3(d)]. Since each of the stalactites has a different length, fewer images contribute to the average the further from the tip one looks, hence the larger error bars further up the stalactite. The agreement between the data and theory is excellent; the Platonic form lies uniformly within 1 standard deviation of the mean.

The dynamic and geometric results presented here illustrate that the essential physics underlying stalactite shape is the locally-varying fluid layer thickness controlling the precipitation rate. Such physics is the basis for a stability analysis that may explain ripples often found on speleothems, similar to those on icicles [15]. Indeed, since icicle formation involves both thin-film fluid flow and diffusion (of latent heat), it is likely that an analysis like that here may explain the characteristic slender shapes of icicles as well. More generally, by highlighting the interplay between surface geometry and growth this work provides a starting point for a comprehensive explanation of the richness of speleothem morphology.

We are grateful to Chris Dombrowski, Ginger Nolan, and Idan Tuval for assistance in photographing stalactites. This work was supported by the Dean of Science, University of Arizona, the Research Corporation, and NSF ITR Grant No. PHY0219411.

- [1] C. Hill and P. Forti, *Cave Minerals of the World* (National Speleological Society, Inc., Huntsville, AL, 1997).
- [2] H. W. Franke, *Studies in Speleology* **1**, 89 (1965).
- [3] W. Dreybrodt, *Boreas* **28**, 347 (1999).
- [4] G. Kaufmann, *Earth Planet. Sci. Lett.* **214**, 251 (2003).
- [5] D. A. Kessler, J. Koplik, and H. Levine, *Adv. Phys.* **37**, 255 (1988).
- [6] J. B. Corliss *et al.*, *Science* **203**, 1073 (1979).
- [7] S. Thouvenel-Romans, W. van Saarloos, and O. Steinbock, *Europhys. Lett.* **67**, 42 (2004).
- [8] E. Bonucci, *Calcification in Biological Systems* (CRC Press, Boca Raton, FL, 1992).
- [9] D. A. Stone and R. E. Goldstein, *Proc. Natl. Acad. Sci. U.S.A.* **101**, 11537 (2004).
- [10] L. C. Huff, *J. Geol.* **48**, 641 (1940).
- [11] *Final Report: Environmental and Geologic Studies for Kartchner Caverns State Park*, edited by R. H. Beucher (Arizona Conservation Projects, Inc., Tucson, AZ, 1992).
- [12] Depletion is negligible only when the rate-limiting step is not surface growth. At high Q and low $[\text{Ca}^{2+}]$, formation of CaCO_3 is rate-limiting and Ca^{2+} depletion, not CO_2 creation, controls the shape.
- [13] D. Buhmann and W. Dreybrodt, *Chemical Geology* **48**, 189 (1984).
- [14] R. C. Brower, D. A. Kessler, J. Koplik, and H. Levine, *Phys. Rev. A* **29**, 1335 (1984).
- [15] K. Ueno, *Phys. Rev. E* **69**, 051604 (2004).

APPENDIX B: STALACTITE GROWTH II

PHYSICS OF FLUIDS

CODEN: PHFLE6

ISSN: 1070-6631

pof.aip.org

Editors: John Kim

University of California, Los Angeles, CA

L. Gary Leal

University of California, Santa Barbara, CA

Associate Editor for Letters: Andrea Prosperetti

Johns Hopkins University, Baltimore, MD

Distinguished Editor (1982–1997): Andreas Acrivos**Founding Editor (1958–1981):** François N. Frenkiel**Associate Editors***Term ending 31 December 2005*

R. P. Behringer (Duke University, Durham, NC)

J. B. Grotberg (University of Michigan, Ann Arbor, MI)

R. D. Moser (University of Illinois, Urbana-Champaign, IL)

F. T. M. Nieuwstadt (Delft Univ. of Tech., The Netherlands)

G. J. F. van Heijst (Tech. Univ. Eindhoven, The Netherlands)

Term ending 31 December 2006

H. Choi (Seoul National University, Seoul, South Korea)

E. J. Hinch (University of Cambridge, Cambridge, UK)

G. M. Homsy (University of California, Santa Barbara, CA)

J. R. Lister (University of Cambridge, Cambridge, UK)

P. A. Monkewitz (Swiss Federal Inst. of Tech., Lausanne)

Term ending 31 December 2007

J. P. Gollub (Haverford College, Haverford, PA)

J. Koplik (Levich Institute, New York, NY)

P. Moin (Stanford University, Stanford, CA)

S. B. Pope (Cornell University, Ithaca, NY)

A. Prosperetti (Johns Hopkins Univ., Baltimore, MD)

Editorial Office StaffMarjorie Hayes, *Assistant to the Editor (UCSB)*

E-mail: pof@engineering.ucsb.edu

Stacey Morse, *Assistant to the Editor (UCLA)*

E-mail: pof@ea.ucla.edu

E-mail Production Staff at AIP: pof@aip.org

Information for Authors

Submissions: Submit manuscripts via Peer X-Press, the journal's online manuscript submission system, located at <http://pof.peerx-press.org>. If preferred, mail printed manuscripts (3 copies) to Editorial Office, *Physics of Fluids*, Department of Chemical Engineering, University of California, Santa Barbara, CA 93106. Tel.: 805-893-3200; E-mail: pof@engineering.ucsb.edu. Submission implies that the manuscript has not been published previously and is not currently submitted for publication elsewhere. For detailed information for contributors, visit the above URL.

Publication Charge: The American Institute of Physics does not require page charges for this Journal.

Free Color Online: If authors supply usable color graphics files in time for the production process, color will appear in the online journal free of charge. Authors or their institutions must bear the cost of any color they wish to use in print. A fixed rate of \$650 for the first color figure and \$325 for each additional color figure applies for color in print. For multipart figures, a single charge will apply only if all parts are submitted as a single piece of artwork.

Reprints: Order reprints with or without covers only in multiples of 50 from AIP, Circulation & Fulfillment/Reprints, Suite 1N01, 2 Huntington Quadrangle, Melville, NY 11747-4502; Fax: 516-349-9704; Tel.: 800-344-6909 (U.S. & Canada), or 516-576-2270.

Supplemental Material may be deposited with AIP's Electronic Physics Auxiliary Publication Service (EPAPS), a low-cost online depository. For a nominal fee, authors may submit multimedia, color figures, data tables, text, etc. Address requests to the Editor; for additional information, see <http://www.aip.org/pubservs/epaps.html>.

Online Status Inquiry: During the production process, authors may access information about their accepted manuscripts at <http://www.aip.org/msinq/status.html>.

Comments: Direct comments on the journal or editorial process to Doreene Berger, Editorial Operations, AIP, Suite 1N01, 2 Huntington Quadrangle, Melville, NY 11747-4502; Tel.: 516-576-2444; Fax: 516-576-2450; E-mail: dberger@aip.org.

Digital Object Identifier (DOI): Each archival article published is assigned a unique DOI that serves to identify the article in a digital environment. In print, the DOI appears at the end of each abstract.

Physics of Fluids is devoted to the publication of original theoretical, computational, and experimental contributions to the dynamics of gases, liquids, and complex or multiphase fluids. It is published monthly by the American Institute of Physics (AIP).

2005 Subscription Prices

Institutions: For information, visit <http://librarians.aip.org>. Institutional rates for *Phys. Fluids* alone and in combination with *Phys. Plasmas* may be found online at http://www.aip.org/journal_catalog/AIP2005NonmemberRateFixed.pdf, or contact AIP Customer Services at subs@aip.org [Tel.: 800-334-6902 (U.S. & Canada) or 516-576-2270; Fax: 516-349-9704].

Members: The following rates are available to all individual members of AIP Member and Affiliate Societies:

		U.S.	Non-U.S. (Surface)	Optional Air
Print & online	<i>Phys. Fluids</i> alone	\$219	\$269	\$299
	With <i>Phys. Plasmas</i>	\$364	\$464	\$519
Microfiche & online	<i>Phys. Fluids</i> alone	\$219	\$269	\$299
	With <i>Phys. Plasmas</i>	\$364	\$464	\$519
Online only	<i>Phys. Fluids</i> alone	\$84	\$84	\$84
	With <i>Phys. Plasmas</i>	\$150	\$150	\$150
Extended backfile access	Online access covers 2000–2005; for access to backfiles from Vol. 1 (1958) to present, add to subscription price: \$45 (for <i>Phys. Fluids</i> alone) or \$65 (for both <i>Phys. Fluids</i> & <i>Phys. Plasmas</i>).			
Annual CD-ROM	Add to subscription price: \$30 (for <i>Phys. Fluids</i> alone) or \$60 (for both <i>Phys. Fluids</i> & <i>Phys. Plasmas</i>).			

Single issue: \$220 for back issues for 2005

Prior years (Members): \$35 Prior years (Institutions): \$215

Additional Availability

Online Access: *Physics of Fluids* is available online at <http://pof.aip.org>.

Microform: *Physics of Fluids* is available on microfiche issued at the same frequency as the printed journal, and annually on microfilm. Direct requests to AIP, Circulation & Fulfillment/Single Copy Sales, Suite 1N01, 2 Huntington Quadrangle, Melville, NY 11747-4502; Fax: 516-349-9704; Tel.: 800-344-6902 (U.S. & Canada) or 516-576-2270.

Document Delivery: Copies of journal articles can be ordered for online delivery from DocumentStore, AIP's online document delivery service (<http://www.documentstore.org>).

Customer Service

Subscription Orders and Renewals should be addressed to American Institute of Physics, P.O. Box 503284, St. Louis, MO 63150-3284. Tel.: 800-344-6902 (U.S. & Canada) or 516-576-2270; Fax: 516-349-9704; E-mail: subs@aip.org. Allow at least six weeks advance notice.

Inquiries, Address Changes, Claims, Single Copy Replacements, and Back Volumes: For address changes, please send both old and new addresses and, if possible, include the mailing label from a recent issue. Missing issue requests will be honored only if received within six months of publication date (nine months for Australia & Asia). Single copies of a journal may be ordered and back volumes are available in print, microfiche, or microfilm. Contact AIP Customer Services at 800-344-6902 (U.S. & Canada) or 516-576-2270; Fax: 516-349-9704; E-mail: subs@aip.org.

Reprint Billing: Contact AIP Publication Charge & Reprints/CFD, Suite 1N01, 2 Huntington Quadrangle, Melville, NY 11747-4502; Tel.: 800-344-6909 (U.S. & Canada) or 516-576-2270; E-mail: pcr@aip.org.

Rights and Permissions

Copying: Single copies of individual articles may be made for private use or research. Authorization is given (as indicated by the Item Fee Code for this publication) to copy articles beyond the use permitted by Sections 107 and 108 of the U.S. Copyright Law, provided the copying fee of \$22.50 per copy per article is paid to the Copyright Clearance Center, 222 Rosewood Drive, Danvers, MA 01923, USA. Persons desiring to photocopy materials for classroom use should contact the CCC Academic Permissions Service. The Item Fee Code for this publication is 1070-6631/2005 \$22.50.

Authorization does not extend to systematic or multiple reproduction, to copying for promotional purposes, to electronic storage or distribution, or to republication in any form. In all such cases, specific written permission from AIP must be obtained.

Other Use: See journal home page for author's web posting guidelines. Permission is granted to quote from the journal with the customary acknowledgment of the source. Reproduction of an article or portions thereof requires formal permission from AIP and may be subject to fees. Permission may be obtained online using Rightslink. Simply click on the Rightslink icon/Permission for Reuse link found in the article abstracts. You may also address requests to: AIP Office of Rights and Permissions, Suite 1N01, 2 Huntington Quadrangle, Melville, NY 11747-4502; Fax: 516-576-2450; Tel.: 516-576-2268; E-mail: rights@aip.org.

Physics of Fluids (ISSN: 1070-6631) is published monthly by the American Institute of Physics. The 2005 print + online base price is US\$2375. POSTMASTER: Send address changes to *Physics of Fluids*, AIP, Suite 1N01, 2 Huntington Quadrangle, Melville, NY 11747-4502. Periodicals postage rate paid at Huntington Station, NY 11746, and additional mailing offices.

Printed on Dependoweb 45# paper, pH 8.0.

Copyright © 2005 American Institute of Physics. All rights reserved.

Stalactite growth as a free-boundary problem

Martin B. Short

Department of Physics, University of Arizona, Tucson, Arizona 85721

James C. Baygents

Department of Chemical and Environmental Engineering and Program in Applied Mathematics, University of Arizona, Tucson, Arizona 85721

Raymond E. Goldstein^{a)}

Department of Physics, Program in Applied Mathematics, and B105 Institute, University of Arizona, Tucson, Arizona 85721

(Received 7 March 2005; accepted 28 June 2005; published online 11 August 2005)

Stalactites, the most familiar structures found hanging from the ceilings of limestone caves, grow by the precipitation of calcium carbonate from within a thin film of fluid flowing down their surfaces. We have recently shown [M. B. Short, J. C. Baygents, J. W. Beck, D. A. Stone, R. S. Toomey III, and R. E. Goldstein, "Stalactite growth as a free-boundary problem: A geometric law and its Platonic ideal," *Phys. Rev. Lett.* **94**, 018501 (2005)] that the combination of thin-film fluid dynamics, calcium carbonate chemistry, and carbon dioxide diffusion and outgassing leads to a local geometric growth law for the surface evolution which quantitatively explains the shapes of natural stalactites. Here we provide details of this free-boundary calculation, exploiting a strong separation of time scales among that for diffusion within the layer, contact of a fluid parcel with the growing surface, and growth. When the flow rate, the scale of the stalactite, and the chemistry are in the ranges typically found in nature, the local growth rate is proportional to the local thickness of the fluid layer, itself determined by Stokes flow over the surface. Numerical studies of this law establish that a broad class of initial conditions is attracted to an ideal universal shape, whose mathematical form is found analytically. Statistical analysis of stalactite shapes from Kartchner Caverns (Benson, AZ) shows excellent agreement between the average shape of natural stalactites and the ideal shape. Generalizations of these results to nonaxisymmetric speleothems are discussed. © 2005 American Institute of Physics. [DOI: [10.1063/1.2006027](https://doi.org/10.1063/1.2006027)]

I. INTRODUCTION

References to the fascinating structures found in limestone caves, particularly stalactites, are found as far back in recorded history as the writings of the Elder Pliny in the first century A.D.¹ Although the subject of continuing inquiry since that time, the chemical mechanisms responsible for growth have only been well-established since the 19th century. These fundamentally involve reactions within the thin fluid layer that flows down speleothems, the term which refers to the whole class of cave formations. As water percolates down through the soil and rock above the cave, it becomes enriched in dissolved carbon dioxide and calcium, such that its emergence into the cave environment, where the partial pressure of CO₂ is lower, is accompanied by outgassing of CO₂. This, in turn, raises the pH slightly, rendering calcium carbonate slightly supersaturated. Precipitation of CaCO₃ adds to the growing speleothem surface. These chemical processes are now understood very well, particularly so from the important works of Dreybrodt,² Kaufmann,³ and Buhmann and Dreybrodt⁴ which have successfully explained the characteristic growth rates seen in nature, typically fractions of a millimeter per year.

Surprisingly, a comprehensive translation of these processes into mathematical laws for the growth of speleothems has been lacking. By analogy with the much studied problems of crystal growth in solidification, interface motion in viscous fingering, and related phenomena,⁵ it would seem only natural for the dynamics of speleothem growth to have been considered as a free-boundary problem. Yet, there have only been a few attempts at this, for the case of stalagmites,^{2-4,6} and they have not been completely faithful to the interplay between fluid mechanics and geometry which must govern the growth. This has left unanswered some of the most basic questions about stalactites (Fig. 1), such as why they are so long and slender, like icicles. Also like icicles,⁷⁻⁹ speleothem surfaces are often found to have regular ripples of centimeter-scale wavelengths, known among speleologists as "crenulations."¹⁰ No quantitative theory for their appearance has been proposed.

Recently, we presented the first free-boundary approach to the axisymmetric growth of stalactites.¹¹ In this, we derived a law of motion in which the local growth rate depends on the radius and inclination of the stalactite's surface. This law holds under a set of limiting assumptions valid for typical stalactite growth conditions. Numerical studies of this surface dynamics showed the existence of an attractor in the space of shapes, toward which stalactites will be drawn regardless of initial conditions. An analysis of the steadily

^{a)}Author to whom correspondence should be addressed; electronic mail: gold@physics.arizona.edu



FIG. 1. Stalactites in Kartchner Caverns. Scale is 20 cm.

growing shape revealed it to be described by a universal, parameter-free differential equation, the connection to an actual stalactite being through an arbitrary magnification factor. As with the Platonic solids of antiquity—the circle, the square, etc.—which are ideal forms independent of scale, this too is a Platonic ideal. Of course, the shape of any single real stalactite will vary from this ideal in a variety of ways due to instabilities such as those producing crenulations, inhomogeneous cave conditions, unidirectional airflow, etc. Mindful of this, we found that an average of natural stalactites appropriately washes out these imperfections, and compares extremely well with the Platonic ideal. Our purpose in this paper is to expand on that brief description by offering much greater detail in all aspects of the analysis.

Section II summarizes the prevailing conditions of speleothem growth, including fluid flow rates, concentrations of carbon dioxide and dissolved calcium which determine the important time scales, and the relevant Reynolds number. In Sec. III we exploit the strong separation of three time scales to derive the asymptotic simplifications important in subsequent analysis. A detailed study of the linked chemical and diffusional dynamics is presented in Sec. IV, culminating in the local growth law and a measure of the leading corrections. That local law is studied analytically in Sec. V and numerically in Sec. VI, where we establish the existence and

TABLE I. Stalactite growth conditions and properties.

Parameter	Symbol	Value
Length	ℓ	10–100 cm
Radius	R	5–10 cm
Fluid film thickness	h	10 μm
Fluid velocity	u_c	1–10 mm/s
Reynolds number	Re	0.01–1.0
Growth rate	ν	1 cm/century
Diffusion time	τ_d	0.1 s
Traversal time	τ_t	100 s
Growth time	τ_g	10^6 s
Forward reaction constant	k_+	0.1 s^{-1}
Backward reaction constant	k'_-	10^{-3} s^{-1}
Henry's law constant	H	0.01

properties of an attractor whose details are described in Sec. VII. The procedure by which a detailed comparison was made with stalactite shapes found in Kartchner Caverns is presented in Sec. VIII. Finally, Sec. IX surveys important generalizations which lie in the future, including azimuthally modulated stalactites and the more exotic speleothems such as draperies. Connections to other free-boundary problems in precipitative pattern formation are indicated, such as terraced growth at hot springs.

II. SPELEOTHEM GROWTH CONDITIONS

Here we address gross features of the precipitation process, making use of physical and chemical information readily obtained from the standard literature, and also, for the case of Kartchner Caverns in Benson, AZ, the highly detailed study¹² done prior to the development of the cave for public access. This case study reveals clearly the *range* of conditions which may be expected to exist in many limestone caves (see Table I). It is a typical rule of thumb that stalactite elongation rates ν are on the order of 1 cm/century, equivalent to the remarkable rate of ~ 2 $\text{\AA}/\text{min}$. One of the key issues in developing a quantitative theory is the extent of depletion of calcium as a parcel of fluid moves down the surface. An estimate of this is obtained by applying the elongation rate ν to a typical stalactite, whose radius at the ceiling might be $R \sim 5$ cm. We can imagine the elongation in a time τ to correspond to the addition of a disk at the attachment point, so $\pi R^2 \nu \tau \sim 80$ cm^3 or ~ 200 g of CaCO_3 (or ~ 80 g of Ca) is added per century, the density of CaCO_3 being 2.7 g/cm^3 . Now, the volumetric flow rate of water over stalactites can vary enormously,¹² but in wet caves it is typically in the range of 10 – 10^3 cm^3/h . If we adopt a conservative value of ~ 50 cm^3/h , the volume of water that flows over the stalactite in a century is ~ 44 000 l. A typical concentration of calcium dissolved in solution is 150 ppm (mg/l), so the total mass of calcium in that fluid volume is 6.6 kg, yielding a fractional precipitation of ~ 0.01 . Clearly, depletion of calcium through precipitation does not significantly alter the chemistry from the top to the bottom of stalactites. Indeed, since stalagmites so often form below stalactites, there must be plenty of calcium carbonate still

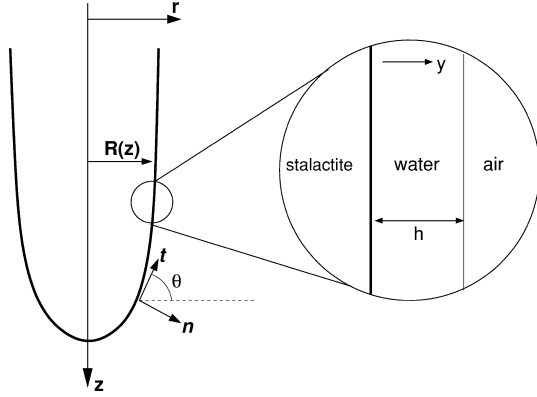


FIG. 2. Geometry of the surface of a stalactite. The tangent and normal vectors, along with the tangent angle θ , are defined.

available in the drip water for precipitation to occur.

Next, we establish the properties of the aqueous fluid layer on the stalactite surface by considering a cylindrical stalactite of radius R , length ℓ , and coated by a film of thickness h . Visual inspection of a growing stalactite confirms that $h \ll R$ over nearly the entire stalactite, except near the very tip where a pendant drop periodically detaches. Given the separation of length scales, we may deduce the velocity profile in the layer by assuming a flat surface. Let y be a coordinate perpendicular to the surface and θ the tangent angle with respect to the horizontal (Fig. 2). The Stokes equation for gravity-driven flow, $\nu d^2 u / dy^2 = g \sin \theta$, with $\nu = 0.01 \text{ cm}^2/\text{s}$ the kinematic viscosity of water, coupled with no-slip and stress-free boundary conditions, respectively, at the solid-liquid and liquid-air interfaces, is solved by the profile

$$u(y) = u_c \left[2 \frac{y}{h} - \left(\frac{y}{h} \right)^2 \right], \quad (1)$$

where

$$u_c \equiv \frac{gh^2 \sin \theta}{2\nu} \quad (2)$$

is the maximum velocity, occurring at the free surface. It is important to note that the extremely high humidity typically in the cave assures that evaporation does not play a significant role and so the fluid flux across any cross section is independent of the position along the stalactite. That volumetric fluid flux,

$$Q = 2\pi R \int_0^h u(y) dy = \frac{2\pi g R h^3 \sin \theta}{3\nu}, \quad (3)$$

allows us to solve for h and u_c in terms of the observables Q and R . Measuring Q in cm^3/h and R in centimeters, we find

$$h = \left(\frac{3Q\nu}{2\pi g R \sin \theta} \right)^{1/3} \approx 11 \mu\text{m} \left(\frac{Q}{R \sin \theta} \right)^{1/3}, \quad (4)$$

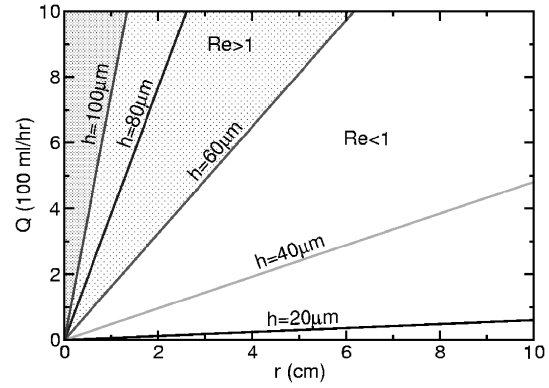


FIG. 3. Contour plot of fluid layer thickness h for various stalactite radii and fluid flow rates evaluated at $\theta = \pi/2$. At a thickness of $60 \mu\text{m}$, the Reynolds number approaches unity, and increases with increasing thickness. The shaded area beginning at a thickness of $100 \mu\text{m}$ denotes the region in which diffusion time across the fluid layer is comparable to the time of the slowest relevant reaction.

$$u_c = \frac{gh^2 \sin \theta}{2\nu} \approx 0.060 \text{ cm s}^{-1} \left(\frac{Q^2 \sin \theta}{R^2} \right)^{1/3}. \quad (5)$$

With the typical flow rates mentioned above and R in the range of 1–10 cm, h is tens of microns and the surface velocities below several mm/s. The Reynolds number on the scale of the layer thickness h is

$$\text{Re} = \frac{u_c h}{\nu} \sim 0.007 \frac{Q}{R}. \quad (6)$$

Using again the typical conditions and geometry, this is much less than unity, and the flow is clearly laminar. Figure 3 is a guide to the layer thickness as a function of Q and R , and the regime in which the Reynolds number approaches unity—only for very thin stalactites at the highest flow rates. The rule for the fluid layer thickness (4) does not hold very near the stalactite tip, where, as mentioned earlier, pendant drops form and detach. Their size is set by the capillary length $l_c = (\sigma/\rho g)^{1/2} \sim 0.3 \text{ cm}$, where $\sigma \approx 80 \text{ ergs/cm}^2$ is the air-water surface tension.

III. SEPARATION OF TIME SCALES

Based on the speleothem growth conditions, we can now see that there are three very disparate time scales of interest. The shortest is the scale for diffusional equilibration across the fluid layer,

$$\tau_d = \frac{h^2}{D} \sim 0.1 \text{ s}, \quad (7)$$

where $D \sim 10^{-5} \text{ cm}^2/\text{s}$ is a diffusion constant typical of small aqueous solutes. Next is the traversal time, the time for a parcel of fluid to move the typical length of a stalactite,

$$\tau_t = \frac{\ell}{u_c} \sim 10^2 \text{ s}. \quad (8)$$

Third is the time scale for growth of one fluid layer depth,

$$\tau_g = \frac{h}{v} \sim 10^6 \text{ s.} \quad (9)$$

Inasmuch as the off gassing of CO_2 leads to the precipitation of CaCO_3 , the concentration distributions of these two chemical species are of interest in the aqueous film. Because the traversal time scale is much less than that for growth, we shall see that solute concentration variations tangent to the growing surface will be negligible and this ultimately permits us to derive a local geometric growth law that governs the evolution of the speleothem shape. To illustrate our approximations, we begin by considering the distribution of Ca^{2+} in a stagnant fluid layer of thickness h . If C and D , respectively, denote the concentration and diffusivity of that species, then

$$\frac{\partial C}{\partial t} = D \frac{\partial^2 C}{\partial y^2}. \quad (10)$$

We require

$$\left. \frac{\partial C}{\partial y} \right|_h = 0 \text{ and } D \left. \frac{\partial C}{\partial y} \right|_0 = F, \quad (11)$$

where the deposition rate F at the solid-liquid boundary ($y=0$) is presumed to depend on the local supersaturation $C - C_{\text{sat}}$. For the sake of discussion, we set

$$F = \gamma(C - C_{\text{sat}}), \quad (12)$$

where γ is a rate constant with units of length/time. Equation (12) implicitly introduces a deposition time scale

$$\tau_{\text{dep}} = \frac{h}{\gamma} \quad (13)$$

that is related to τ_g . Because the observed growth rate of stalactites is so low, for the time being we take $\tau_{\text{dep}} \gg \tau_t \gg \tau_d$. Toward the end of Sec. IV we obtain an expression for F that confirms this ordering of time scales and makes it apparent that γ depends on the acid-base chemistry of the liquid film.

If we define a dimensionless concentration

$$\Theta \equiv \frac{C - C_{\text{sat}}}{C_0 - C_{\text{sat}}}, \quad (14)$$

where C_0 is the initial concentration of the solute in the liquid, we can write Eq. (10) as

$$\frac{\partial^2 \Theta}{\partial y^2} = N \frac{\partial \Theta}{\partial t}, \quad (15)$$

where time t is now scaled on τ_{dep} and the coordinate y is scaled on h . The parameter

$$N \equiv \frac{\gamma h}{D} \quad (16)$$

is a dimensionless group that weighs the relative rates of deposition and diffusion. The boundary conditions become

$$\left. \frac{\partial \Theta}{\partial y} \right|_1 = 0 \text{ and } \left. \frac{\partial \Theta}{\partial y} \right|_0 = N\Theta. \quad (17)$$

Though it is possible to write out an analytical solution to Eqs. (15)–(17), we elect to construct an approximate solution by writing

$$\Theta(y, t) = \bar{\Theta}(t) + N\Theta'(y, t), \quad (18)$$

which is useful when $N \ll 1$, as it is here. $\bar{\Theta}(t)$ represents, to leading order in N , the mean concentration of solute in the fluid layer. Upon substituting (18) into (15)–(17), one obtains

$$\bar{\Theta}(t) = Ae^{-t}, \quad (19)$$

where A is an $O(1)$ constant. At short times then, $\bar{\Theta}(t) \approx A(1-t)$ and $\partial\bar{\Theta}/\partial t \sim -A$. This means the time rate of change of the solute concentration is constant, and there is little depletion of the solute, on time scales that are long compared to τ_d but short compared to τ_{dep} . This latter point concerning solute depletion and time scales will become more important as we consider the role of advection in the film.

Consider again diffusion of the solute across a liquid film of thickness h , but now suppose that the liquid flows along the solid surface, which is taken to be locally flat and characterized by a length scale $\ell \gg h$ in the direction of the flow. If the flow of the liquid is laminar, the (steady) balance law for the solute (Ca^{2+}) reads as

$$u(y) \frac{\partial C}{\partial x} = D \frac{\partial^2 C}{\partial y^2}. \quad (20)$$

Here diffusion in the x direction has been neglected. In dimensionless form, Eq. (20) is

$$Nf(y) \frac{\partial \Theta}{\partial x} = \frac{\partial^2 \Theta}{\partial y^2}, \quad (21)$$

where x has been scaled on $u_c h / \gamma$ and $f(y) = 2y - y^2$. Note that the small parameter N appears on the left-hand side of (20), implying that advection plays a lesser role than one might anticipate from a cursory evaluation of the Peclet number,

$$\text{Pe} = \frac{u_c h}{D} \sim \gamma \frac{Q}{R}, \quad (22)$$

which is $\sim 10-100$. This is, of course, due to the fact that the gradient in concentration is nearly perpendicular to the fluid velocity field, i.e., the extremely low deposition rate does not lead to a significant reduction in calcium concentration along the length of the stalactite. Boundary conditions (17) still apply and the problem statement is made complete by the requirement that Θ be unity at $x=0$.

To construct an approximate solution to Eq. (21), we write

$$\Theta \equiv \Theta_b(x) + N\Theta'(x, y), \quad (23)$$

where

$$\Theta_b(x) \equiv \frac{\int_0^1 f(y)\Theta(x,y)dy}{\int_0^1 f(y)dy} \quad (24)$$

is the bulk average concentration of the solute at position x . Substituting (23) into (21) yields

$$\Theta_b(x) = A_b e^{-3/2x}, \quad (25)$$

where A_b is unity if $\Theta(0,y)=1$.

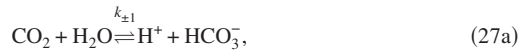
Recall that the x coordinate is scaled on $u_c h/\gamma$. This means $x \ll 1$ as long as $\ell \ll u_c h/\gamma$ or, equivalently, $\tau_t \ll \tau_{\text{dep}}$. The bulk concentration Θ_b is thus

$$\Theta_b(x) \approx A_b \left(1 - \frac{3}{2}x\right), \quad (26)$$

indicating that, to leading order, the concentration of the solute in the film diminishes linearly with position, i.e., $\partial\Theta/\partial x$ is approximately constant, which is analogous to the behavior obtained for the stagnant film. More importantly, Eq. (26) reveals the approximate functional form for the calcium depletion and verifies the existence of a length scale over which significant depletion occurs that is much greater than typical stalactite lengths.

IV. CHEMICAL KINETICS AND THE CONCENTRATION OF CO₂

Deposition of CaCO₃ is coupled to the liquid-phase concentration of CO₂ through the acid-base chemistry of the film. As the pH of the liquid rises, the solubility of CaCO₃ decreases. Much work has been done to determine the rate limiting step in the chemistry of stalactite growth under various conditions.²⁻⁴ For typical concentrations of chemical species, an important conclusion is that the slowest chemical reactions involved in the growth are those that couple carbon dioxide to bicarbonate,



All other chemical reactions are significantly faster than these and can be considered equilibrated by comparison. It is also critical to note that these reactions are directly coupled to the deposition process; for each molecule of CaCO₃ that adds to the surface of the crystal, pathways (27a) and (27b) must generate one molecule of CO₂, which then exits the liquid and diffuses away in the atmosphere. We express the local rate of production of CO₂ by chemical reaction as

$$R_{\text{CO}_2} = k_-[\text{HCO}_3^-] - k_+[\text{CO}_2], \quad (28)$$

where

$$k_- \equiv k_{-1}[\text{H}^+] + k_{-2}, \quad (29a)$$

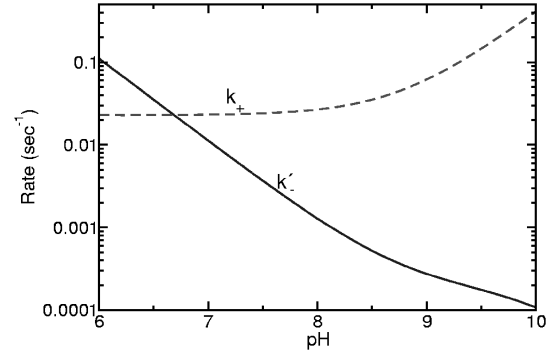


FIG. 4. Values for k_+ and k'_- [Eq. (51)] as functions of pH are shown as dashed and solid lines, respectively. Note that k_+ is much larger than k'_- at pH values typical of caves (~ 9), so $[\text{Ca}^{2+}]$ must be significantly larger than $[\text{CO}_2]$ for growth to occur.

$$k_+ \equiv k_{+1} + k_{+2}[\text{OH}^-]. \quad (29b)$$

The pH dependence of the rate constant k_+ (which is much greater than k_-) is shown in Fig. 4. The inverse of this constant defines an additional time scale. At a pH typical of cave water (~ 9), the value of k_+ is $\sim 0.1 \text{ s}^{-1}$, giving a chemical reaction time of about 10 s, much greater than the diffusional time scale τ_d . This implies that variations from the average of $[\text{CO}_2]$ (or of other chemical species) in the normal direction within the fluid layer will be quite small. The two time scales are not of comparable magnitude until the thickness reaches $\sim 100 \mu\text{m}$, significantly thicker than typically seen.

The dependence of the precipitation rate on fluid layer thickness is crucial; we follow and extend an important earlier work⁴ to derive this. As previously noted, the dynamics of CO₂ plays a critical role in stalactite formation, and the growth of the surface can be found directly from the amount of carbon dioxide leaving the fluid layer into the atmosphere. To that end, we begin with the full reaction-diffusion equation for $[\text{CO}_2]$ within the fluid layer, taken on a plane with coordinates x and y tangent and normal to the surface, respectively. That is,

$$\frac{\partial C}{\partial t} + u \frac{\partial C}{\partial x} + w \frac{\partial C}{\partial y} = D \left(\frac{\partial^2 C}{\partial y^2} + \frac{\partial^2 C}{\partial x^2} \right) - k_+ C + k_- [\text{HCO}_3^-], \quad (30)$$

where $C = [\text{CO}_2]$, u and w are the fluid velocity components in the x and y directions, and $D \sim 10^{-5} \text{ cm}^2/\text{s}$ is the diffusion constant associated with CO₂ in water. We now stipulate that only an equilibrium solution is desired, so the partial time derivative will be ignored. We also note that, insofar as the plane is considered flat, the velocity w will be zero everywhere, eliminating a second term. Finally, we rescale quantities as

$$x = \ell \tilde{x}, \quad y = h \tilde{y}, \quad u = u_c \tilde{u}, \quad C = C_0(1 + \phi). \quad (31)$$

Then, omitting the tildes, Eq. (30) can be rewritten as

$$\frac{\tau_d u}{\tau_t} \frac{\partial \phi}{\partial x} = \frac{\partial^2 \phi}{\partial y^2} + \left(\frac{h}{\ell} \right)^2 \frac{\partial^2 \phi}{\partial x^2} + \delta^2(\omega - \phi), \quad (32a)$$

$$\delta \equiv \sqrt{\frac{h^2 k_+}{D}}, \quad (32b)$$

$$\omega \equiv \frac{k_- [\text{HCO}_3^-]}{k_+ [\text{CO}_2]_0} - 1. \quad (32c)$$

Now, since both h/ℓ and τ_d/τ_i are $\sim 10^{-4}$, we will ignore the terms corresponding to diffusion and advection in the x direction. This is further justified by the estimation above regarding the very low fractional depletion of Ca^{2+} as the fluid traverses the stalactite; there is clearly very little change in the concentrations of species from top to tip. The parameter $\delta \sim 10^{-1}$, so we will desire a solution to lowest order in δ only. Furthermore, as δ represents the influence of chemical reactions in comparison to diffusion, it is clear that for very small δ , the concentrations of species will vary only slightly (order of δ^2 at most) from their average throughout the layer. Indeed, the definition of δ indicates that there is an important characteristic distance in this problem, the reaction length

$$\ell_r = \sqrt{\frac{D}{k_+}} \sim 100 \mu\text{m}. \quad (33)$$

When the layer thickness is smaller than ℓ_r , the concentration profile is nearly constant; beyond ℓ_r , it varies significantly. This criterion is illustrated in Fig. 3. To lowest order in δ , we need not account for the fact that $[\text{HCO}_3^-]$ and $[\text{H}^+]$ are functions of y , and instead simply use their average values. The result of these many approximations is the equation

$$\frac{\partial^2 \phi}{\partial y^2} = \delta^2 (\phi - \omega). \quad (34)$$

The first boundary condition imposed on Eq. (34) is that of zero flux of CO_2 at the stalactite surface. Second, we demand continuity of flux between the fluid and atmosphere at the surface separating the two. Third, the concentration of CO_2 in the water at the free fluid surface is proportional to the atmospheric concentration at the same position, the proportionality constant being that of Henry's law.¹⁶ Finally, the atmospheric concentration approaches a limiting value $[\text{CO}_2]_\infty$ far from the stalactite. Since the solution to Eq. (34) is dependent upon the atmospheric carbon dioxide field $[\text{CO}_2]_a$, we stipulate that this quantity obeys Laplace's equation

$$\nabla^2 [\text{CO}_2]_a = 0, \quad (35)$$

as is true for a quiescent atmosphere.

At this point, we alter the geometry of the model to that of a sphere covered with fluid (Fig. 5), as Laplace's equation is more amenable to an exact solution in these coordinates. We do not anticipate that this will affect the model in any significant way, as we have already condensed the problem to variations of the CO_2 concentrations in the direction normal to the stalactite surface only. This approximation would be problematic if atmospheric diffusion played a significant role; this turns out to be not the case, as explained below. In these new coordinates, the atmospheric carbon dioxide concentration is

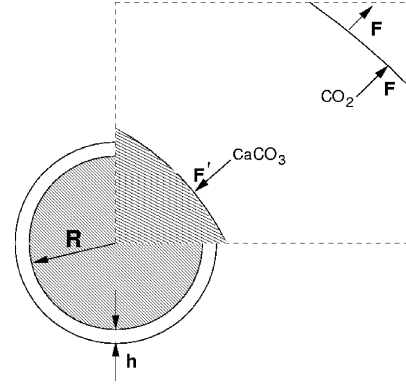


FIG. 5. Spherical model for calculating the growth rate. F and F' are the magnitudes of the fluxes of carbon dioxide and calcium carbonate.

$$[\text{CO}_2]_a = [\text{CO}_2]_\infty + \frac{A}{r}, \quad (36)$$

where r is the radial position relative to the center of the sphere and A is a constant to be determined. To first order in $\epsilon \equiv h/R \sim 10^{-3}$ the value of $[\text{CO}_2]_a$ at the water-air interface, $r=R+h$, is

$$[\text{CO}_2]_{a|R+h} = [\text{CO}_2]_\infty + (1 - \epsilon) \frac{A}{R}. \quad (37)$$

Likewise, the flux of CO_2 exiting the fluid at this interface is found to be

$$F = (1 - 2\epsilon) \frac{D_a A}{R^2}, \quad (38)$$

where $D_a \sim 10^{-2} \text{ cm}^2/\text{s}$ is the atmospheric diffusion coefficient of carbon dioxide.

Now we turn to the aqueous $[\text{CO}_2]$. If we express (34) in spherical coordinates with the rescaling $r=R+hy$, and expand to first order in ϵ we obtain

$$\frac{\partial^2 \phi}{\partial y^2} + 2\epsilon \frac{\partial \phi}{\partial y} = \delta^2 (\phi - \omega). \quad (39)$$

The first boundary condition of zero flux at the stalactite surface can be expressed as

$$\left. \frac{\partial \phi}{\partial y} \right|_{y=0} = 0. \quad (40)$$

The Henry law boundary condition is rewritten as

$$\phi(1) = (1 - \epsilon) \frac{A}{R[\text{CO}_2]_\infty}, \quad (41)$$

where we have taken $[\text{CO}_2]_0$ to be $H[\text{CO}_2]_\infty$. Finally, using (38) and our definition of $[\text{CO}_2]_0$, the condition of flux continuity between the fluid and atmosphere can be written as

$$\left. \frac{\partial \phi}{\partial y} \right|_{y=1} = -\epsilon \frac{D_a A}{DRH[\text{CO}_2]_\infty}. \quad (42)$$

Eliminating A between Eqs. (41) and (42) we obtain

$$\left. \frac{\partial \phi}{\partial y} \right|_{y=1} = -\epsilon \frac{D_a}{DH} \phi(1). \quad (43)$$

After straightforwardly solving Eq. (39) subject to the boundary conditions (40) and (43), we expand to lowest order in δ and first order in ϵ . From this, we find that the function ϕ is

$$\phi = \omega \delta^2 \left(\frac{1-y^2}{2} - \epsilon \frac{1-y^3}{3} + \frac{DH}{D_a} \frac{1-\epsilon-\epsilon^2}{\epsilon} \right). \quad (44)$$

We then easily calculate the amount of carbon dioxide leaving the fluid by multiplying the CO_2 flux by the surface area of the outside of the liquid layer. The final step is to equate the amount of CO_2 leaving with the amount of CaCO_3 adding to the surface and divide by the surface area of the sphere to find the CaCO_3 flux. The result is

$$F' = h(k_-[\text{HCO}_3^-] - k_+H[\text{CO}_2]_\infty)(1 + \epsilon). \quad (45)$$

We see then that atmospheric diffusion is negligible at lowest order and that the flux is directly proportional to the fluid layer thickness. Finally, though the spherical approximation used above is useful, it is not strictly necessary, and the calculations can be repeated using a cylindrical model instead. The result in this geometry is

$$F' = h(k_-[\text{HCO}_3^-] - k_+H[\text{CO}_2]_\infty)(1 - \epsilon/2), \quad (46)$$

differing from the spherical model only at order ϵ . As we will neglect this term for the remainder of the paper, the choice of geometry is irrelevant.

As information regarding typical $[\text{HCO}_3^-]$ is less available than that regarding $[\text{Ca}^{2+}]$, we wish to reexpress Eq. (45) in terms of the calcium ion concentration. This is readily accomplished by first imposing an electroneutrality condition on the fluid at any point,

$$2[\text{Ca}^{2+}] + [\text{H}^+] = 2[\text{CO}_3^{2-}] + [\text{HCO}_3^-] + [\text{OH}^-]. \quad (47)$$

Next, we note that $[\text{OH}^-]$ and $[\text{H}^+]$ are related through the equilibrium constant of water K_w , and that $[\text{CO}_3^{2-}]$, $[\text{H}^+]$, and $[\text{HCO}_3^-]$ are related through another equilibrium constant, K . Hence, we can express $[\text{HCO}_3^-]$ solely in terms of these constants, $[\text{Ca}^{2+}]$, and $[\text{H}^+]$ as

$$[\text{HCO}_3^-] = \frac{2[\text{Ca}^{2+}] + (1 - \beta)[\text{H}^+]}{1 + 2\alpha}, \quad (48)$$

where

$$\beta = \frac{K_w}{[\text{H}^+]^2}, \quad \alpha = \frac{K}{[\text{H}^+]}. \quad (49)$$

Upon substitution of this formula into Eq. (45), we obtain (ignoring the order ϵ correction)

$$F' = h(k'_-[\text{Ca}^{2+}] + k_0[\text{H}^+] - k_+H[\text{CO}_2]_\infty), \quad (50)$$

$$k'_- = \frac{2}{1 + 2\alpha}k_-, \quad k_0 = \frac{1 - \beta}{1 + 2\alpha}k_-. \quad (51)$$

As one can now see *a posteriori*, the calcium ion flux is indeed given by a formula of the form supposed in Eq. (12), where the values of γ and C_{sat} are given by

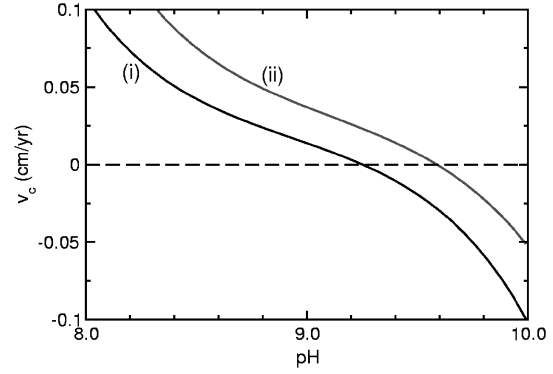


FIG. 6. Growth velocity v_c vs pH, using CO_2 partial pressure in the cave of 3×10^{-4} atm, a temperature of 20°C , and (i) $[\text{Ca}^{2+}]$ of 200 ppm and volumetric fluid flow $Q=30$ cm^3/h and (ii) $[\text{Ca}^{2+}]$ of 500 ppm and $Q=5$ cm^3/h . The formulas for the constants are taken from Ref. 4.

$$\gamma = hk'_-, \quad C_{\text{sat}} = \frac{k_+}{k'_-}H[\text{CO}_2]_\infty - \frac{k_0}{k'_-}[\text{H}^+]. \quad (52)$$

With these definitions, $\tau_{\text{dep}} = 1/k'_- \sim 10^4$, and our previous time-scale orderings are vindicated. In addition, the expression for C_{sat} is consistent with the underlying chemical kinetics.

V. LOCAL GEOMETRIC GROWTH LAW

The two ingredients of the local growth law are now at hand: the relation (50) for the flux as a function of fluid layer thickness and internal chemistry, and the result (4) connecting the layer thickness to the geometry and imposed fluid flux Q . Combining the two, we obtain at leading order a *geometrical* law for growth. It is most appropriately written as a statement of the growth velocity \mathbf{v} along the unit normal to the surface ($\hat{\mathbf{n}}$ in Fig. 2),

$$\hat{\mathbf{n}} \cdot \mathbf{v} = v_c \left(\frac{\ell_Q}{r \sin \theta} \right)^{1/3}. \quad (53)$$

Here, $r(z)$ is the local radius and $\theta(z)$ is the local tangent angle of the surface, and

$$v_c = v_m \ell_Q (k'_-[\text{Ca}^{2+}] + k_0[\text{H}^+] - k_+H[\text{CO}_2]_\infty) \quad (54)$$

is the characteristic velocity, with v_m being the molar volume of CaCO_3 , and

$$\ell_Q = \left(\frac{3\nu Q}{2\pi g} \right)^{1/4} \sim 0.01 \text{ cm} \quad (55)$$

a characteristic length. The velocity v_c depends upon the pH not only through $[\text{H}^+]$ but also through the definitions of k'_- and k_+ , crossing from positive (growth) to negative (dissolution) at a critical pH that depends on the average calcium ion concentration, the partial pressure of CO_2 in the cave atmosphere, and the fluid flux. Figure 6 shows some examples of this behavior. Cave water is often close to the crossing point, implying values for v_c on the order of 0.1 mm/year.

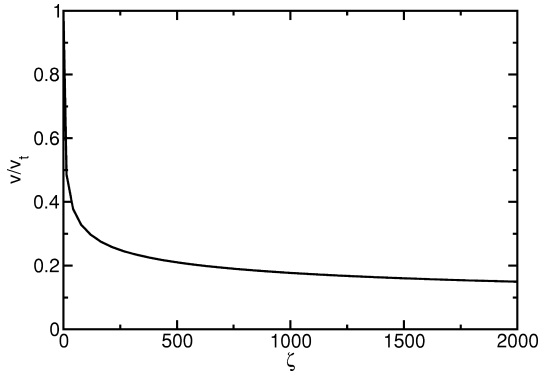


FIG. 7. The dimensionless growth velocity, v/v_t , vs. ζ , defined in Eq. (56), evaluated for the ideal stalactite shape (Fig. 9). Note the precipitous drop away from the stalactite's tip.

In comparison to many of the classic laws of motion for surfaces, the axisymmetric dynamics (53) is rather unusual. First, unlike examples such as “motion by mean curvature”¹³ and the “geometrical” models of interface motion,¹⁴ it depends not on geometric invariants but on the absolute orientation of the surface through the tangent angle, and on the radius r of the surface. As remarked earlier,¹¹ the fact that it depends on the tangent angle θ is similar to the effects of surface tension anisotropy,¹⁵ but without the periodicity in θ one finds in that case. The variation (Fig. 7) is extreme near the tip, where θ and r are both small, and minor in the more vertical regions, where $\theta \sim \pi/2$ and r is nearly constant.

Note also that the geometric growth law takes the form of a product of two terms, one dependent only upon chemistry, the other purely geometric. This already implies the possibility that while individual stalactites may grow at very different rates as cave conditions change over time (for instance, due to variations in fluid flux, and carbon dioxide and calcium levels), the geometric relationship for accretion does not change. Therein lies the possibility of an underlying common form, as we shall see in subsequent sections.

VI. NUMERICAL STUDIES

In order to understand the shapes produced by the growth law (53), numerical studies were performed to evolve a generic initial condition. The method of these simulations is based on well-known principles.¹⁴ Here, because of the axisymmetric nature of our law, we take the stalactite tangent angle θ to be the evolving variable. The time-stepping algorithm is an adaptive, fourth-order Runge-Kutta method. For simplicity, all simulations were performed with the boundary condition that the stalactite be completely vertical at its highest point (i.e., the cave ceiling). The growth law breaks down very near the tip, where the precipitation dynamics becomes much more complex. However, it is safe to assume that the velocity of the stalactite's tip v_t is a monotonically increasing function of flow rate Q . For the numerics then, velocities at radii smaller than the capillary length are extrapolated from those near this region, with the tip velocity scaling at a rate

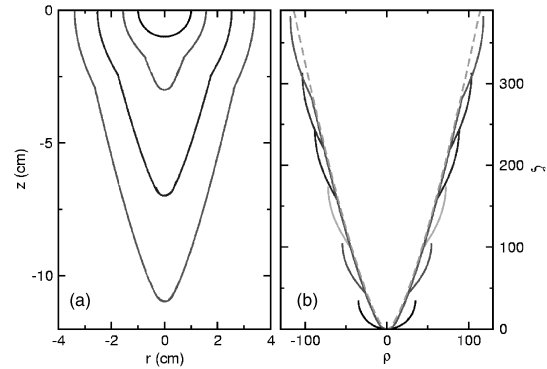


FIG. 8. Numerical results. (a) A rounded initial condition evolves into a fingered shape. (b) Aligning the tips of the growing shapes shows rapid collapse to a common form. Here, the profiles have been scaled appropriately [Eq. (60)] and are shown with the ideal curve (dashed line).

greater than $Q^{1/3}$ (this choice will be explained in more detail in Sec. VII). The volumetric fluid flux is a user-defined parameter and sets the value of ℓ_Q .

Figure 8 shows how a shape which is initially rounded develops an instability at its lowest point. The mechanism of the instability follows from the flux conservation that is an integral part of the dynamics. The downward protuberance has a locally smaller radius than the region above and therefore a thicker fluid layer. According to (45) this increases the precipitation rate, enhancing the growing bump. We find numerically that the growing protuberance approaches a uniformly translating shape for a wide range of initial conditions (Fig. 8). The aspect ratio of this shape, defined here as the length ℓ divided by maximum width W , is influenced by the flow rate chosen for the simulation, with a high flow giving a higher aspect ratio stalactite than a low flow for equal stalactite lengths.

VII. THE TRAVELING SHAPE

The asymptotic traveling shape $z(r)$ can be found by noting that the normal velocity (53) at any point on such a surface must equal $v_t \cos \theta$, where, as noted previously, v_t is the tip velocity. Observing that $\tan \theta = dz/dr$, and rescaling symmetrically r and z as

$$\rho \equiv \frac{r}{\ell_Q} \left(\frac{v_t}{v_c} \right)^3 \quad \text{and} \quad \zeta \equiv \frac{z}{\ell_Q} \left(\frac{v_t}{v_c} \right)^3, \quad (56)$$

we find the differential equation

$$\frac{\zeta'(\rho)}{[1 + \zeta'(\rho)^2]^2} - \frac{1}{\rho} = 0. \quad (57)$$

Let us now examine Eq. (57) in detail. A first observation is that for large ζ' the balance of terms is $(\zeta')^{-3} \sim \rho^{-1}$, implying a power law,

$$\zeta \sim \rho^\alpha, \quad \alpha = \frac{4}{3}. \quad (58)$$

This particular power can be traced back to the flux relation $Q \sim h^3$, and if this were more generally $Q \sim h^\psi$ then $\alpha = (\psi$

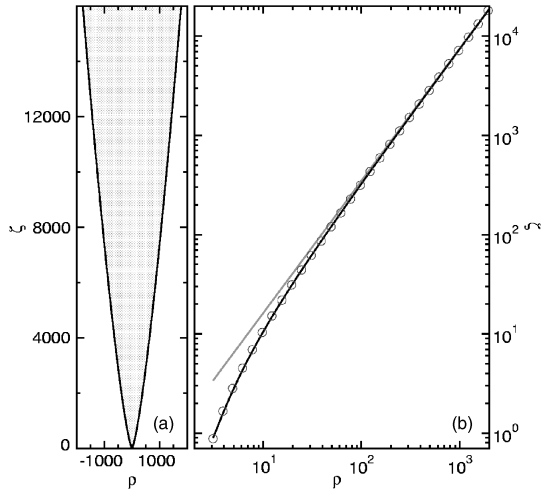


FIG. 9. Platonized ideal of stalactite shapes. (a) The shape is from the numerical integration of Eq. (57). (b) The gray line shows comparison of that integration with the pure power law given by the first term in (59), while the circles represent the complete asymptotic form in (59).

$+1/\psi$ which is always greater than unity for the physically sensible $\psi > 0$. As this is steeper than linear the associated shape is convex outward, and therefore has an aspect ratio that increases with overall length—just as the classic carrot-like shape of stalactites.

The differential Eq. (57) has some mathematical subtleties. The term involving ζ' vanishes at $\zeta'(\rho) = 0$ and also as $\zeta'(\rho) \rightarrow \infty$, is positive at all points in between, and has a maximum of magnitude $3\sqrt{3}/16$ at the point $\zeta'(\rho) = 1/\sqrt{3}$. The rightmost term will then shift this function downward by an amount $1/\rho$. So, at $\rho = 0$, there is no real solution to Eq. (57). Of course, this is acceptable to us because we do not expect the velocity law (53) to be valid exactly at the tip of the stalactite, where capillarity must modify the thickness of the film. As ρ moves away from zero, we first encounter a real solution at $\rho = \rho_m \equiv 16/3\sqrt{3}$, at which point $\zeta'(\rho)$ is equal to $1/\sqrt{3}$. This minimum radius cutoff, which is intrinsic to the mathematics and, therefore, inescapable, should not be confused with the somewhat arbitrary capillary length cutoff used earlier in the numerical studies. For all ρ greater than this minimal ρ_m , there will be two distinct real solutions of the equation for $\zeta'(\rho)$. One solution is a decreasing function of ρ , the other an increasing function. Since the physically relevant shape of a stalactite has a large slope at a large radius, the second root is of greater interest.

The astute reader will notice that Eq. (57) is essentially a fourth-order polynomial equation for $\zeta'(\rho)$, and thus admits an exact solution. This solution is quite complex, though, and does not readily allow for an exact analytic formula for $\zeta(\rho)$, though it is useful for numerical integration. Figure 9 shows the shape so determined. At large values of ρ , this formula can be expanded and integrated to yield the approximation

$$\zeta(\rho) \approx \frac{3}{4}\rho^{4/3} - \rho^{2/3} - \frac{1}{3}\ln \rho + \mathcal{O}(\rho^{-2/3}). \quad (59)$$

It is important to note that this ideal shape is completely parameter-free; all of the details of the flow rate, characteristic velocity, and tip velocity are lost in the rescaling. Hence, the stalactites created by our numerical scheme should all be of the same dimensionless shape, the only difference between them arising from the different magnification factors

$$a \equiv \ell_Q \left(\frac{v_c}{v_t} \right)^3 \quad (60)$$

that translate that shape into real units. Clearly, when comparing stalactites of equal length, the one with the lower magnification factor will occupy a greater extent of the universal curve, hence it will also have a higher aspect ratio. This explains our earlier choice that the tip velocity should scale at a rate greater than $Q^{1/3}$; with such a scaling, higher flow rates lead to lower magnification factors and higher aspect ratios, as is the case with real stalactites.

VIII. COMPARISONS WITH STALACTITES IN KARTCHNER CAVERNS

In this section we describe a direct comparison between the ideal shape described by the solution to Eq. (57) and real stalactites found in Kartchner Caverns in Benson, AZ. As is readily apparent to any cave visitor, natural stalactites may experience a wide range of morphological distortions; they may be subject to air currents and grow deformed along the direction of flow: they may be part of the sheet-like structures known as “draperies,” ripples may form (see below), etc. To make a comparison with theory we chose stalactites not obviously deformed by these processes. Images of suitable stalactites were obtained with a high-resolution digital camera (Nikon D100, 3008 × 2000 pixels), a variety of telephoto and macrolenses, and flash illumination where necessary. To provide a local scale on each image, a pair of parallel green laser beams 14.5 cm apart was projected on each stalactite.

Let us emphasize again that because the rescalings used to derive Eq. (57) are symmetric in r and z , a direct comparison between actual stalactites and the ideal requires only a global rescaling of the image. Moreover, as the aspect ratio for the ideal increases with the upper limit of integration, our theory predicts that all stalactites will lie on the ideal curve provided the differential equation defining that curve is integrated up to a suitable length. Therefore, we can visually compare stalactite images to the ideal shape rather simply. Figure 10 shows three representative examples of such a direct comparison, and the agreement is very good. Small deviations are noted near the tip, where capillarity effects associated with the pendant drops alter the shape.

For a more precise comparison, we extracted the contours of 20 stalactites by posterizing each image and utilizing a standard edge detection algorithm to obtain $r(z)$ for each [Fig. 11(a)]. The optimal scale factor a for each was found by a least-squares comparison with the ideal function [Fig. 11(b)]. This set of rescaled data was averaged and compared directly to the theoretical curve, yielding the master plot in Fig. 12. The statistical uncertainties grow with distance from

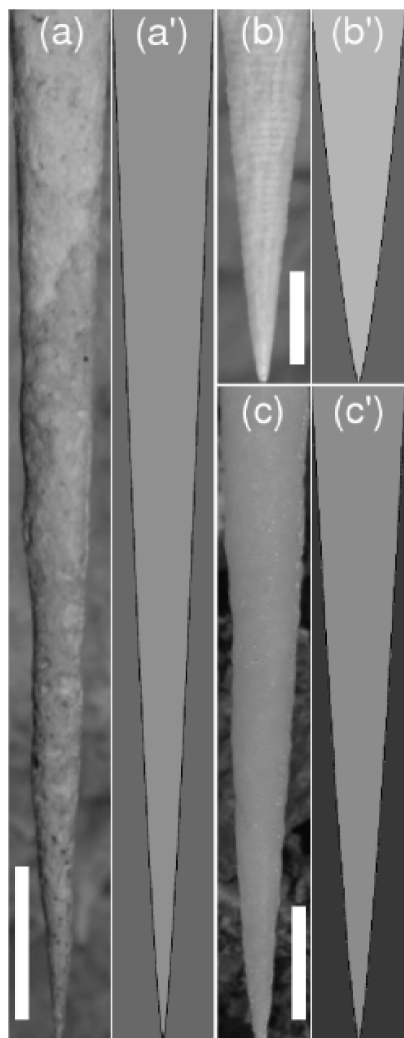


FIG. 10. Comparison between observed stalactite shapes and the Platonic ideal. Three examples [(a)—(c)] are shown, each next to an ideal shape of the appropriate aspect ratio and size [(a')—(c')]. Scale bars in each are 10 cm.

the stalactite tip because there are fewer long stalactites contributing to the data there. We see that there is excellent agreement between the data and the Platonic ideal, the latter falling uniformly within one standard deviation from the former. A plot of the residuals to the fit, shown in Fig. 13, indicates that there is a small systematic positive deviation near the tip. This is likely traced back to capillary effects ignored in the present calculation. These results show that the essential physics underlying stalactite growth is the spatially varying fluid layer thickness along the surface, which gives rise to extreme enhancement of growth near the tip. The characteristic, slightly convex form is an explicit consequence of the cubic relationship between flux and film thickness.

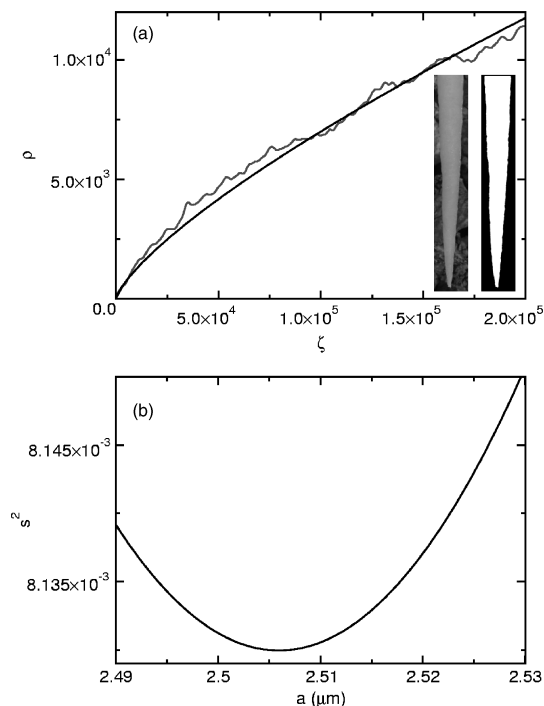


FIG. 11. Analysis of natural stalactites. (a) Posterization of an image to yield a contour, shown with the optimum scaling to match the ideal form. (b) Variance of the fit as a function of the scale factor a , showing a clear minimum.

IX. CONCLUSIONS

The dynamic and geometric results presented here illustrate that the essential physics underlying the familiar shape of stalactites is the locally varying fluid layer thickness controlling the precipitation rate, under the global constraint on that thickness provided by fluid flux conservation. Since so many speleothem morphologies arise from precipitation of calcium carbonate out of thin films of water, it is natural to conjecture that these results provide a basis for a quantitative understanding of a broad range of formations. Generalizations of this analysis to other speleothem morphologies can be divided into two classes: axisymmetric and nonaxisymmetric. Chief among the axisymmetric examples are stalagmites, the long slender structures growing up from cave floors, often directly below stalactites. These present significant complexities not found with stalactites. First, the upper ends of stalagmites are decidedly not pointed like the tips of stalactites, for the fluid drops that impact it do so from such a height as to cause a significant splash, although, when a stalagmite grows close to the stalactite above, it does tend to adopt a mirror-image form, the more so the closer the two are to fusing. Like stalactites, stalagmites and indeed most speleothem surfaces may display centimeter-scale ripples, further emphasizing the importance of a linear stability analysis of the coupled fluid flow and reaction-diffusion dynamics. A key question is why some stalactites display

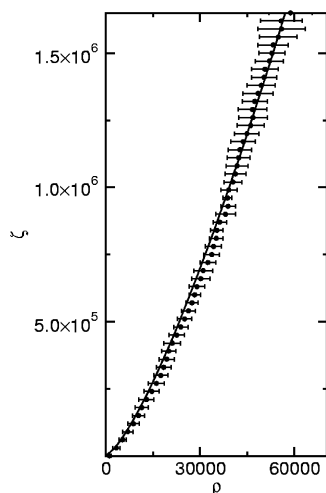


FIG. 12. Master plot of stalactite shapes, rescaled as described in text. The average of 20 stalactites is shown, compared with the ideal (black curve).

ripples while others do not. This will be discussed elsewhere. Many stalagmites also display a series of wedge-like corrugations on a scale much larger than the crenulations. We conjecture that these may be a signature of a secondary instability, the identification of which would require a fully nonlinear theory to describe the saturated amplitude of crenulations.

Two kinds of nonaxisymmetric forms are of immediate interest, those which arise from instabilities of axisymmetric shapes, and those which are formed by a mechanism with a fundamentally different intrinsic symmetry. A likely physical explanation of these forms is that a small azimuthal perturbation on an inclined surface, effectively a ridge, will accumulate fluid, thereby growing faster. Such deviations from axisymmetry present an interesting challenge for free-boundary theories, for the constraint of global flux conservation translates into a single azimuthal constraint on the variable film thickness at a given height on the speleothem. Formations of fundamentally different symmetry include draperies, sheet-like structures roughly 1 cm thick, with undulations on a scale of 20 cm. These grow typically from slanted ceilings along which flow rivulets of water, and increase in size by precipitation from fluid flowing along the lower edge. That flow is susceptible to the Rayleigh–Taylor instability, and not surprisingly there are often periodic undulations with a wavelength on the order of the capillary length seen on the lower edges of draperies. Since it is known that jets flowing down an inclined plane can undergo a meandering instability, it is likely that the same phenomenon underlies the gentle sinusoidal forms of draperies.

Other structures in nature formed by precipitation from solution likely can be described by a similar synthesis of fluid dynamics and geometric considerations. Examples include the hollow soda straws in caves, whose growth is templated by pendant drops (analogous to tubular growth templated by gas bubbles in an electrochemical setting¹⁶).

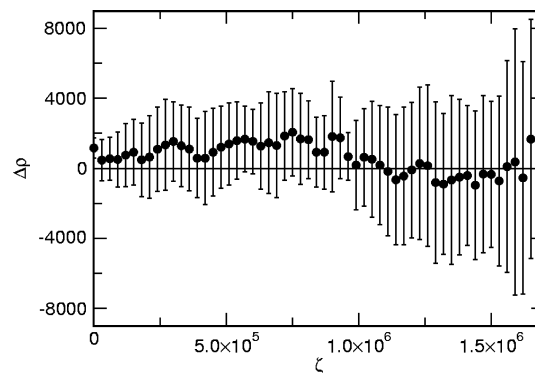


FIG. 13. Residuals of the fit to ideal shape, from Fig. 12.

Likewise, the terraces that form at mineral-rich hot springs like those at Yellowstone National Park provide a striking example of precipitative growth from solution. Moreover, the striking similarity between the geometry of stalactites and icicles, and especially the ripples on icicles (as discussed in recent works^{7–9}), suggests a commonality in their geometric growth laws. In both cases there is a thin film of fluid flowing down the surface, and a diffusing scalar field (carbon dioxide in the case of stalactites and latent heat for icicles) controlling the growth of the underlying surface. While the extreme separation between diffusional, traversal, and growth time scales found in the stalactite problem likely does not hold in the growth of icicles, that separation appears large enough to allow a significant equivalence between the growth dynamics of icicles and stalactites. Finally we note that it would be desirable to investigate model experimental systems whose time scale for precipitation is vastly shorter than natural stalactites. Many years ago Huff¹⁷ developed one such system based on gypsum. Further studies along these lines would provide a route to real-time studies of a whole range of free-boundary problems in a precipitative pattern formation.

ACKNOWLEDGMENTS

We are grateful to David A. Stone, J. Warren Beck, and Rickard S. Toomey for numerous important discussions and ongoing collaborations, to C. Jarvis for important comments at an early stage of this work, and to Chris Dombrowski, Ginger Nolan, and Idan Tuval for assistance in photographing stalactites. This work was supported by the Dean of Science, University of Arizona, the Research Corporation, and NSF ITR Grant No. PHY0219411.

¹C. Hill and P. Forti, *Cave Minerals of the World* (National Speleological Society, Huntsville, AL, 1997)

²W. Dreybrodt, “Chemical kinetics, speleothem growth and climate,” *Boreas* **28**, 347 (1999).

³G. Kaufmann, “Stalagmite growth and palaeo-climate: the numerical perspective,” *Earth Planet. Sci. Lett.* **214**, 251 (2003).

⁴D. Buhmann and W. Dreybrodt, “The kinetics of calcite dissolution and precipitation in geologically relevant situations of karst areas. 1. Open system,” *Chem. Geol.* **48**, 189 (1984).

⁵M. C. Cross and P. C. Hohenberg, “Pattern formation outside of equilib-

- rium," *Rev. Mod. Phys.* **65**, 851 (1993).
- ⁶H. W. Franke, "The theory behind stalagmite shapes," *Stud. Speleol.* **1**, 89 (1965).
- ⁷N. Ogawa and Y. Furukawa, "Surface instability of icicles," *Phys. Rev. E* **66**, 041202 (2002).
- ⁸K. Ueno, "Pattern formation in crystal growth under parabolic shear flow," *Phys. Rev. E* **68**, 021603 (2003).
- ⁹K. Ueno, "Pattern formation in crystal growth under parabolic shear flow. II," *Phys. Rev. E* **69**, 051604 (2004).
- ¹⁰C. A. Hill, "On the waves," *Sci. News (Washington, D. C.)* **163**, 111 (2003).
- ¹¹M. B. Short, J. C. Baygents, J. W. Beck, D. A. Stone, R. S. Toomey III, and R. E. Goldstein, "Stalactite growth as a free-boundary problem: A geometric law and its platonic ideal," *Phys. Rev. Lett.* **94**, 018510 (2005).
- ¹²*Final Report: Environmental and Geologic Studies for Kartchner Caverns State Park*, edited by R. H. Beucher (Arizona Conservation Projects, Tucson, AZ, 1992).
- ¹³M. Gage and R. S. Hamilton, "The heat equation shrinking convex plane-curves," *J. Diff. Geom.* **23**, 69 (1986).
- ¹⁴R. C. Brower, D. A. Kessler, J. Koplik, and H. Levine, "Geometrical models of interface evolution," *Phys. Rev. A* **29**, 1335 (1984).
- ¹⁵D. A. Kessler, J. Koplik, and H. Levine, "Pattern selection in fingered growth phenomena," *Adv. Phys.* **37**, 255 (1988).
- ¹⁶D. A. Stone and R. E. Goldstein, "Tubular precipitation and redox gradients on a bubbling template," *Proc. Natl. Acad. Sci. U.S.A.* **101**, 11537 (2004).
- ¹⁷L. C. Huff, "Artificial helictites and gypsum flowers," *J. Geol.* **48**, 641 (1940).

APPENDIX C: ICICLE GROWTH

PHYSICS OF FLUIDS

CODEN: PHFLE6

ISSN: 1070-6631

pof.aip.org

Editors: John Kim
University of California, Los Angeles, CA
L. Gary Leal
University of California, Santa Barbara, CA

Associate Editor for Letters: Andrea Prosperetti
Johns Hopkins University, Baltimore, MD

Distinguished Editor (1982–1997): Andreas Acrivos

Founding Editor (1958–1981): François N. Frenkiel

Associate Editors

Term ending 31 December 2006

H. Choi (Seoul National University, Seoul, South Korea)
E. J. Hinch (University of Cambridge, Cambridge, UK)
G. M. Homsy (University of California, Santa Barbara, CA)
J. R. Lister (University of Cambridge, Cambridge, UK)
P. A. Monkewitz (Swiss Federal Inst. of Tech., Lausanne)

Term ending 31 December 2007

J. P. Gollub (Haverford College, Haverford, PA)
J. Koplik (Levich Institute, New York, NY)
P. Moin (Stanford University, Stanford, CA)
S. B. Pope (Cornell University, Ithaca, NY)
A. Prosperetti (Johns Hopkins University, Baltimore, MD)

Term ending 31 December 2008

R. P. Behringer (Duke University, Durham, NC)
J. B. Grotberg (University of Michigan, Ann Arbor, MI)
R. D. Moser (University of Texas, Austin, TX)
E. S. G. Shaqfeh (Stanford University, Stanford, CA)
G. J. F. van Heijst (Tech. Univ. Eindhoven, The Netherlands)

Editorial Office Staff

Marjorie Hayes, *Assistant to the Editor (UCSB)*
E-mail: pof@engineering.ucsb.edu
Stacey Morse, *Assistant to the Editor (UCLA)*
E-mail: pof@ea.ucla.edu

E-mail Production Staff at AIP: pof@aip.org

Information for Authors

Submissions: Submit manuscripts online at <http://pof.peeerpress.org>. If preferred, mail printed manuscripts (3 copies) to Editorial Office, *Physics of Fluids*, Department of Chemical Engineering, University of California, Santa Barbara, CA 93106. Tel.: 805-893-3200; E-mail: pof@engineering.ucsb.edu. Submission implies that the manuscript has not been published previously and is not currently submitted for publication elsewhere. For detailed information for Contributors, visit <http://pof.aip.org/pof/submit.jsp>.

Publication Charge: The American Institute of Physics does not require page charges for this Journal.

Open Access: Through participation in *Author Select*SM and payment of a \$1500 fee, authors may choose open access publication for their accepted papers. See information during manuscript submission at <http://pof.peeerpress.org>.

Free Color Online: If authors supply usable color graphics files in time for the production process, color will appear in the online journal free of charge. Authors or their institutions must bear the cost of any color they wish to use in print. A fixed rate of \$650 for the first color figure and \$325 for each additional color figure applies for color in print. For multipart figures, a single charge will apply only if all parts are submitted as a single piece of artwork.

Reprints: Order reprints with or without covers only in multiples of 50 from AIP, Circulation & Fulfillment/Reprints, Suite 1N01, 2 Huntington Quadrangle, Melville, NY 11747-4502; Fax: 516-349-9704; Tel.: 800-344-6909 (U.S. & Canada), or 516-576-2270.

Supplemental Material may be deposited with AIP's Electronic Physics Auxiliary Publication Service (EPAPS), a low-cost online depository. For a nominal fee, authors may submit multimedia, data tables, text, etc. Address requests to the Editor; for additional information, see <http://www.aip.org/pubservs/epaps.html>.

Online Status Inquiry: During the production process, authors may access information about their accepted manuscripts at <http://www.aip.org/msinfo/status.html>.

Comments: Direct comments on the journal or editorial process to Doreene Berger, Editorial Operations, AIP, Suite 1N01, 2 Huntington Quadrangle, Melville, NY 11747-4502; Tel.: 516-576-2444; Fax: 516-576-2450; E-mail: dberger@aip.org.

Physics of Fluids is devoted to the publication of original theoretical, computational, and experimental contributions to the dynamics of gases, liquids, and complex or multiphase fluids. It is published monthly by the American Institute of Physics (AIP).

2006 Subscription Prices

Institutions: For information, visit <http://librarians.aip.org>. Institutional rates for *Phys. Fluids* alone and in combination with *Phys. Plasmas* may be found online at http://www.aip.org/journal_catalog/AIP2006NonmemberRateFixed.pdf, or contact AIP Customer Services at subs@aip.org [Tel.: 800-334-6902 (U.S. & Canada) or 516-576-2270; Fax: 516-349-9704].

Members: The following rates are available to all individual members of AIP Member and Affiliate Societies:

		U.S.	Non-U.S. (Surface)	Optional Air
Print & online	<i>Phys. Fluids</i> alone	\$252	\$307	\$337
	With <i>Phys. Plasmas</i>	\$428	\$533	\$593
Microfiche & online	<i>Phys. Fluids</i> alone	\$252	\$307	\$337
	With <i>Phys. Plasmas</i>	\$428	\$533	\$593
Online only	<i>Phys. Fluids</i> alone	\$88	\$88	\$88
	With <i>Phys. Plasmas</i>	\$158	\$158	\$158
Extended backfile access	Online access covers 2001–2006; for access to backfiles from Vol. 1 (1958) to present, add to subscription price: \$45 (for <i>Phys. Fluids</i> alone) or \$65 (for both <i>Phys. Fluids</i> & <i>Phys. Plasmas</i>).			
Annual CD-ROM	Add to subscription price: \$30 (for <i>Phys. Fluids</i> alone) or \$60 (for both <i>Phys. Fluids</i> & <i>Phys. Plasmas</i>).			

Single issue: \$225 for back issues for 2006

Prior years (Members): \$40 Prior years (Institutions): \$225

Additional Availability

Online Access: *Physics of Fluids* is available online at <http://pof.aip.org>.

Microform: *Physics of Fluids* is available on microfiche issued at the same frequency as the printed journal, and annually on microfilm. Direct requests to AIP, Circulation & Fulfillment/Single Copy Sales, Suite 1N01, 2 Huntington Quadrangle, Melville, NY 11747-4502; Fax: 516-349-9704; Tel.: 800-344-6902 (U.S. & Canada) or 516-576-2270.

Document Delivery: Copies of journal articles can be ordered for online delivery from DocumentStore, AIP's online document delivery service (<http://www.documentstore.org>).

Customer Service

Subscription Orders and Renewals should be addressed to American Institute of Physics, P.O. Box 503284, St. Louis, MO 63150-3284. Tel.: 800-344-6902 (U.S. & Canada) or 516-576-2270; Fax: 516-349-9704; E-mail: subs@aip.org. Allow at least six weeks advance notice.

Inquiries, Address Changes, Claims, Single Copy Replacements, and Back Volumes: For address changes, please send both old and new addresses and, if possible, include the mailing label from a recent issue. Missing issue requests will be honored only if received within six months of publication date (nine months for Australia & Asia). Single copies of a journal may be ordered and back volumes are available in print, microfiche, or microfilm. Contact AIP Customer Services at 800-344-6902 (U.S. & Canada) or 516-576-2270; Fax: 516-349-9704; E-mail: subs@aip.org.

Reprint Billing: Contact AIP Publication Charge & Reprints/CFD, Suite 1N01, 2 Huntington Quadrangle, Melville, NY 11747-4502; Tel.: 800-344-6909 (U.S. & Canada) or 516-576-2270; E-mail: pcr@aip.org.

Rights and Permissions

Copying: Single copies of individual articles may be made for private use or research. Authorization is given to copy articles beyond the free use permitted under Sections 107 and 108 of the U.S. Copyright Law, provided that the copying fee of \$23.00 per copy per article is paid to the Copyright Clearance Center, 222 Rosewood Drive, Danvers, MA 01923, USA, <http://www.copyright.com>. (Note: The ISSN for this journal is 1070-6631.)

Authorization does not extend to systematic or multiple reproduction, to copying for promotional purposes, to electronic storage or distribution, or to republication in any form. In all such cases, specific written permission from AIP must be obtained. Note: Copies of individual articles may also be purchased online via AIP's DocumentStore service (<http://www.documentstore.org>).

Other Use: See journal home page for author's web posting guidelines. Permission is granted to quote from the journal with the customary acknowledgment of the source. Republication of an article or portions thereof requires formal permission from AIP and may be subject to fees. Permission may be obtained online using Rightslink. Simply click on the Rightslink icon/Permission for Reuse link found in the article abstracts. You may also address requests to: AIP Office of Rights and Permissions, Suite 1N01, 2 Huntington Quadrangle, Melville, NY 11747-4502; Fax: 516-576-2450; Tel.: 516-576-2268; E-mail: rights@aip.org.

Digital Object Identifier (DOI): Each archival article published is assigned a unique DOI that serves to identify the article in a digital environment. In print, the DOI appears at the end of each abstract.

Physics of Fluids (ISSN: 1070-6631) is published monthly by the American Institute of Physics. The 2006 print + online base price is US\$2445. POSTMASTER: Send address changes to *Physics of Fluids*, AIP, Suite 1N01, 2 Huntington Quadrangle, Melville, NY 11747-4502. Periodicals postage rate paid at Huntington Station, NY 11746, and additional mailing offices.

Printed on Dependoweb 45# paper, pH 8.0.

Copyright © 2006 American Institute of Physics. All rights reserved.

Reprinted with permission from M.B. Short, J.C. Baygents, and R.E. Goldstein, *Physics of Fluids* 18, 083101 (2006). Copyright 2006, American Institute of Physics.

A free-boundary theory for the shape of the ideal dripping icicle

Martin B. Short

Department of Physics, University of Arizona, Tucson, Arizona 85721

James C. Baygents

Department of Chemical and Environmental Engineering and Program in Applied Mathematics, University of Arizona, Tucson, Arizona 85721

Raymond E. Goldstein^{a)}

Department of Physics, Program in Applied Mathematics, and BIO5 Institute, University of Arizona, Tucson, Arizona 85721

(Received 16 January 2006; accepted 10 July 2006; published online 18 August 2006)

The growth of icicles is considered as a free-boundary problem. A synthesis of atmospheric heat transfer, geometrical considerations, and thin-film fluid dynamics leads to a nonlinear ordinary differential equation for the shape of a uniformly advancing icicle, the solution to which defines a parameter-free shape which compares very favorably with that of natural icicles. Away from the tip, the solution has a power-law form identical to that recently found for the growth of stalactites by precipitation of calcium carbonate. This analysis thereby explains why stalactites and icicles are so similar in form despite the vastly different physics and chemistry of their formation. In addition, a curious link is noted between the shape so calculated and that found through consideration of only the thin coating water layer. © 2006 American Institute of Physics. [DOI: [10.1063/1.2335152](https://doi.org/10.1063/1.2335152)]

The formation of patterns in snow and ice has been a source of fascination since antiquity. As early as 1611, Johannes Kepler¹ sought a physical explanation for the beautiful forms of snowflakes. While attention has been lavished upon snowflakes ever since,² their wintry cousins, icicles, have remained largely ignored. The basic mechanisms of icicle growth are well known,^{3–5} but there are few mathematical analyses describing their long, slender forms, most notably those of Makkonen³ and of Szilder and Lozowski.⁴ Icicle surfaces are typically covered with ripples a few centimeters in wavelength, but only recently^{6–8} has theoretical work begun to address the underlying dynamic instability that produces them. On a more basic level, the growth of dripping icicles has not been studied from the perspective of a true free-boundary approach.

As one can see in Fig. 1, icicles and stalactites—the iconic structures found in limestone caves⁹—can bear a striking resemblance, particularly insofar as they evince a slightly convex carrot-like form that is distinct from a cone. Of course visual similarity does not imply mechanistic similarity, but there is reason to think that a common mathematical structure might link the two phenomena.¹⁰ In each case, the evolving solid structure is enveloped by a thin flowing layer of fluid which regulates the rate of growth. For stalactites, this is the coating water film flowing down the surface in which carbon dioxide is produced and through which it diffuses. In icicles there is a similar water layer, but the controlling fluid is the upward flowing natural convection

boundary layer in the surrounding air through which latent heat is transported by diffusion and convection.

Recent work^{11,12} examining stalactite growth as a free boundary problem established a novel geometrical growth law based on the coupling of thin-film fluid dynamics and calcium carbonate chemistry.^{13–15} Numerical studies showed an attractor in the space of shapes whose analytical form was determined and found to compare very favorably with that of natural stalactites. Is there an analogous ideal shape for icicles? It is tempting to view icicle growth as a classic Stefan problem, as explored extensively for solidification from the melt.¹⁶ There, growth is controlled by a quasistatic diffusive field and the growth rate is determined by a gradient of that variable. However, such systems generally lack the previously mentioned thin layer of moving fluid (water or air) that separates the developing solid from its surroundings, and thus they do not conceptually match the conditions of growth. Exceptions occur, for instance, in the presence of surface premelting.¹⁷ One context in which progress has been made is the formation of “ice stalactites,” hollow tubular structures formed below sea ice as salt is rejected during solidification,^{18,19} but these formations are quite distinct from typical icicles. Here, we suggest an approach to the problem of icicle growth which synthesizes geometrical principles, heat flow in the water and atmosphere, and thin-film fluid dynamics, to arrive at the existence of an ideal growing shape for icicles. This approach can be viewed as a generalization of the important works mentioned above^{3,4} to a true free-boundary formulation. The ideal growing shape found here compares well with observations. Interestingly, the shape far from the tip has the same mathematical form as that recently derived^{11,12} for the growth of stalactites.

We first consider the water layer flowing down the surface of a growing icicle to set some initial scales. The volu-

^{a)} Author to whom correspondence should be addressed. Address after September 1, 2006: Department of Applied Mathematics and Theoretical Physics, Center for Mathematical Sciences, Wilberforce Road, University of Cambridge, Cambridge CB3 0WA, United Kingdom. Electronic mail: gold@physics.arizona.edu



FIG. 1. (Color online) Icicles and stalactites. (a) A collection of icicles (Ref. 23). (b) Stalactites in Katchner Caverns, Benson, AZ.

metric flow rate Q over icicles is typically^{3,20} on the order of tens of milliliters per hour ($\sim 0.01 \text{ cm}^3/\text{s}$), and icicle radii are usually in the range of 1–10 cm. To understand the essential features of the flow, consider a cylindrical icicle of radius r , over the surface of which flows an aqueous film of thickness h (Fig. 2). Since $h \ll r$ over nearly the entire icicle surface, the velocity profile in the layer may be determined as that flowing on a flat surface. Furthermore, we expect the Reynolds number to be low enough that the Stokes approximation is valid. If y is a coordinate normal to the surface and θ is the angle that the tangent vector \hat{t} makes with respect to the horizontal, then the Stokes equation for gravity-driven flow is $\nu_w d^2 u / dy^2 = g \sin \theta$, where g is the gravitational acceleration and $\nu_w = 0.01 \text{ cm}^2/\text{s}$ is the kinematic viscosity of water. Enforcing no-slip and stress-free boundary conditions at the solid-liquid and liquid-air interfaces, the thickness is

$$h = \left(\frac{3Q\nu_w}{2\pi g r \sin \theta} \right)^{1/3}. \quad (1)$$

Using typical flow rates and radii, we deduce a layer thickness that is tens of microns and surface velocities

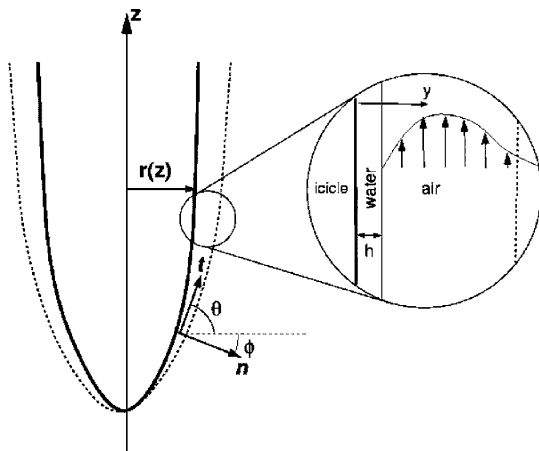


FIG. 2. Features of a hanging axisymmetric shape used in development of the theory. The flowing water layer, not to scale, is much thinner than the rising thermal boundary layer.

$u_s \approx (gh^2/2\nu_w)\sin \theta$ below several mm/s, consistent with known values,^{3,20} yielding $\text{Re} = 0.01 - 0.1$, well in the laminar regime as anticipated. At distances from the icicle tip comparable to the capillary length (several millimeters), the complex physics of pendant drop detachment takes over and the thickness law (1) ceases to hold.

Of course, if the icicle is growing, the volumetric flux Q must vary along the arc length s of the icicle as water is converted to ice. With the icicle profile described by $r(z)$ (Fig. 2) and the growth velocity normal to the ice at any point being v_g , Q varies along the surface as

$$\frac{dQ}{ds} = 2\pi r v_g, \quad (2)$$

the positive sign on the right-hand side reflecting the choice of origin at the tip, with s increasing upward. We seek to find a final answer in the form of a uniformly translating shape,^{11,12} for which every point on the icicle must grow at a rate such that $v_g = v_t \cos \theta$, where v_t is the growth velocity of the tip, usually millimeters per hour ($\sim 10^{-4} \text{ cm/s}$)^{3,20} (given the complexities of droplet detachment,³ the tip velocity here will be considered a parameter of the theory). Therefore, we substitute this rule into (2), using $dr = ds \cos \theta$, and find that an exact integration may be performed, yielding

$$Q = Q_t + \pi r^2 v_t, \quad (3)$$

where Q_t is the flow rate at the icicle's tip. This result, which neglects evaporation, conforms to the obvious fact that, for a given Q , Q_t will eventually approach zero as the icicle becomes so long as to allow all of the feeding water to freeze before it reaches the tip. For further analysis, we will only consider the growth of icicles up to this point, and not beyond, and only consider growth into a calm environment.

Turning now to heat transport, note that the curvature of the icicle surface is sufficiently small everywhere that the Gibbs-Thompson correction²¹ to the melting temperature T_m is negligible. Thus, the temperature of the water at the ice-water interface is well-approximated as T_m along the entire icicle, neglecting the tip. Furthermore, since most icicles possess an unfrozen liquid core,³⁻⁵ heat does not travel radially outward from the center of the icicle, as it would if the core were solid and the temperature inside were decreasing over time. Hence, any flux of heat present at the ice-water interface consists solely of latent heat being removed as the water changes phase. The issue of advective heat transport by the flowing water is addressed by considering the Peclet number $\text{Pe} = u_s h / \alpha_w$, where $\alpha_w \approx 10^{-3} \text{ cm}^2/\text{s}$ is the thermal diffusivity of water. Using our previous estimates for the flow velocity u_s and thickness, we find $\text{Pe} \approx 0.1 - 1$, indicating that energy transport down the icicle is generally subordinate to conduction of heat across the water layer. The heat flux across the water, then, is $F_w = \kappa_w (T_m - T_i) / h$, where κ_w is the thermal conductivity of water and T_i , the temperature at the air-water interface, is found below.

The rate-limiting, and hence, controlling, step in growth occurs once the heat has traversed the water layer and must then be transported through the air surrounding the icicle. This transport can be greatly influenced by the presence of

forced convection, as considered in previous works,^{3,4} but we shall ignore this in the present study, assuming a calm environment for growth. Instead, we will consider natural convection, such as found in the study by Makkonen.³ As is well known, objects warmer than their surroundings create rising thermal boundary layers in the adjacent atmosphere due to the buoyancy of the heated surrounding air. Similarity solutions for the coupled Navier-Stokes and heat transport equations in the Boussinesq approximation can provide the basis for understanding this boundary layer. For instance, for a flat, vertical, isothermal plate, solutions show that the rising warm air is confined to a boundary layer whose thickness δ as a function of the vertical coordinate z is²²

$$\delta = C\ell \left(\frac{z}{\ell}\right)^{1/4}, \quad \text{with } \ell \equiv \left(\frac{\nu_a^2}{g\beta\Delta T}\right)^{1/3}, \quad (4)$$

where C is a dimensionless constant that depends on the Prandtl number of air (0.68) and is of order unity, $\nu_a \approx 0.13 \text{ cm}^2/\text{s}$ is the kinematic viscosity of air, $\beta \approx 3.7 \times 10^{-3} \text{ K}^{-1}$ is the volumetric coefficient of expansion for air, and ΔT is the temperature difference between the plate and the ambient temperature T_a far away. For a temperature difference of 10 K the characteristic length scale $\ell \approx 0.01\text{--}0.1 \text{ cm}$.

To justify our future use of (4) to approximate the boundary layer thickness for our icicle, we submit the following. First, using a temperature difference of 10 K, one finds a boundary layer thickness on the order of a few millimeters to a centimeter, much greater than the thickness of the water layer on a typical icicle, but less than a typical icicle radius, so that flatness is approximated. Second, the peak velocity of the warm air in the layer is

$$u_p \approx \frac{2}{3}\sqrt{g\Delta T\beta z}, \quad (5)$$

around 5–10 cm/s, much greater than the downward water velocity, so the no slip condition used in the flat plate analysis is nearly attained. Third, the atmospheric heat flux can be written as $F_a = \kappa_a(T_i - T_a)/\delta$, where κ_a is the thermal conductivity of air, differing from the exact form only by the multiplication of an order one constant. If we equate this heat flux with that through the water layer, which we previously described, one finds that T_i is given by

$$T_i = T_m - (T_m - T_a) \frac{h\kappa_a/\delta\kappa_w}{1 + h\kappa_a/\delta\kappa_w}. \quad (6)$$

On account of the vast difference in scale between h and δ mentioned above, the ratio $h\kappa_a/\delta\kappa_w \approx 0.01$, so T_i is lower than T_m by only $10^{-3}\text{--}10^{-2} \text{ K}$. Hence, from the view of atmospheric heat transport, the icicle walls are essentially isothermal at T_m (although the tip is cooler³). Finally, we note that (4) can be used to describe a slightly nonvertical plate by simply replacing g with $g \cos \phi$ and z with $z/\cos \phi$ (the arc length along the plate). Since, barring the tip region, an icicle's surface is nearly vertical and has a very slowly varying slope, this is a valid approximation in our case; we treat the order one factor of $\cos \phi$ as a constant and fold it into the

parameter C . A more sophisticated treatment would account for the effects of wall curvature.³

At this point, we are in a position to derive a formula for the growth velocity v_g of the icicle's surface. We divide the heat flux as calculated through the atmospheric boundary layer by the latent heat of fusion per volume L of water (334 J/cm^3) to obtain the velocity

$$v_g = v_c \left(\frac{\ell}{z}\right)^{1/4}, \quad (7)$$

where v_c is a characteristic velocity given by

$$v_c \equiv \frac{\kappa_a \Delta T}{L C \ell}, \quad (8)$$

and is, with $\Delta T = 10 \text{ K}$, around 10^{-4} cm/s , which is in good agreement with the known velocities cited earlier. To find the equation governing the icicle profile, we enforce the condition for uniformly translating shapes, $v_g = v_t \sin \phi$, upon (7) and scale the variables r and z both by the factor $a = \ell(v_c/v_t)^4$, thereby defining the new dimensionless variables ρ and ζ . After rewriting trigonometric functions in terms of the slope of the profile ρ' , one finds the equation

$$\rho' = \frac{1}{\sqrt{\zeta^{1/2} - 1}}, \quad (9)$$

which can be exactly integrated to yield the final expression for our ideal icicle shape,

$$\rho = \frac{4}{3}(\zeta^{1/2} + 2)\sqrt{\zeta^{1/2} - 1}. \quad (10)$$

This shape is shown in Fig. 3(a). Note that this shape at large ζ goes as $\rho \sim \zeta^{3/4}$ and therefore the thickness of the thermal boundary layer relative to the icicle radius scales as $\delta/r \sim \zeta^{-1/2}$ and the two-dimensional boundary layer calculation becomes ever more satisfactory further up the icicle, albeit slowly.

As promised, this asymptotic power law is identical to that found in the case of stalactites,^{11,12} finally explaining their strikingly similar appearances. Furthermore, if we evaluate this asymptotic form at some point on the surface (ρ^*, ζ^*) where the aspect ratio (length/width) is $A = \zeta^*/\rho^*$, then the shape can be rewritten as $\zeta/\zeta^* \approx (\rho/\rho^*)^{4/3}$, a universal, self-similar form. Hence, we can compare our ideal shape to natural icicles by simply finding the correct aspect ratio, or, equivalently, the correct scaling factor a , that best equates the two forms. The results of such comparisons are seen in Figs. 3 and 4. Figures 3(b)–3(d) show overlays of the appropriately scaled theoretical shape with three images of natural icicles. To find the appropriate scaling, each image was passed through an edge-detection algorithm to extract the profile $r(z)$. Each profile was then compared to the ideal form through a least-squares analysis to determine the best fit a . For the more quantitative analysis of Fig. 4, we first found a for each of the eight icicle images, then scaled the image profiles by this best-fit factor. All eight of the now-dimensionless profiles were then averaged together, forming the data points and associated error bars seen in the graph in Fig. 4, which are to be compared with the theoretical shape

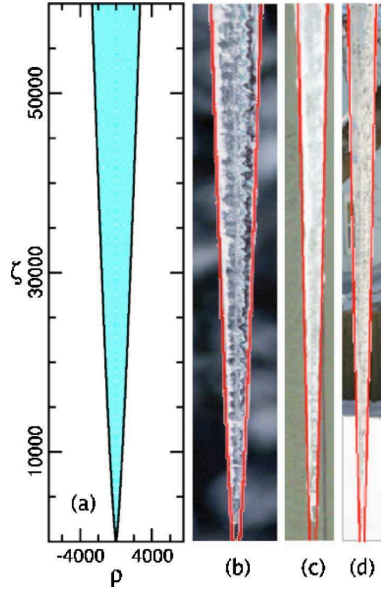


FIG. 3. (Color online) Ideal shape of an icicle and comparison with natural icicles. (a) Ideal shape in dimensionless units of radius and height. (b)–(d) A selection of natural icicles (Ref. 23) each with the appropriately scaled ideal form overlaid.

shown. Clearly, there is good agreement between the two, with no obvious systematic deviations present. On the far right, possible ripples can be seen as the data oscillates around the theoretical curve. Moreover, the shape is quite distinct from a conical geometry; indeed, an analogous least-squares fit of the data to a conical shape displays quite significant systematic deviations. Of course, controlled experiments on the growth of icicles are needed to check in detail various aspects of the theory, such as the assumption that a traveling shape is indeed an attractor of the dynamics.

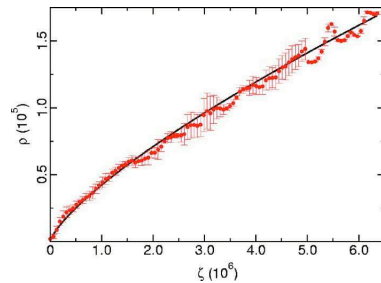


FIG. 4. (Color online) A comparison between the theoretical shape and natural icicles. The solid line represents the shape as calculated in the text, while the data points and error bars represent the averaging of the scaled profiles of eight icicles. In order to perform this averaging, each icicle's profile was scaled by the appropriate factor a through a least squares analysis. Error bars generally increase with ζ due to the fact that there are fewer icicles with appropriate aspect ratios at those points. After $\zeta=5 \times 10^6$ only one icicle is represented, and the displayed error bars represent discretization uncertainties.

As a final interesting side note, we now calculate the ideal shape by analyzing the growth velocity using the heat flux through the thin water layer rather than the air. First, let us look at the thickness law (1) in conjunction with the depletion predicted in (3). Clearly, at large ρ , the fluid layer thickness will *grow* as

$$h \approx \left(\frac{3v_t v_w \rho}{2g \sin \theta} \right)^{1/3}. \quad (11)$$

Using this and the ideal shape we have calculated, the ratio of h to δ in this regime must then look like

$$\frac{h}{\delta} \approx \left(\frac{2v_w a v_t^4}{g} \right)^{1/3} \frac{L}{\kappa_a \Delta T}. \quad (12)$$

So, if we substitute this ratio into (6), we see that, asymptotically, the temperature drop across the water layer goes to a fixed value of

$$\Delta T_w \rightarrow \left(\frac{2v_w a v_t^4}{g} \right)^{1/3} \frac{L}{\kappa_w}, \quad (13)$$

which is on the order of 10^{-3} K, as previously indicated. It is curious that this factor turns out as it does; for a different thickness law (1), as could be the case for a non-Newtonian fluid, the temperature drop could either approach zero or even increase at large ζ . In any case, we can now use this ΔT_w , along with the heat flux through the water layer, to find that, asymptotically, the profile ζ' should follow the scaling law

$$\zeta' \approx \left(\frac{3}{4\rho} \right)^{1/3}. \quad (14)$$

Equation (14) is another interesting result, as it shows that the shape obtained by a method that focuses on the liquid film yields the same shape as that found from the foregoing analysis of the natural convection boundary layer. We are unsure at this point whether it is mere happenstance that these two methods agree as they do, or perhaps this four-thirds scaling law has a deeper underlying significance in this class of problems.

Clearly, the scenario presented here, by which a free boundary dynamics for icicle growth is derived, contains a number of simplifications and approximations whose quantitative accuracy merits further study. Chief among these is the use of a boundary layer theory which assumes a flat and vertical surface. Both of these assumptions are justifiable only far away from the icicle's tip. A full numerical study would likely prove most illuminating. We expect the analysis presented here to serve as a basis for further understanding of ice structures, including axisymmetric perturbations such as the ripples so commonly found on icicles, as well as strongly nonaxisymmetric forms such as the sheets which are analogous to “draperies” in limestone caves. In this regard, recent work on solidification on surfaces of arbitrary curvature²⁴ may prove quite relevant.

The authors thank J. G. Dash, S. R. Morris, J. S. Wettlaufer, and M. G. Worster for important discussions, and

an anonymous referee who emphasized the importance of heat transport through the convective boundary layer. This work was supported in part by NSF ITR Grant No. PHY0219411.

- ¹J. Kepler, *A New Year's Gift, or On the Six-Cornered Snowflake* (Clarendon, Oxford, 1966).
- ²K. G. Libbrecht, *The Snowflake: Winter's Secret Beauty* (Voyageur, Stillwater, 2003).
- ³L. Makkonen, "A model of icicle growth," *J. Glaciol.* **34**, 64 (1988).
- ⁴K. Szilder and E. P. Lozowski, "An analytical model of icicle growth," *Ann. Glaciol.* **19**, 141 (1994).
- ⁵J. Walker, "Icicles ensheathe a number of puzzles: just how does the water freeze?" *Sci. Am.* **258**, 114 (1988).
- ⁶N. Ogawa and Y. Furukawa, "Surface instability of icicles," *Phys. Rev. E* **66**, 041202 (2002).
- ⁷K. Ueno, "Pattern formation in crystal growth under parabolic shear flow," *Phys. Rev. E* **68**, 021603 (2003).
- ⁸K. Ueno, "Pattern formation in crystal growth under parabolic shear flow. II," *Phys. Rev. E* **69**, 051604 (2004).
- ⁹C. Hill and P. Forti, *Cave Minerals of the World* (National Speleological Society, Huntsville, 1997).
- ¹⁰C. A. Knight, "Icicles as crystallization phenomena," *J. Cryst. Growth* **49**, 193 (1980).
- ¹¹M. B. Short, J. C. Baygents, J. W. Beck, D. A. Stone, R. S. Toomey, and R. E. Goldstein, "Stalactite growth as a free boundary problem: A geometric law and its Platonic ideal," *Phys. Rev. Lett.* **94**, 018501 (2005).
- ¹²M. B. Short, J. C. Baygents, and R. E. Goldstein, "Stalactite growth as a free-boundary problem," *Phys. Fluids* **17**, 083101 (2005).
- ¹³W. Dreybrodt, "Chemical kinetics, speleothem growth and climate," *Boreas* **28**, 347 (1999).
- ¹⁴G. Kaufmann, "Stalagmite growth and palaeo-climate: the numerical perspective," *Earth Planet. Sci. Lett.* **214**, 251 (2003).
- ¹⁵D. Buhmann and W. Dreybrodt, "The kinetics of calcite dissolution and precipitation in geologically relevant situations of karst areas. 1. Open system," *Chem. Geol.* **48**, 189 (1984).
- ¹⁶D. A. Kessler, J. Koplik, and H. Levine, "Pattern selection in fingered growth phenomena," *Adv. Phys.* **37**, 255 (1988).
- ¹⁷J. S. Wettlaufer and M. G. Worster, "Dynamics of premelted films: frost heave in a capillary," *Phys. Rev. E* **51**, 4679 (1995).
- ¹⁸S. Martin, "Ice stalactites: Comparison of a laminar flow theory with experiment," *J. Fluid Mech.* **63**, 51 (1974).
- ¹⁹D. K. Perovich, J. A. Richter-Menge, and J. H. Morison, "The formation and morphology of ice stalactites observed under deforming lead ice," *J. Glaciol.* **41**, 305 (1995).
- ²⁰N. Maeno, L. Makkonen, K. Nishimura, K. Kosugi, and T. Takahashi, "Growth-rates of icicles," *J. Glaciol.* **40**, 319 (1994).
- ²¹J. S. Rowlinson and B. Widom, *Molecular Theory of Capillarity* (Clarendon, Oxford, 1982).
- ²²H. Schlichting, *Boundary Layer Theory* (McGraw-Hill, New York, 1979).
- ²³Icicle images: www.artlebedev.com/posters [Figs. 1(a) and 3(b)]; smartacus.org/albums/tahoe/icicles.jpg [Fig. 3(c)]; cyren.org/Mambo/images/stories/icicles.jpg [Fig. 3(d)].
- ²⁴T. G. Myers, J. P. F. Charpin, and S. J. Chapman, "The flow and solidification of a thin fluid film on an arbitrary three-dimensional surface," *Phys. Fluids* **14**, 2788 (2002).

APPENDIX D: EVOLUTIONARY TRANSITIONS IN *VOLVOX*

PNAS

Proceedings of the National Academy of Sciences of the United States of America

www.pnas.org

PNAS (ISSN-0027-8424) is published weekly in print by the National Academy of Sciences.

Correspondence: PNAS, 500 Fifth Street, NW, NAS 340, Washington, DC 20001 USA or 2101 Constitution Avenue, NW, NAS 340, Washington, DC 20418 USA (for courier or express mail). E-mail: PNAS@nas.edu.

Information for Authors: Information for Authors and the Editorial Board listing by discipline are available at www.pnas.org.

Copyright: Volumes 90–103, copyright © 1993–2006 by the National Academy of Sciences of the United States of America, all rights reserved. Volumes 1–89, copyright as a collective work only; author(s) retains copyright to individual articles.

Requests for Permission: See www.pnas.org/misc/rightperm.shtml for details. Address requests to reproduce material published in Volumes 1–89 to the original author(s); e-mail other requests to PNASpermissions@nas.edu, fax 1-202-334-2739, or PNAS Permissions Editor, 500 Fifth Street, NW, NAS 340, Washington, DC 20001 USA. Please cite the exact material to be reprinted and state specifically where it will be used. **Photocopies:** PNAS is registered with the Copyright Clearance Center (CCC), 222 Rosewood Drive, Danvers, MA 01923 USA, fax 1-978-750-4470, or www.copyright.com. Authorization to photocopy items for the internal or personal use of specific clients is granted by the National Academy of Sciences provided that the proper fee is paid directly to CCC. **Microforms:** Contact UMI at www.umi.com or P.O. Box 1346, Ann Arbor, MI 48106-1346 USA. This journal is printed on acid-free paper effective with Volume 84, Issue 1.

Advertising: Sarah Frances Scarborough, PNAS Advertising Sales, 500 Fifth Street, NW, NAS 340, Washington, DC 20001 USA. Phone 1-202-334-2348, fax 1-202-334-1346, e-mail sscarborough@nas.edu.

Subscriptions: Address correspondence to: PNAS, % AIP, P.O. Box 503284, St. Louis, MO 63150-3284 USA. For subscription help, e-mail subs@aip.org, phone 1-516-576-2270, or visit www.pnas.org. Subscriptions are entered on a calendar-year basis. The 2006 rates for print are as follows—in the U.S.: personal, \$290; institutional, \$1,510—U.S. by First Class at a surcharge of \$160—elsewhere (institutional includes expedited delivery): personal, \$455; institutional, \$1,865—elsewhere by expedited delivery at a surcharge of \$355. **Exclusive Agent for Subscribers in Japan:** USACO Corporation, 17-12 Higashi-Azabu, 2-Chome, Minato-ku, Tokyo 106-0044, Japan. Phone 81 3 3505 3256, fax 81 3 3505 6282, e-mail agent@usaco.co.jp. **Change of Address:** Notify the Circulation Office 6 weeks in advance and list the old and new addresses. **Claims:** Requests for replacement copies will not be honored more than 60 days after the issue date for domestic subscribers and not more than 90 days after the issue date for foreign subscribers. Claims will not be honored for more than 2 issues per calendar year for the same subscriber. **Single Copies:** \$40 per issue in the U.S., \$50 elsewhere. **Canadian GST:** Registration Number R-133130880.

Postmaster: Send address changes to PNAS, % AIP, P.O. Box 503284, St. Louis, MO 63150-3284 USA. Periodicals postage paid at Washington, DC, and additional mailing offices.

PNAS is available online at www.pnas.org.
PRINTED IN THE USA

President of the Academy
Ralph J. Cicerone

Editor-in-Chief
Nicholas R. Cozzarelli

Senior Editor
Solomon H. Snyder

Associate Editors
William C. Clark
Alan Fersht
Jack Halpern
Jeremy Nathans

Editorial Board
Susan G. Amara
Kathryn V. Anderson
Francisco J. Ayala
Linda M. Bartoshuk
Adriaan Bax
Roger N. Beachy
Michael L. Bender
Stephen J. Benkovic
May R. Berenbaum
Bruce J. Berne
Barry R. Bloom
David Botstein
James H. Brown
Patrick O. Brown
Charles R. Cantor
Stephen R. Carpenter
Maarten J. Chrispeels
Thomas W. Cline
Enrico Coen
John M. Coffin
Stanley N. Cohen
Peter Cresswell
Partha Sarathi Dasgupta
Eric H. Davidson
Pietro V. De Camilli
Francisco de la Cruz
David L. Denlinger
Charles A. Dinarello
W. Ford Doolittle
Charles T. Esmon
Douglas T. Fearon
Christopher B. Field
Richard A. Flavell
L. B. Freund
Fred H. Gage
Joseph L. Goldstein
Shafira Goldwasser
Emil C. Gotschlich
Harry B. Gray
Philip P. Green
E. Peter Greenberg
Diane E. Griffin
Mark T. Groudine
John B. Gurdon
Jeffrey C. Hall
Philip C. Hanawalt
Susan Hanson
Robert Haselkorn
Peter M. Howley
Richard L. Haganir
Tony Hunter
Vernon Martin Ingram
L. L. Iversen

Rudolf Jaenisch
Ronald W. Jones
David Julius
Richard V. Kadison
Robert W. Kates
James P. Kennett
Robion C. Kirby
Edward D. Korn
John Kuriyan
Robert A. Lamb
Alan M. Lambowitz
Ramon Latorre
Robert J. Lefkowitz
Anthony Leggett
Michael Levitt
Steven E. Lindow
Dan R. Littman
George H. Lorimer
Philip W. Majerus
Tak Wah Mak
Geoffrey W. Marcy
Paul C. Martin
Pamela A. Matson
Robert May
Stephen L. Mayo
John J. Mekalanos
Barbara J. Meyer
Kiyoshi Mizuuchi
Paul L. Modrich
Salvador Moncada
Nancy A. Moran
Newton E. Morton
Shigetada Nakanishi
Masatoshi Nei
Tomoko Ohta
Eric N. Olson
Gordon H. Orians
Elinor Ostrom
David C. Page
Peter Palese
William E. Paul
Stanley B. Prusiner
Dale Purves
Charles M. Radding
Marcus E. Raichle
Tom A. Rapoport
Mark A. Ratner
R. Michael Roberts
Robert G. Roeder
Michael Rosbash
David D. Sabatini
Jeremy A. Sabloff
Linda J. Saif
Hans Joachim Schellnhuber
Gertrud M. Schupbach
Michael Sela
Thomas E. Shenk
Obaid Siddiqi
David O. Siegmund
Thomas J. Silhavy
Brian Skyrms
Edward E. Smith
Ralph M. Steinman
Charles F. Stevens
M. S. Swaminathan
Joseph S. Takahashi
Hans Thoenen
Craig B. Thompson

Janet Thornton
Robert Tjian
Barry M. Trost
Nicholas J. Turro
Inder M. Verma
Peter K. Vogt
Peter Walter
Michael S. Waterman
James A. Wells
Susan R. Wessler
Sue H. Wickner
William T. Wickner
Ryuzo Yanagimachi
Masashi Yanagisawa
George D. Yancopoulos

Publisher
Kenneth R. Fulton

Executive Editor
Diane M. Sullenberger

Managing Editor
Daniel H. Salsbury

Editorial Staff
James B. Allison
Josiah W. Armour
Jennifer Byers
Michael Campbell
Heather A. Ehlers
Carolyn Elliott
Benjamin E. Ellis
Arijit Guha
Moses M. Jackson
Renita M. Johnson
Elise Laffman
Jaime Lees
Leslie Malone
Michael C. Mullins
Tom Myers
Allison Ross

**Production, Marketing,
and Licensing Manager**
George Kendall

Production Staff
Barbara A. Bacon
Timothy Bauer
Anne C. Field
Christopher Lashomb
Tiffany A. Miller

Finance Manager
Simone Marshall-Campbell

Business Staff
Andrew Huff
LaTarrea S. Jackson
Julia A. Little
Sarah Frances Scarborough

Media Staff
Regina Nuzzo
Jennifer L. Smith
Oliver J. Yun
Nick Zagorski

Flows driven by flagella of multicellular organisms enhance long-range molecular transport

Martin B. Short*, Cristian A. Solari†, Sujoy Ganguly*, Thomas R. Powers‡, John O. Kessler*, and Raymond E. Goldstein*§¶

Departments of *Physics and †Ecology and Evolutionary Biology, §Program in Applied Mathematics, and ¶BIOS Institute, University of Arizona, Tucson, AZ 85721; and ‡Division of Engineering, Box D, Brown University, Providence, RI 02912

Edited by Robert H. Austin, Princeton University, Princeton, NJ, and approved April 18, 2006 (received for review January 22, 2006)

Evolution from unicellular organisms to larger multicellular ones requires matching their needs to the rate of exchange of molecular nutrients with the environment. This logistic problem poses a severe constraint on development. For organisms whose body plan is a spherical shell, such as the volvocine green algae, the current (molecules per second) of needed nutrients grows quadratically with radius, whereas the rate at which diffusion alone exchanges molecules grows linearly, leading to a bottleneck radius beyond which the diffusive current cannot meet metabolic demands. By using *Volvox carteri*, we examine the role that advection of fluid by the coordinated beating of surface-mounted flagella plays in enhancing nutrient uptake and show that it generates a boundary layer of concentration of the diffusing solute. That concentration gradient produces an exchange rate that is quadratic in the radius, as required, thus circumventing the bottleneck and facilitating evolutionary transitions to multicellularity and germ-soma differentiation in the volvoclean green algae.

advection | multicellularity | *Volvox*

The motility of microorganisms is primarily thought to enable access to optimum environments. Yet some species of colonial motile algae thrive in restrictive habitats such as shallow evanescent puddles, all the while paddling energetically with their flagella. What is the significance, beyond locomotion, of this collective coordinated beating of flagella? Algal metabolism requires exchange, between organisms and water, of small molecules and ions such as CO_2 , O_2 , and PO_4^{3-} . Rapidly growing organisms that are “large” in the sense explained below must augment diffusion with effective modes of transport from remote reaches of their environment (1). The volvocine green algae (2–5) can serve as a model system for understanding how exchange of nutrients and wastes varies with organism size, as in the transition from unicellular to ever-larger multicellular colonies. The Volvocales range from the unicellular *Chlamydomonas* to large colonies of cells, eventually leading to *Volvox*, comprising 1,000–50,000 cells (Fig. 1). They include closely related lineages with different degrees of cell specialization in reproductive and vegetative function (germ-soma separation), which seem to represent “alternative stable states” (6). Phylogenetic studies show that these transitions in cell specialization have occurred multiple times, independently (7–9), to geometrically and functionally similar configurations, suggesting that there is a selective advantage to that morphology. The volvoclean range of sizes, >3 orders of magnitude, enables the study of scaling laws; from a theoretical perspective, the spherical form of the Volvocales simplifies mathematical analysis.

Volvox, the largest colonies in the lineage, are formed by sterile biflagellated *Chlamydomonas*-like somatic cells, with outwardly oriented flagella, which are embedded at the surface of a transparent extracellular matrix, which also contains the germ cells that develop into flagellated daughter colonies. In some species, germ cells start flagellated, but after their first mitotic division the flagella are absorbed (e.g., *V. aureus*), whereas in others (e.g., *V. carteri*) the germ cells are never flagellated.

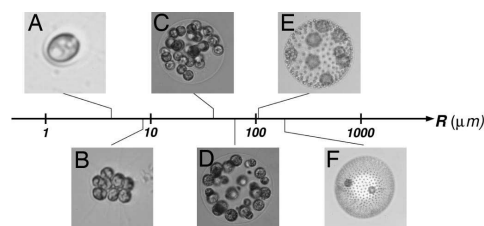


Fig. 1. Volvocine green algae arranged according to typical colony radius R . The lineage ranges from the single-cell *Chlamydomonas reinhardtii* (A), to undifferentiated *Gonium pectorale* (B), *Eudorina elegans* (C), to the soma-differentiated *Pleodorina californica* (D), to the germ-soma differentiated *V. carteri* (E), *V. aureus* (F), and even larger (e.g., *V. gigas* with a radius of 1 mm). In species in which two cell types can be identified, the smaller are somatic cells and the larger are reproductive cells. Note that the number of cells in *Volvox* species ranges from 1,000 (e.g., *V. carteri*) to 50,000 (e.g., *V. barberi*).

Directional swimming due to the coordinated beating of these flagella also is accompanied by rotation; *Volvox* is from the Latin “*volvare*,” to roll (2). Bell (10) and Koufopanou (11) suggested that the extracellular matrix is a storehouse (“source”) of nutrients for the germ cells (“sink”). They interpret this source-sink coupling as a mechanism that increases the uptake of nutrients by the developing germ cells located within the colony. Moreover, they showed (11) that germ cells from *Volvox carteri*, when liberated from their mother colony and freely suspended in the growth medium, grow more slowly than those embedded in intact colonies. Those experimental studies did not consider the external flow created by collective flagellar beating of the mother colonies. Our studies (3, 4) were designed to investigate the effects of such fluid flows and showed in fact that these flows positively influence germ-cell growth rates. Indeed, externally supplied flows can replace those due to flagella and return germ cells to normal growth rates. Flagella obviously confer motility; we infer that they also play a subtle but crucial role in metabolism. Niklas (1) suggested that as organisms increase in size, stirring of boundary layers, yielding transport from remote regions, can be fundamental in maintaining a sufficient rate of metabolite turnover, one not attainable by diffusive transport alone. Yet there has not been a clear quantitative analysis of this putative connection between flagella-driven stirring and nutrient uptake. Here we investigate the hypothesis that those flows facilitate, even “encourage,” the transition to large multicellular forms. We analyze the idealized problem of the scaling that relates nutrient uptake to body size. Measurements of the actual

Conflict of interest statement: No conflicts declared.

This paper was submitted directly (Track II) to the PNAS office.

¶To whom correspondence should be addressed. E-mail: gold@physics.arizona.edu.

© 2006 by The National Academy of Sciences of the USA

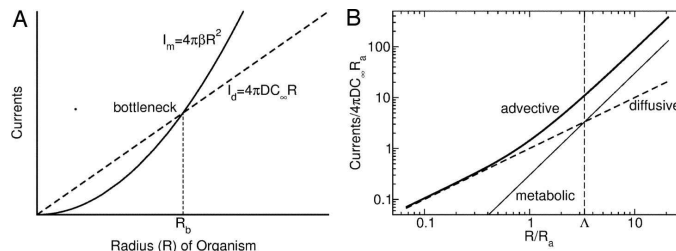


Fig. 2. Molecular currents (molecules per second) and requirements. (A) A schematic diagram illustrating the existence of the diffusive bottleneck R_b . When the metabolic demand current (solid line), which is quadratic in organism radius R , exceeds the diffusive current (dashed line), which is only linear in R , the metabolism is constrained by diffusion. (B) Log-log plot showing how the advective current (thick solid line) circumvents the diffusive bottleneck for the choice $\Lambda \equiv R_b/R_a = 3.3$. At radii greater than the advective radius R_a (Eq. 7), the advective current grows quadratically with R , allowing metabolic needs to be satisfied for any arbitrary size.

flow fields generated by colonies confirm the analysis. Because we also aim to understand the physical constraints leading to germ-soma differentiation, we investigate a body plan without such differentiation and examine its failure to deal with those constraints.

Results

Bottleneck Radius. Consider the case in which only molecular diffusion in the suspending fluid governs transport (uptake or rejection) of a chemical species whose concentration is $C(r)$, where r is the radial distance from the center of the colony. When more than even a few percent of the colony surface is covered by an array of absorbers or emitters, the diffusion-limited rate is well approximated by that of a sphere uniformly covered with absorbers/emitters (12). We now focus, for simplicity, on nutrient acquisition. By Fick's law, a gradient in concentration yields a flux. We define the uptake rate or current at the surface of the sphere as the integral of the flux over the area of the sphere. Our sign convention is that the current is positive if the sphere takes up nutrients. Therefore, if C_∞ is the concentration far from the colony of radius R , then the steady-state concentration is $C(r) = C_\infty(1 - R/r)$. Furthermore, if D is the diffusion constant and dS is the element of surface area of the colony, then the inward current $I_d = D \int dS (\partial C / \partial r)$ is linear in the colony radius R

$$I_d = 4\pi DC_\infty R. \quad [1]$$

The timescale τ_D on which this steady-state profile develops from an initially uniform concentration is $\tau_D \approx R^2/D$. For a typical colony of radius 200 μm and diffusion constant of $D = 2 \times 10^{-5} \text{ cm}^2/\text{s}$, $\tau_D \approx 20 \text{ s}$, which is very long compared with the flagellar beat period but short compared with the life cycle. The current (Eq. 1) can be compared with the metabolic requirements of a colony with surface-mounted cells

$$I_m = 4\pi R^2 \beta, \quad [2]$$

where β is the time-dependent nutrient demand rate per unit area, including the requirements of internal "tissue" (e.g., germ cells), and storage by the extracellular matrix. The availability by diffusion can exceed the nutritional requirements at small radii. At sizes greater than the bottleneck radius

$$R_b = \frac{DC_\infty}{\beta}, \quad [3]$$

at which $I_d = I_m$, diffusion is insufficient to feed the organism (Fig. 2A). The diffusive rejection of waste products also is limited

by a bottleneck radius of the same form as Eq. 3, with β signifying the forced emission rate of waste and C_∞ replaced by the difference between a molecular waste concentration at the surface and at infinity.

Estimation of the bottleneck radius includes several considerations. First, the demand/consumption rate β varies with time and environmental parameters (e.g., light, temperature, nutrient availability) during the life cycle of *Volvox*. Second, there is uncertainty as to which of the key nutrients is limiting. Third, it is arguable whether the boundary condition for waste rejection at the colony surface involves a specified flux or a concentration. Mindful of these difficulties, we can make a rough estimate using parameters appropriate for either phosphate (13) ($D \approx 10^{-5} \text{ cm}^2/\text{s}$, $C_\infty \approx 6 \times 10^{14} \text{ cm}^{-3}$, and $\beta \approx 10^{12} \text{ cm}^{-2}\text{s}^{-1}$) or oxygen ($D \approx 2 \times 10^{-5} \text{ cm}^2/\text{s}$, $C_\infty \approx 10^{17} \text{ cm}^{-3}$, and $\beta \approx 10^{14} \text{ cm}^{-2}\text{s}^{-1}$) measured in *V. carteri* using standard biological oxygen demand (BOD) bottles. We find $R_b \approx 50\text{--}200 \mu\text{m}$. Intriguingly, the low range of the estimated R_b is comparable with *Pleodorina* (Fig. 1D), the smallest species where soma differentiation occurs; the high range is comparable with the smallest germ-soma differentiated *Volvox* colonies (e.g., Fig. 1E). Note that *Pleodorina* is considerably smaller than *Volvox*. In the latter, the number of flagellated surface-mounted somatic cells is much higher, and germ cells, which are nonflagellated, lie in the interior of the colony.

As a consequence of the dual role played by the flagellar basal bodies as both anchoring points for flagella and as microtubule organizing centers active in cell division, undifferentiated colonies are subject to the "flagellation constraint" (5, 14), which prevents the use of flagella during cell division. It is therefore appropriate that the largest colonies without true germ-soma differentiation would have a maximum size comparable with the bottleneck radius. For the nonmotile part of the life cycle, which also has the greatest metabolic needs, these colonies would just barely be able to obtain sufficient nutrients by diffusion alone.

Flows, Advection, and Nutrient Uptake. How does advection, the transport of solutes by flow, modify this picture? The governing advection-diffusion equation is

$$\frac{\partial C}{\partial t} + \vec{u} \cdot \vec{\nabla} C = D \nabla^2 C, \quad [4]$$

where $\vec{u} \cdot \vec{\nabla} C$ is the advective rate of change of the concentration field $C(\vec{r}, t)$, and $D \nabla^2 C$ is the diffusive rate of change. Here, the vector $\vec{u}(\vec{r}, t)$ is the spatially and temporally varying fluid velocity. The standard measure of the competition between advection and diffusion is the (dimensionless) Péclet number

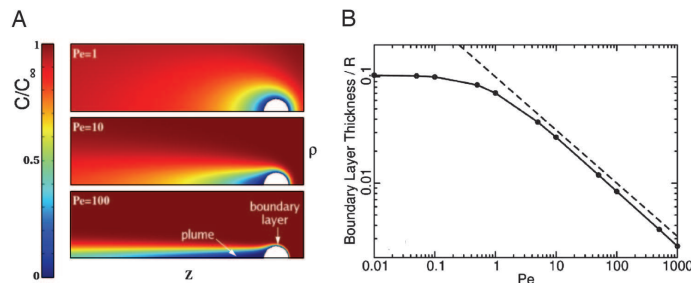


Fig. 4. Results from numerical calculations of spatial dependence of the concentration field using the theoretically obtained velocity field. (A) Concentration, normalized by C_∞ , near a perfectly absorbing [$C(R) = 0$] swimming spherical colony for various Péclet numbers, illustrating the development of a thin localized anterior boundary layer and long narrow posterior plumes at high swimming speeds. Colors represent the dimensionless concentration C/C_∞ . The concentration fields near an immobilized colony are quantitatively very similar. (B) The relationship between boundary layer thickness and Péclet number. The thickness was determined from the computations as the distance from the front surface of the sphere to the point at which $C/C_\infty = 0.1$. When displayed as shown on a log-log plot (black line), the boundary layer thickness, divided by sphere radius R , is parallel to a line (dashed) proportional to $Pe^{-1/2}$, indicating that it also varies as the $-1/2$ power at Péclet numbers greatly exceeding unity.

concentration field C/C_∞ near a swimming colony for a range of Péclet numbers. When $Pe \sim 1$, the concentration field is only slightly distorted from spherical symmetry, whereas for $Pe \gg 1$, a thin concentration boundary layer forms around the leading edge of the sphere; furthermore, a solute plume, analogous to the “tail” behind sedimenting marine snow (21), the organic detritus falling from the upper layers of the ocean, extends to ever-greater length. This plume of nutrient depletion or waste product accumulation is left behind a swimming colony. As an increasing Péclet number is associated with increasing radius, we may imagine the three frames in Fig. 4A as corresponding to organisms comparable in size with the advective radius, larger, and then much larger. Because R_a is the measure of the size of the boundary layer, the boundary layer width R_b/R , in units of the colony radius, is proportional to $Pe^{-1/2}$. Computations are consistent with this scaling (Fig. 4B), where the boundary layer thickness is taken to be the distance over which the scaled concentration $C/C_\infty = 0.1$ in front of the colony. The absorption current I_a follows from Fick's law as an integral, $I_a = \int_S dS (\partial C / \partial r)$, over S , the colony surface. We approximate $\partial C / \partial r \approx C_\infty / R_a$ at the surface, yielding

$$I_a \approx \frac{4\pi R^2 D C_\infty}{R_a}. \quad [8]$$

The right-hand side of Eq. 8 also may be expressed as $4\pi D C_\infty R P e^{1/2}$, the same power law found by Magar *et al.* (17, 18), whose velocity field included only the first few Legendre polynomial terms. The key point here is that the quadratic dependence of the Péclet number on radius (quite miraculously!) leads to a solute current that scales with the surface area, just as required. Fig. 2B revisits the competition between pure diffusive current and metabolic needs first illustrated in Fig. 2A but now presented on a log-log plot. It shows how the total molecular current crosses over from a diffusion-dominated linear behavior for $R < R_a$ to advection-dominated quadratic scaling for $R > R_a$. This scaling is the same power as that for the metabolic needs. We therefore conclude that transport by the collective beating of flagella eliminates the diffusion-only inhibition of growth and thus facilitates the transition to enlargement and multicellularity.

Discussion

Viewed from a different perspective, the flows we have described enhance the molecular or metabolite exchange rate per unit area

of a colony. This advective contribution confers an advantage to increasing size, because it rises precipitously from the smallest organisms up to those whose size is several times the advection radius (Fig. 5). These results suggest that “a greater rate of nutrient acquisition per unit area” is one answer to the often-posed question regarding the advantages of increased size (22), particularly for colonial forms with only a few cells. Significantly, the leveling out of the exchange rate for even larger colonies implies size neutrality in that regime, i.e., that an increase of size in this range no longer affords any greater rate of nutrient acquisition per unit area. Perhaps this characteristic contributes to the polyphyletic origin of the Volvocales.

It should be emphasized that the details of the boundary conditions for nutrient uptake and/or waste removal can have a large effect on the degree to which advection can enhance these processes. It is also quite possible that the dynamics of waste removal are coupled to those of nutrient uptake.

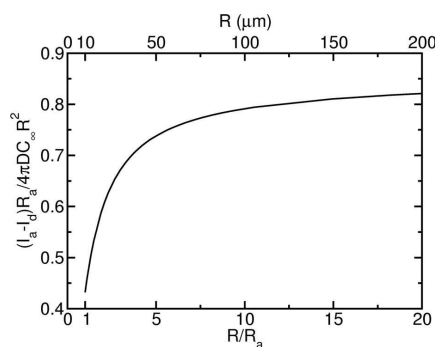


Fig. 5. Difference between molecular flux (current/area) with advection and without, plotted as a function of the colony radius R , in units of the advective radius R_a . Numerical results derived using flagella-driven flow show that beyond R_a the advective contribution overpowers pure diffusion. Beyond $\approx 100 \mu\text{m} = 10R_a$, the approximate size where germ/soma differentiation occurs in the Volvocales, that difference saturates, indicating onset of size neutrality, in the sense that increasing size no longer increases the advective advantage in nutrient acquisition per unit area.

Although we have focused on the central issue of metabolite exchange in the presence of strong fluid transport by flagella, the solute plumes (Fig. 4A), representing either depletion or waste, also provide spatially and temporally extended signals for the presence of a colony, perhaps significant for intercolony communication, as in sexual induction (23) and quorum sensing (24), and for spatial patterning by means of chemotaxis. In the context of predation, a solute plume increases the probability of detection.

Methods

Colonies of *V. carteri f. nagariensis* harvested from synchronized populations grown in standard *Volvox* medium (25) under controlled dark/light cycles (16 h light, 10,760 lux, 28°C/8 h dark, 26°C) were held fixed by micropipette aspiration (Fig. 2), viewed at 4× magnification on the stage of an inverted microscope (Nikon Diaphot 200). Movies were acquired with an analog charge-coupled device camera (SSC-M374; Sony; 480 × 640 pixels) and were typically composed of ≈1,000 images taken at ≈30 frames per s. The resulting flow fields were smoothed by

averaging >200 frames. For particle imaging velocimetry (PIV) studies, the medium was seeded with microspheres (Molecular Probes; F8825 carboxylate modified, 1.0 μm, Nile red), viewed by using laser epifluorescence (80 mW, 532 nm) or darkfield illumination. Commercial PIV software (Dantec Dynamics, Skovlunde, Denmark) was used. Averaged velocity fields were used to obtain the tangential velocity component as a function of polar angle θ (Fig. 2), with typically 20 measurements between $\theta = 0$ and $\theta = \pi$. Apart from minor distortions due to the micropipette, symmetry between the two halves of the profile was observed; we combined those data and partitioned them into 10 bins.

We thank H. C. Berg, T. E. Huxman, R. E. Michod, R. Stocker, and especially A. M. Nedelcu for important discussions and L. Cisneros, C. Dombrowski, and C. Smillie for experimental assistance. This work was supported in part by National Science Foundation Grants DEB-0075296 (to C.A.S.), PHY-0551742 (to M.B.S., S.G., J.O.K., and R.E.G.), and CMS-0093658 (to T.R.P.).

- Niklas, K. J. (1994) *Plant Allometry* (Univ. of Chicago Press, Chicago).
- Kirk, D. L. (1998) *Volvox: Molecular-Genetic Origins of Multicellularity and Cellular Differentiation* (Cambridge Univ. Press, Cambridge, U.K.).
- Solari, C. A., Kessler, J. O. & Michod, R. E. (2006) *Am. Nat.* **167**, 537–554.
- Solari, C. A., Ganguly, S., Michod, R. E., Kessler, J. O. & Goldstein, R. E. (2006) *Proc. Natl. Acad. Sci. USA* **103**, 1353–1358.
- Koufopanou, V. (1994) *Am. Nat.* **143**, 907–931.
- Larson, A., Kirk, M. M. & Kirk, D. L. (1992) *Mol. Biol. Evol.* **9**, 85–105.
- Coleman, A. W. (1999) *Proc. Natl. Acad. Sci. USA* **96**, 13892–13897.
- Nozaki, H., Ohta, N., Takano, H. & Watanabe, M. M. (1999) *J. Phycol.* **35**, 104–112.
- Nozaki, H. (2003) *Biologia* **58**, 425–431.
- Bell, B. (1985) in *The Origin and Evolution of Sex*, eds Halvorson, H. O. & Monroy, A. (Liss, New York), pp. 221–256.
- Koufopanou, V. & Bell, G. (1993) *Proc. R. Soc. London Ser. B* **254**, 107–113.
- Berg, H. C. & Purcell, E. M. (1977) *Biophys. J.* **20**, 193–219.
- Senft, W. H., Hunchberger, R. A. & Roberts, K. E. (1981) *J. Phycol.* **17**, 323–329.
- King, N. (2004) *Dev. Cell* **7**, 313–325.
- Guyon, E., Hulin, J. P., Petit, L. & Mitescu, C. D. (2001) *Physical Hydrodynamics* (Oxford Univ. Press, Oxford).
- Acrivos, A. & Taylor, T. D. (1962) *Phys. Fluids* **5**, 387–394.
- Magar, V., Goto, T. & Pedley, T. J. (2003) *Q. J. Mech. Appl. Math.* **56**, 65–91.
- Magar, V. & Pedley, T. J. (2005) *J. Fluid Mech.* **539**, 93–112.
- Hand, W. G. & Haupt, W. (1971) *J. Protozool.* **18**, 361–364.
- Hiatt, J. D. F. & Hand, W. G. (1972) *J. Protozool.* **19**, 488–489.
- Kjørboe, T. & Jackson, G. A. (2001) *Limnol. Oceanogr.* **46**, 1309–1318.
- Bonner, J. T. (1998) *Integr. Biol.* **1**, 27–36.
- Nedelcu, A. M., Marcu, O. & Michod, R. E. (2004) *Proc. R. Soc. London Ser. B* **271**, 1591–1596.
- Bassler, B. L. (2002) *Cell* **109**, 421–424.
- Kirk, D. L. & Kirk, M. M. (1983) *Dev. Biol.* **96**, 493–506.